Innovative Ironless Loudspeaker Motor Adapted to Automotive Audio

Mathias Rémy

Académie de Nantes

École Doctorale Sciences Pour l'Ingénieur, Géosciences, Architecture
Université du Maine, Le Mans, France

Thèse De Doctorat
Spécialité : ACOUSTIQUE

présentée par

Mathias REMY

pour obtenir le titre de Docteur d'Université

Innovative Ironless Loudspeaker Motor Adapted to Automotive Audio

---

Moteur de Haut-parleur Sans Fer Innovant Adapté à l'Audio Automobile

---

Thèse préparée au **L**aboratoire d'**A**coustique de l'**U**niversité du **M**aine

soutenue le 9 septembre 2011

devant le jury composé de :

A. DOBRUCKI	Professeur, Wroclaw University of Technology	Rapporteur
B. MULTON	Professeur, ENS Cachan, Bruz	Rapporteur
N. DAUCHEZ	Professeur, SUPMECA, Saint-Ouen	Examinateur
C. HENAUX	Maître de Conférence, INP Toulouse	Examinateur
Y. AUREGAN	Professeur, LAUM, Université du Maine	Examinateur
B. CASTAGNEDE	Professeur, LAUM, Université du Maine	Examinateur
M.F. SIX	Docteur, Hutchinson, Chalette sur Loing	Invité
R. TOPPI	Docteur, Faital S.p.A., Milan	Invité
G. GUYADER	Docteur, Renault, Guyancourt	Examinateur
G. LEMARQUAND	Professeur, LAUM, Université du Maine	Directeur de thèse

Abstract

This PhD work (CIFRE, Renault, LAUM) deals with the conception, development and pre-industrialization of a new kind of ironless loudspeaker motor using bonded magnets, which allows substantial reduction of the distortion due to the motor, as well as making the loudspeaker lighter thanks to an optimization of the useful magnetic mass. This structure led to the filing of five patents by Renault and the LAUM [1, 2, 3, 4, 5].

The first part is dedicated to reminding the reader of the general laws that describe the functioning of a loudspeaker: how it is modelled, the different intrinsic non-linearities and their impact on the radiated acoustic pressure. This is done in order to understand the stakes of reducing these imperfections, and more particularly those directly linked to the loudspeaker motor. In addition, a history of the different ironless motor structures realized in sintered magnets known today is presented.

The second part presents a new ironless structure made of a bonded magnet that we developed during these three years. The use of this material, fabricated by injection molding, allows one to realize a great variety of magnet physical shapes and complex magnetization shapes. A complete theoretical study of this new structure, presenting the magnetic model and the design of the motor, is then proposed. This theoretical study is completed with several measurements realized on a prototype in order to verify the theoretical expectations, with regard to harmonic and intermodulation distortion reduction. The same measurements were done on the standard loudspeaker in order to quantify the advantages and disadvantages of this new kind of motor. This prototype was based on the design of a standard automotive loudspeaker in which the motor was replaced by a bonded magnet motor. The motor was fabricated by Paulstra/Hutchinson and then assembled on the loudspeaker by Faital S.p.A., both of whom are certified automotive suppliers. The methods used to realize this prototype could be directly applied for mass production. This PhD work is used as a tool by the people in charge of the development of this technology with a view to potential industrialization for the mass market.

Résumé

Ce travail de thèse (CIFRE, Renault, LAUM) porte sur la conception, le développement et la pré-industrialisation d'un nouveau type de moteur de haut-parleur sans fer utilisant des plasto-aimants, permettant à la fois de réduire très nettement la distorsion due au moteur, ainsi que d'alléger le haut-parleur grâce à une optimisation de la masse magnétique utile. Cette structure a donné lieu à cinq brevets déposés par Renault et le LAUM [1, 2, 3, 4, 5].

La première partie est consacrée à un rappel sur le fonctionnement du haut-parleur, sa modélisation, les différentes non-linéarités qui lui sont propres et leur impact sur la pression acoustique rayonnée par celui-ci, afin de mieux comprendre les enjeux de la réduction de ces imperfections, et plus particulièrement celles liées au moteur du haut-parleur. L'accent est mis sur la suppression du fer dans le moteur qui représente une des principales sources de distorsion de la transduction électro-mécanique. Un historique des différentes structures de moteurs de haut-parleur sans fer réalisées en aimants frittés existant à ce jour est alors présenté.

La seconde partie présente ensuite une nouvelle structure de moteur de haut-parleur tout aimant réalisée en plasto-aimant. Cette matière permet de réaliser par injection, des aimants de formes très variées et surtout, possédant des profils d'aimantation nettement plus complexes que ceux qu'il est possible d'obtenir avec des aimants traditionnels frittés. Une étude théorique complète de cette nouvelle structure est alors proposée, puis agrémentée d'un certain nombre de mesures réalisées sur un prototype afin de vérifier les attentes théoriques. Les mêmes mesures ont également été effectuées sur le haut-parleur équipé du moteur standard afin de pouvoir quantifier les avantages et les inconvénients de ce nouveau type de moteur. Ce prototype a été réalisé sur la base d'un haut-parleur automobile standard sur lequel le moteur a été changé. Les prototypes ont été réalisés par des sous-traitants automobiles (Paulstra/Hutchinson et Faital S.p.A.) dans des conditions telles que ces haut-parleurs soient industrialisables. Ce travail de thèse sert d'outil aux personnes en charge du développement de cette technologie en vue d'une éventuelle industrialisation et d'une mise en série sur véhicule.

Remerciements

J'adresse mes vifs remerciements à Andrzej Dobrucki et Bernard Multon pour avoir accepté d'être rapporteurs de ce travail. Je tiens également à remercier Bernard Castagnède, qui a accepté de présider la soutenance de ma thèse, ainsi que Nicolas Dauchez, Carole Henaux, Yves Aurégan, Marc-François Six et Romolo Toppi de m'avoir fait l'honneur de participer à ce jury de thèse.

Je souhaite remercier Guy Lemarquand, mon directeur de thèse, pour avoir accepté d'encadrer cette thèse proposée par Renault et m'avoir permis de développer mes connaissances dans les domaines de l'électroacoustique et du magnétisme, plus particulièrement appliquées au sujet passionnant qu'est le haut-parleur.

Je tiens également à exprimer ma vive gratitude à Gaël Guyader, mon tuteur industriel, pour son encadrement, ses conseils, son soutien, ses encouragements dans les moments difficiles, son grain de folie, ses idées parfois saugrenues, son enthousiasme à toute épreuve, ainsi que pour les nombreux bons moments partagés aussi bien au travail qu'en dehors, autour d'une bonne bouteille de vin par exemple.

Je me dois également de remercier Benoit Merit pour nos nombreuses discussions fructueuses, pour son aide et son soutien, ainsi qu'Antonin Novak, qui m'a été d'une aide précieuse dans la réalisation d'un certain nombre de mesures réalisées lors de cette thèse.

Je remercie les deux partenaires industriels que sont Paulstra/Hutchinson et Faital S.p.A. pour la réalisation des différents prototypes de haut-parleur. Je pense bien sûr plus particulièrement à Benoit Rousselot, Marc-François Six, Romolo Toppi, Alessandro Morelli et Daniele Ceruti.

Mes remerciements se dirigent également vers tous les gens avec qui j'ai eu le plaisir de travailler chez Renault, et plus particulièrement les gens de l'équipe dont je faisais partie : Gaël Guyader, Aurélie Frère, Claire Peteul-Brouillet, Nathalie Le-Hir, Yann Leduc, Chantao Blumenfeld et Kevin Reynier. Un grand merci également à tous les doctorants que j'ai côtoyé chez Renault, notamment Aurélie Frère, Abbas Hekmati, Ludovic Desvard, Franck Barillon, Alex Elmaian, Yann Recoquillon, Marion DHondt, Amélie Da-Costa, Marine Masson et bien d'autres... Je m'arrêterai là dans la liste, mais c'est bien sûr sans oublier de nombreuses autres personnes que j'ai eu le bonheur de connaître pendant ces trois années.

Je remercie également l'ensemble des membres du LAUM qui m'ont toujours réservé un excellent accueil lors de chacun de mes séjours au laboratoire et m'ont permis d'y travailler dans des conditions optimales et dans la bonne humeur. Je remercie bien évidemment Benoit Merit, Antonin Novak, Adrien Pelat, Olivier Doutres, Marcos Pinho, Pierrick Lotton, Laurent Simon, Joël Gilbert, Hervé Mezière, Eric Egon, James Blondeau, Emmanuel Brasseur, Stéphane Lebon et beaucoup d'autres qui se reconnaîtront...

I would like to thank as well Andrew Nagel and Robert Cochran for the time they spent proofreading my thesis and their pertinent advice.

Enfin, je tiens à remercier mes amis, ma famille bien sûr, et surtout mes parents que je ne remercierai jamais assez, entre autre, pour leur soutien inconditionnel, et sans qui rien de tout cela n'aurait été possible.

Table of Contents

Introduction

Loudspeakers are transducers that generate sound in response to an electrical input signal. The mechanism behind this conversion varies from loudspeaker to loudspeaker, but in most cases involves some form of motor assembly attached to a diaphragm. The alternating force generated by the motor assembly, in response to the electrical signal, causes the diaphragm to vibrate. This in turn moves the air in contact with the diaphragm and gives rise to the radiation of sound.

Ernst W. Siemens described the first transducer realizing the principle of electrodynamic conversion thanks to a coil wire suspended in the magnetic field of an electro-magnet in 1874 [6]. But transducer history really began with Alexander Graham Bell's patent of 1876 [7]. Bell had been involved in trying to teach the deaf to speak and wanted a way of displaying speech graphically to help with that. He needed a transducer for the purpose and ended up inventing the telephone. The moving-coil motor used in a loudspeaker was patented by Sir Oliver Lodge in 1898 [8] but, in the absence of suitable amplification equipment, it could not enter wide use. Prior to 1925, the maximum output available from a radio set was in the order of milliwatts, normally only used for listening via earphones. So, the earliest 'speakers' only needed to handle a limited frequency range at low power levels, since it was not until the 1940s that microphones could capture the full audible frequency range, and the 1950s before it could be delivered commercially to the public via the microgroove, vinyl record. The six inch, rubber surround device of Rice and Kellogg used a powerful electro-magnet (not a permanent magnet) [9], and as it could 'speak' to a whole room-full of people, as opposed to just one person at a time via an earpiece, it became known as a *loud* speaker. The inventors were employed by the General Electric Company, in the USA, and they began by building a mains-driven power amplifier which could supply the then huge power of one watt. This massive increase in the available drive power meant that they no longer needed to rely on resonances and rudimentary horn loading, which typically gave very coloured responses. With a whole watt of amplified power, the stage was set to go for a flatter, cleaner response, the result of which became the Radiola Model 104, with its built in power amplifier. The idea of passing the DC supply current through the energising coil of the loudspeaker, to use it instead of the usual, separate smoothing choke to filter out the mains hum from the amplifier, was later patented by Marconi.

Concurrently with the work going on at General Electric, Paul Voight was busy developing somewhat similar systems at the Edison Bell company. By 1924 he had developed a huge electro-magnet assembly weighing over $35kg$ and using $250watts$ of energising

power. By 1926 he had coupled this to his Tractrix horn, which rejuvenated interest in horn loudspeakers due to its improved sensitivity and acoustic output of the moving coil loudspeakers, and when properly designed did not produce the 'honk' sound associated with the older horns. Voight then moved on to use permanent magnets, with up to $3.5kg$ of Ticonal and $9kg$ of soft iron, paving the way for the permanent magnet devices and the much higher acoustic outputs that we have today. Developments in magnet technology made it possible to replace the field coil with a suitable permanent magnet towards the end of the 1930s and there has been little change in the concept since then.

Many detailed studies have been run about the electrodynamic loudspeaker mechanism since its creation, aimed at improving its sound quality as well as its efficiency. The efficiency or sensitivity of a loudspeaker, which is a measurable, objective parameter, represents the loudspeaker's ability to convert the electrical energy that is fed to it into acoustic energy. The sound quality, on the other hand, is a subjective parameter that many people are still trying to understand and predict by knowing the physical parameters of the loudspeaker. It seems that the global sound quality perceived by the auditory system depends on the total harmonic distortion (THD) among other parameters such as intermodulation distortion (IMD) of the considered loudspeaker. Indeed, the loudspeaker is a non-linear system, which means that its acoustic response contains frequency components that are not in the original electrical signal driving the transducer, also known as non-linear distortion.

Therefore, loudspeaker manufacturers try to produce loudspeakers that have a great sensitivity on the one hand, and that are as linear as possible on the other hand. A great part of the non-linearity sources of a loudspeaker has been clearly identified. Among the most significant in terms of generated distortions are found the mechanical non-linearities, mainly due to the suspension systems that are used to make the voice-coil oscillate without rubbing in the magnetic field created by the magnet or electro-magnet. On the acoustic side, the mechanical modes of the diaphragm are a great source of non-linearities as well. They mainly appear at high frequencies, depending on the size, shape and material of the membrane, and particularly impact the directivity of the loudspeaker and create peaks and notches in the sound pressure level (SPL) versus frequency response. Finally, the non-linearities due to the electrodynamic (or electromechanical) conversion have a strong contribution to the total distortion of a loudspeaker.

Nowadays, many people spend more time listening to music in their cars than they do in their living rooms, and considering that the interiors of vehicles now have the potential to house a large array of multimedia devices, R&D organizations around the world have allocated increased resources to improve the sound quality of these environments. However, a vehicle's passenger compartment contains a certain amount of problems that are likely to noticeably affect the audio quality. Contrary to a living room, a vehicle does not contain a lot of space for speakers and enclosures. Also, the seats are fixed, causing the listener to be close to some speakers and far from others, making sound balancing difficult. Furthermore, the seats and interior trim absorb sound whereas glass and metal reflect it. All these elements form a complex listening environment for an audio system.

If we look at it from a different angle, these problems can become advantages. Contrary to living rooms - which differ in size, shape and layout - materials, passenger cell shape and seat positions in a personal car stay unchanged. It thus goes the same way for the acoustics. The audio system can therefore adapt to the vehicle acoustics, making this environment propitious for high quality music listening.

That being said, it goes without saying that one of the most important steps between the music (or speech) recording and the listener's ears is the electroacoustic transduction, that is to say, the loudspeaker. However, the classical electrodynamic loudspeakers with standard ferrite or neodymium motors are not really suited to the new automotive constraints (i.e. weight and room limitations) and to the emerging usage of mass market automotive audio: individual listening, varied audio and video media, security constraints... That is why car manufacturers now start putting into use new technologies that could fulfill these needs. Many configurations have already been proposed, or are under study. Some good examples are for instance the rigid vibrating plates, the use of ultra-thin ribbon transducers, electroactive polymers or high-directivity systems such as 'audio-spot-light'.

In 2008, Renaut launched a study through a PhD thesis supervised by the University of Maine Acoustics Laboratory (LAUM, France), regarding innovative sound reproduction systems adapted to automotive audio. The main research axis that has been chosen to follow during this PhD is the optimization of the classical electrodynamic loudspeaker and more particularly its motor. We decided to study two parameters of optimization that are fundamental for automotive audio: weight reduction, and sound quality enhancement, while of course, satisfying cost constraints that are quite predominant within the automotive industry. One solution that satisfies both criteria is to remove the iron from the loudspeaker motor. However, realizing an ironless motor with traditional sintered magnets can be quite difficult and expensive. We chose to use bonded magnets to design a new innovative motor. This study led to five patents [1, 2, 3, 4, 5].
The first part is dedicated to remind the reader about the general laws that describe the functioning of a loudspeaker: how it is modelled, the different intrinsic non-linearities and their impact on the radiated acoustic pressure. This is done in order to understand the stakes of reducing these imperfections, and more particularly those directly linked to the loudspeaker motor. In addition, a history of the different ironless motor structures realized in sintered magnets known today is presented.
The second part presents a new ironless structure made of a bonded magnet that we developed during these three years. The use of this material, fabricated by injection molding, allows us to realize a great variety of magnet physical shapes and complex magnetization shapes. A complete theoretical study of this new structure, presenting the magnetic model and the design of the motor, is then proposed. This theoretical study is completed with several measurements realized on a prototype in order to verify the theoretical expectations, with regard to harmonic and intermodulation distortion reduction. This prototype was based on the design of a standard automotive loudspeaker on which the motor was replaced by a bonded magnet motor. The motor was fabricated by Paulstra/Hutchinson and then assembled on the loudspeaker by Faital S.p.A., both of whom are certified au-

tomotive suppliers. The methods used to realize this prototype could be directly applied for mass production.

Introduction

Les haut-parleurs sont des transducteurs transformant un signal électrique en son. Le mécanisme de cette conversion varie d'un haut-parleur à l'autre, mais dans la plupart des cas implique un moteur relié à un diaphragme. La force alternative générée par le moteur, en réponse au signal électrique qui lui est appliqué, fait vibrer le diaphragme. A son tour, le mouvement de ce diaphragme fait bouger l'air en contact avec lui et donne naissance à un rayonnement sonore.

Ernst W. Siemens décrivit le premier transducteur réalisant le principe de conversion électrodynamique grâce à une bobine de fil suspendue dans le champ magnétique d'un électro-aimant en 1874 [6]. Mais l'histoire des transducteurs commença réellement avec le brevet de Alexander Graham Bell en 1876 [7]. Bell essayait d'apprendre aux sourds à parler et voulait une manière de représenter graphiquement la parole afin de les aider dans cet apprentissage. Il avait besoin d'un transducteur dans ce but et finit par inventer le téléphone. Le moteur à bobine mobile utilisé dans un haut-parleur fut breveté par Sir Oliver Lodge en 1898 [8] mais, en l'absence d'un équipement d'amplification adapté, il ne put jamais être utilisé à grande échelle. Avant 1925, la puissance de sortie maximale d'un équipement de radio, normalement uniquement utilisé pour écouter avec des écouteurs, était de l'ordre de quelques milliwatts. De plus, les premiers "haut-parleurs" n'avaient besoin de reproduire qu'une bande de fréquences limitée à faible puissance, étant donné que les microphones capables de capturer le spectre audible complet n'arrivèrent que dans les années 1940, et il fallut attendre jusque dans les années 1950 afin de pouvoir délivrer le signal au grand public grâce au disque vinyle. Le dispositif à suspension caoutchouc de 6 pouces construit par Rice et Kellogg utilisait un électro-aimant puissant (et non pas un aimant permanent) [9], et comme il était capable de "parler" à une salle entière, contrairement aux écouteurs qui étaient dédiés à une seule personne, le nom de *haut*-parleur apparut. Les inventeurs était employés aux États-Unis par General Electric, et ils commencèrent par construire un amplificateur capable de délivrer la puissance, énorme pour l'époque, de un watt. Cette forte augmentation de la puissance disponible permit de ne plus dépendre des résonances et de pavillons rudimentaires qui donnaient des réponses très colorées. Avec une puissance d'un watt, il était possible d'obtenir une réponse plus plate et plus propre, dont le résultat fut le Radiola Model 104, avec son amplificateur de puissance intégré.

En concurrence avec le travail mené par General Eletric, Paul Voight travaillait sur des systèmes similaires chez Edison Bell. En 1924, il développa un énorme électro-aimant pesant plus de $35kg$ et utilisant une puissance de $250watts$ pour l'alimenter. En 1926, il

le coupla à son pavillon Tractrix, qui relança l'intérêt dans les haut-parleurs à pavillon permettant d'améliorer la sensibilité et la puissance acoustique des haut-parleurs à bobine mobile, et ne produisant pas le son de "klaxon" associé aux vieux pavillons à condition que ces derniers soient conçus correctement. Voight utilisa ensuite des aimants permanents, avec jusqu'à $3,5kg$ de Ticonal and $9kg$ de fer doux, traçant la voie aux modèles à aimants permanents et à la puissance acoustique élevée que nous connaissons aujourd'hui. C'est vers la fin des années 1930 que le développement des technologies d'aimants rendit possible de remplacer la bobine fixe créant le champ magnétique permanent par des aimants permanents convenables. Le concept du haut-parleur n'a que très peu évolué depuis.

De nombreuses études ont été menées à propos du mécanisme du haut-parleur électrodynamique depuis sa création, dans le but d'améliorer sa qualité sonore ainsi que son efficacité. L'efficacité ou sensibilité d'un haut-parleur, qui est une grandeur objective et mesurable, représente la capacité du haut-parleur à convertir l'énergie électrique qui lui est fournie en énergie acoustique. La qualité acoustique, d'autre part, est un paramètre subjectif que de nombreuses personnes essayent toujours de comprendre et de prévoir à partir des paramètres physiques du haut-parleur. Il semblerait que la qualité sonore globale perçue par le système auditif dépende à la fois de la distorsion harmonique totale (THD) et de la distorsion d'intermodulation (IMD) du haut-parleur considéré. En effet, le haut-parleur est un système non-linéaire, ce qui signifie que sa réponse acoustique contient des composantes fréquentielles qui ne sont pas présentes dans le signal électrique original alimentant le transducteur.

De ce fait, les fabricants de haut-parleurs essaient de produire des haut-parleurs ayant une efficacité élevée d'une part, et étant le plus linéaires possible d'autre part. Une bonne partie des sources de non-linéarité d'un haut-parleur a été identifiée. Les sources principales de distorsion sont les non-linéarités mécaniques, essentiellement dues aux systèmes de suspension utilisés pour faire osciller la bobine mobile dans le champ magnétique créé par l'aimant ou l'électro-aimant, sans que celle-ci ne frotte. Du côté acoustique, les modes propres du diaphragme sont également une source de non-linéarités non négligeable. Ils apparaissent essentiellement aux hautes fréquences, en fonction de la taille, de la forme et de la matière de la membrane. Ils impactent particulièrement la directivité du haut-parleur et créent des pics et des creux dans la pression acoustique en fonction de la fréquence. Finalement, les non-linéarités dues à la conversion électrodynamique (ou électromécanique) contribuent fortement à la distorsion totale d'un haut-parleur.

De nos jours, beaucoup de gens passent plus de temps à écouter de la musique dans leur voiture qu'ils ne le font dans leur salon. Prenant donc en compte le fait fait que les véhicules ont maintenant la possibilité d'accueillir de nombreux équipements multimédia, les services R&D à travers le monde ont alloué des ressources importantes afin d'améliorer la qualité sonore de ces environnements. Cependant, l'habitacle d'une automobile contient un certain nombre de problèmes susceptibles d'affecter sensiblement la qualité audio. Contrairement à un salon, un véhicule ne contient pas beaucoup d'espace pour les haut-parleurs et les enceintes. En outre, les sièges sont fixes, forçant l'auditeur à être proche de certains haut-parleurs et loin des autres, rendant la balance sonore difficle. De plus,

les sièges et différents habillages intérieurs absorbent le son alors que le métal et le verre le refléchisse. Tous ces éléments forment un environnement d'écoute complexe pour un système audio.
En regardant ces différents paramètres sous un autre angle, ces problèmes peuvent devenir des avantages. Contrairement aux salons, dont la taille, la forme et l'aménagement varient, les habitacles et la position des sièges restent inchangés. Il en va donc de même pour l'acoustique. Le système audio peut alors s'adapter à l'acoustique du véhicule, faisant de cet environnement un lieu propice à une écoute de haute qualité.

Ceci étant, il va sans dire que l'une des étapes les plus importantes entre l'enregistrement de la musique (ou de la parole) et les oreilles de l'auditeur est la transduction électroacoustique, autrement dit, le haut-parleur. Cependant, les haut-parleurs électrodynamiques classiques utilisant des moteurs standard ne sont pas vraiment adaptés aux nouvelles contraintes de l'automobile (c.-à-d. poids et encombrement) et à l'usage émergent de l'audio automobile de masse : écoute individuelle, média audio et vidéo variés, contraintes de sécurité... C'est pourquoi les constructeurs automobiles commencent à mettre en application de nouvelles technologies qui pourraient satisfaire ces besoins. Beaucoup de configurations ont déjà été proposées, ou sont encore à l'étude. Quelques bons exemples sont ainsi les plaques vibrantes, l'utilisation de transducteurs à ruban ultra-fins, les polymères électroactifs ou encore les systèmes à haute directivité tel que "l'audio-spot-light".

En 2008, Renault a lancé une étude par le biais d'une thèse de doctorat supervisée par le Laboratoire d'Acoustique de l'Université du Maine (LAUM, Le Mans), afin d'étudier les systèmes de restitution sonore innovants adaptés à l'automobile. L'axe de recherche principal qui a été choisi durant cette thèse est l'optimisation du haut-parleur électrodynamique standard et plus particulièrement son moteur. Nous avons décidé d'étudier deux paramètres d'optimisation fondamentaux pour l'audio automobile: la réduction du poids et l'amélioration de la qualité sonore, en satisfaisant bien évidemment les contraintes de coût qui sont prédominantes dans l'industrie automobile. Une solution permettant de satisfaire ces deux critères est la suppression du fer dans le moteur du haut-parleur. Cependant, la réalisation de moteurs sans fer avec des aimants frittés traditionnels peut être difficile et coûteuse. Nous avons donc choisi d'utiliser des aimants liés afin de développer un nouveau moteur innovant. Cette étude a donné lieu à cinq brevets [1, 2, 3, 4, 5].
La première partie est dédiée à rappeler au lecteur les lois fondamentales décrivant le fonctionnement du haut-parleur: la façon dont il est modélisé, les différentes non-linéarités intrinsèques et leur impact sur la pression acoustique rayonnée. Ceci est réalisé de manière à bien comprendre les enjeux qu'il y a à réduire ces imperfections, et plus particulièrement celles directement liées au moteur du haut-parleur. De plus, un historique des différentes structures de moteurs sans fer réalisées en aimants frittés connues à ce jour est présenté.
La seconde partie présente une nouvelle structure sans fer faite en aimant lié, développée pendant ces trois années. L'utilisation de cette matière mise en forme par injection, permet de réaliser une grande variété de formes d'aimants ayant des orientations d'aimantation complexes. Une étude théorique complète de cette nouvelle structure, présentant le modèle magnétique utilisé et le design du moteur, est alors proposée. Cette étude théorique est complétée par une étude expérimentale réalisée sur un prototype afin de vérifier

les attentes théoriques, en ce qui concernce la réduction des distorsions harmonique et d'intermodulation. Ce prototype est basé sur un haut-parleur automobile standard sur lequel le moteur a été remplacé par un moteur en aimant lié. Le moteur a été fabriqué par Paulstra/Hutchinson puis assemblé sur le haut-parleur pour Faital S.p.A., qui sont tous deux des fournisseurs automobiles certifiés et reconnus. Les méthodes utilisées pour réaliser ce prototype pourraient être directement appliquées à une production de masse.

Chapter 1

Loudspeaker motor equations

1.1 Introduction

Ideally, an acoustical source dedicated to sound reproduction must emit an acoustical energy that is proportional to the electrical stimulus coming from the source through a power amplifier, which means that the complex frequency response has to be linear as a function of frequency and sound level. We assume that the electrical source signal coming from a given sensor and then being amplified is a perfect image of the original acoustical pressure over the whole audio bandwidth (i.e. $20Hz$ to $20kHz$). In other words, we consider that all the devices put prior to the speaker are ideal. Before giving more details about the electrodynamic loudspeaker and the electroacoustic analogies that permit us to describe it, we propose a quick reminder of the different physical principles that can be used to convert a electrical signal into an acoustic signal.

The term *loudspeaker* refers to any transducer capable of transforming an electrical energy into an acoustic energy over a certain frequency band. This energy conversion can be realized using different physical principles that are described in [10] and that we summarize as:

- Electrodynamic principle: a conductor of length $\vec{dl}$ placed in a uniform magnetic induction field $\vec{B}$ in which a current $i(t)$ flows is subjected to an electromagnetic force $\vec{f}(t)$ proportional to the current, such as predicted in Laplace's law: $\vec{f}(t) = i(t)\vec{dl}\times\vec{B}$,

- Electrostatic principle: a polarized plane electrode having a surface S and a normal $\vec{n}$ placed between two other electrodes in which a current $i(t)$ flows is subjected to a force $\vec{f}(t)$ proportional to the inter-electrodes electrical field q: $\vec{f}(t) = qSi(t)\vec{n}$,

- Piezoelectric principle: a piezoelectric material, having a volume V, submitted to a electrical field q is subjected, in the linear case, to a deformation that is proportional to the electrical current flowing through it,

- Electromagnetic principle: A ferromagnetic frame placed in a magnetic field $\vec{B}(t)$ created by a solenoid is subjected to a force that depends on the current $i(t)$ flowing through the solenoid wire,

- Ionic principle: an air mass ionized by a high frequency electric discharge between two electrodes generates a local variation of pressure that is proportional to the thermal gradient induced by the inter-electrodes low frequency current modulation,

- Pneumatic principle: a compressed air tank feeds an orifice whose section variation modulated by an electrical actuator modifies the outgoing air flow with time. The addition of the same device along the opposite axis permits to obtain an inverse flow, the overall producing an alternative flow.

As for the applications of these technologies, the ionic principle is by far the least used. The piezoelectric principle, sometimes used for tweeters, is essentially used for ultrasonic applications. The use of pneumatic principle is limited to high sound pressure level but low quality music reproduction or horns for trucks, trains or boats for instance. The most commonly used transducers for audio reproduction are either electrostatic (sound panels, microphones, very high sensitivity when the polarization voltage is high) or electromagnetic (phone speakers, car horns, easy to fabricate, excellent sensitivity but brings harmonic distortion even at low level) or electrodynamic. The first two are well suited for medium and high frequencies (i.e. between approximately $200Hz$ and $20kHz$) because in this case, the displacement of the vibrating membranes is limited to small amplitudes. Finally, the electrodynamic principle turns out to be the most efficient for low frequencies and a good compromise for the whole audio bandwidth because of the way this technology works, as explained in details in the next part.

1.2 Electrodynamic loudspeaker

When Rice and Kellog developed the moving coil cone loudspeaker (i.e. the electrodynamic loudspeaker), and the one watt amplifier able to power it, in the early 1920s [9], they were already well aware of the complexity of radiating an even frequency balance of sound from such a device. Although Sir Oliver Joseph Lodge had patented the concept in 1898 [8] (following on from earlier work in the 1870s by Ernst Werner Siemens at the Siemens company in Germany [6] and Alexander Graham Bell [7]), it was not until Rice and Kellog that practical devices began to evolve. Sir Oliver had had no means of electrical amplification; the vacuum tube had still not been invented, and the transistor was not to follow for 50 years. Remarkably, the concept of loudspeakers was worked out from fundamental principles; it was not a case of men playing with bits of wire and cardboard and developing things by trial and error. Indeed, what Rice and Kellog developed is still the essence of the modern moving coil loudspeaker. Although they lacked the benefit of modern materials and technology, they had the basic principles very well within their understanding, but their goals at the time were not involved with achieving a flat frequency response from below $20Hz$ to above $20kHz$ at sound pressure levels in excess of $110dB$ SPL.
Of all types of drive units, there is probably none so varied in size, shape, materials of construction or performance as the moving coil cone loudspeaker. They basically all follow the concept shown in Fig. 1.1, and little has changed in the underlying principles of their operation in the 80 years of existence so far. However, this technology is today the only

one capable of reproducing frequencies lower than $200Hz$ at high sound pressure level with a quite compact transducer.
The magnetic circuits are designed to concentrate the magnetic field in a circular gap, as shown in Fig. 1.2. In this gap is inserted the moving coil, which receives the electrical drive current from the power amplifier. This current produces its own alternating magnetic field, whose phase and amplitude depend on the drive signal. The variable field interacts with the static field in the circular gap, and creates a force which either causes the voice coil to move into or out of the gap, depending of the voice-coil current sign. Of course, a means is required to maintain the coil centralized in the gap, and this is achieved by the use of a centering device, or inner suspension, which is still often referred to as a spider. A chassis, also known as a frame or basket, supports the whole assembly and enables it to be mounted on a front baffle or a cabinet. The cone is connected rigidly to the former upon which the voice-coil is wound, and is also connected more or less at the same point to the inner suspension. At the chassis' outer edge the cone is attached via a flexible outer suspension, or surround, which may take the form of half-rolls, corrugations, or pleats. A dust cap is then normally placed in the apex of the cone in order to prevent the ingress of dust and any abrasive dirt, and may also be used as an air pump to cool the voice-coil and gap when the cone assembly moves in and out.

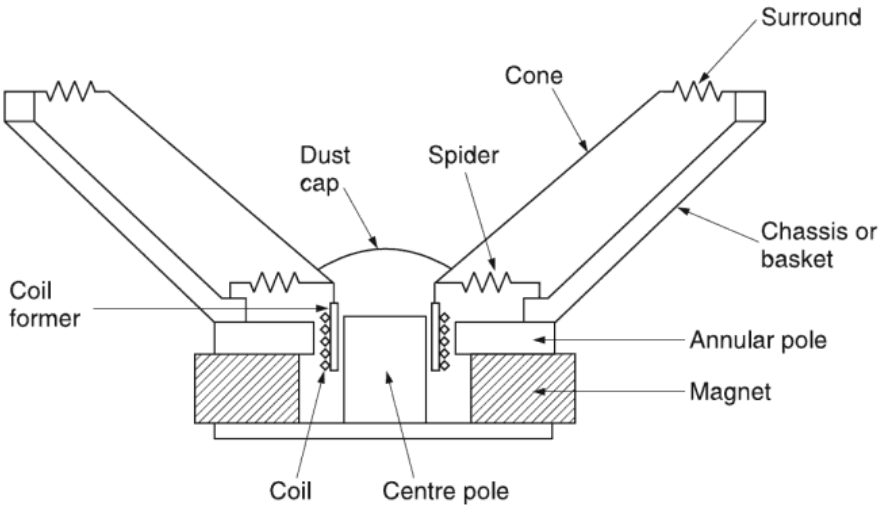

Figure 1.1: The components of a moving coil loudspeaker

1.3 Loudspeaker fundamental equations

As a first approximation, we consider a perfectly linear loudspeaker.

1.3.1 Current-Magnetic field interaction

The loudspeaker voice-coil constitutes a closed contour $\partial\Sigma$ within which an electrical current can circulate. The movement of the voice-coil is assured by the interaction between

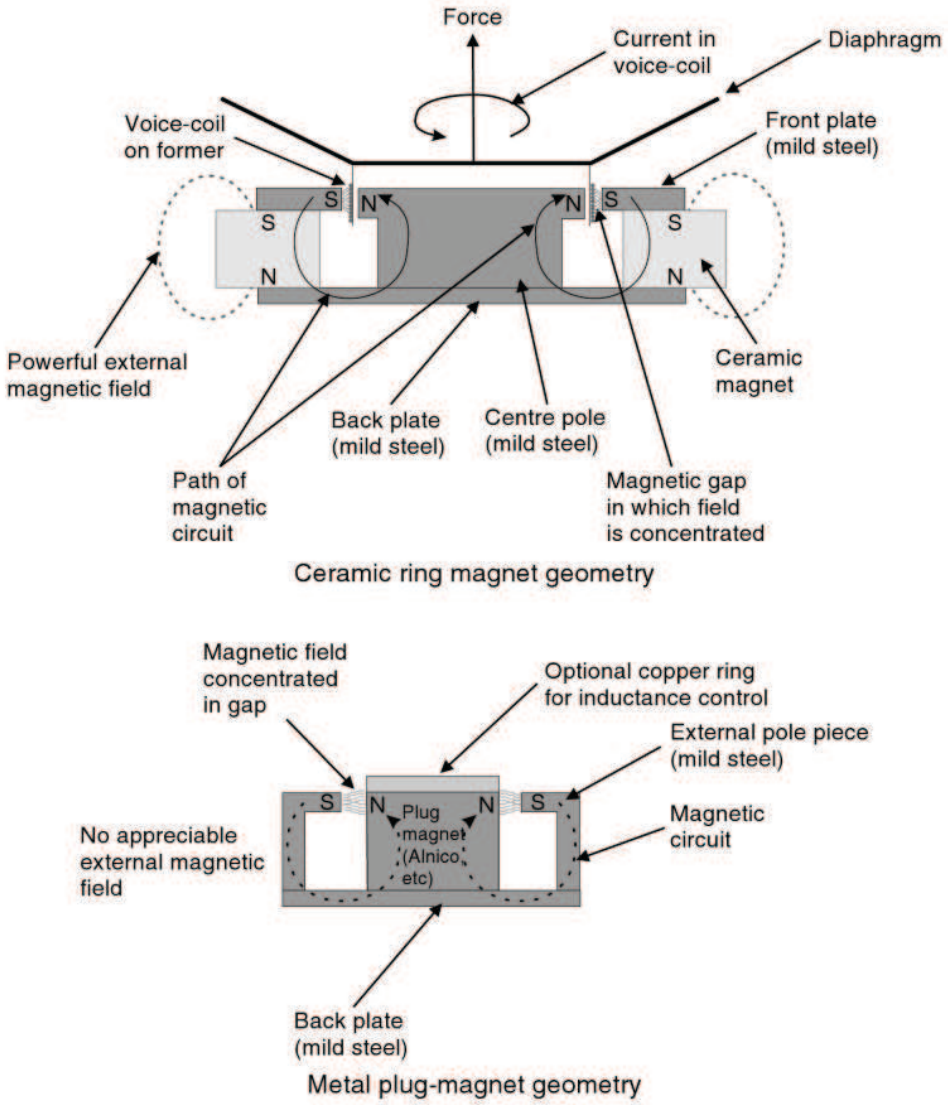

Figure 1.2: Typical motor topologies

this current and the magnetic induction field $\vec{B}_0$ generated by the magnet and flowing through the air gap. This interaction is the origin of the magnetic component of the Lorentz force:

$$\vec{F}_{mag} = q\vec{v}_q \otimes \vec{B}_0, \tag{1.1}$$

where q is an elementary charge flowing through the coil with a velocity $\vec{v}_q$, and $\otimes$ represents the vector product. On a macroscopic scale, the Lorentz force action on the charged particles q of a coil wire element $d\vec{l}$, then creating a current $i(t)$ running through the coil, leads to the Laplace force expression:

$$\vec{F}_L(t) = \int_{\partial\Sigma} i(t)d\vec{l} \otimes \vec{B}_0. \tag{1.2}$$

This force $\vec{F}_L$ exerted on the voice-coil, kept rigid thanks to the voice-coil former, leads this one to move, and more generally makes the whole moving part move.

1.3.2 Towards Thiele and Small parameters

Let us consider a speaker voice-coil having a radius b and a direct current resistance R_{dc}. This resistance is defined by the physical properties of the material that is used to make the coil (copper, aluminum, silver...):

$$R_{dc} = \frac{\xi_b l_b}{S_b}, \tag{1.3}$$

where ξ_b is the material resistivity, l_b the length of the wire and S_b the section of wire. Thus, as for any resistive element, when a direct current i runs through the voice-coil, the voltage u at its extremities is given by Ohm's law:

$$u = R_{dc} i. \tag{1.4}$$

When an alternative current $i(t)$ flows through this coil, it generates a magnetic flux that, following Faraday's law, generates an electromotive force, or *emf*, at the terminals of any electrical conductor that is run across by this flux. An *emf*, noted $e_{mf}(t)$, is then generated at its input terminals. Thus, the voltage $u(t)$ at the coil's terminals is written:

$$u(t) = R_{dc} i(t) - e_{mf}(t). \tag{1.5}$$

By definition, this *emf* at the coil's terminals, representing the total induced voltage including the self induction, is equal to the electrical field circulation $\vec{E}(t)$ across the contour $\partial\Sigma$ [11]:

$$e_{mf}(t) = \oint_{\partial\Sigma} \vec{E}(t).\vec{dl}, \tag{1.6}$$

where the electrical field $\vec{E}(t)$ is linked to the total magnetic field $\vec{B}_\Sigma(t)$ flowing through a section Σ based on the contour $\partial\Sigma$ with Maxwell-Faraday equation [12, 13]:

$$\nabla \otimes \vec{E}(t) = -\frac{\partial \vec{B}_\Sigma(t)}{\partial t}, \tag{1.7}$$

in which ∇ is the del operator. The *emf* expression is then linked to the magnetic field variation inside any section closed by the voice-coil contour. In a loudspeaker, this surface Σ is then crossed by the magnetic field created by the voice-coil and the one created by the magnet. The total field $\vec{B}_\Sigma(t)$ then represents the resultant of these two magnetic fields. The integration of eq. (1.7) over the surface Σ leads to the following relation:

$$\iint_\Sigma \left(\nabla \otimes \vec{E}(t)\right).\overrightarrow{d\Sigma} = \iint_\Sigma -\frac{\partial \vec{B}_\Sigma(t)}{\partial t}.\overrightarrow{d\Sigma}, \tag{1.8}$$

in which the vector $\overrightarrow{d\Sigma}$ is orthogonal to the surface Σ. Using Kelvin-Stokes theorem, it is possible to evaluate the electrical field circulation $\vec{E}(t)$, and thus, the sought *emf*:

$$\oint_{\partial\Sigma} \vec{E}(t).\vec{dl} = e_{mf}(t) = \iint_\Sigma -\frac{\partial \vec{B}_\Sigma(t)}{\partial t}.\overrightarrow{d\Sigma}. \tag{1.9}$$

Due to the interaction between the voice-coil current and the static magnetic field $\vec{B}_0$, the voice-coil is moving and Leibniz's rule for differentiation under the integral sign applied to eq. (1.9), taking into account that $\nabla.\vec{B} = 0$, gives:

$$e_{mf}(t) = -\frac{\partial}{\partial t}\iint_{\Sigma} \vec{B}_{\Sigma}(t).\overrightarrow{d\Sigma} - \int_{\partial\Sigma} (\vec{v}(t) \otimes \vec{B}_{\partial\Sigma}(t)).d\vec{l}, \tag{1.10}$$

where $\vec{v}(t)$ is the voice-coil displacement speed and $\vec{B}_{\partial\Sigma}(t)$ is the resultant magnetic field over the contour $\partial\Sigma$. The first right member term in eq. (1.10) represents the variation of the total magnetic flux $\phi_t(t)$ of the sum of both fields $\vec{B}_0$ and $\vec{B}_{\Sigma}(t)$ across the voice-coil surface Σ, where $\phi_t(t)$ is then written:

$$\phi_t(t) = \iint_{\Sigma} \vec{B}_{\Sigma}(t).\overrightarrow{d\Sigma}. \tag{1.11}$$

Therefore, eq. (1.5) expressing the voltage $u(t)$ at the coil's terminals becomes:

$$u(t) = R_{dc}i(t) + \frac{d\phi_t(t)}{dt} + \int_{\partial\Sigma} (\vec{v}(t) \otimes \vec{B}_{\partial\Sigma}(t)).d\vec{l}. \tag{1.12}$$

This relation (1.12) describes the electrical phenomena happening in a loudspeaker motor, in which no simplifying hypothesis has been made. The first reduction step consists in simplifying the integral calculation defined in eq. (1.10).

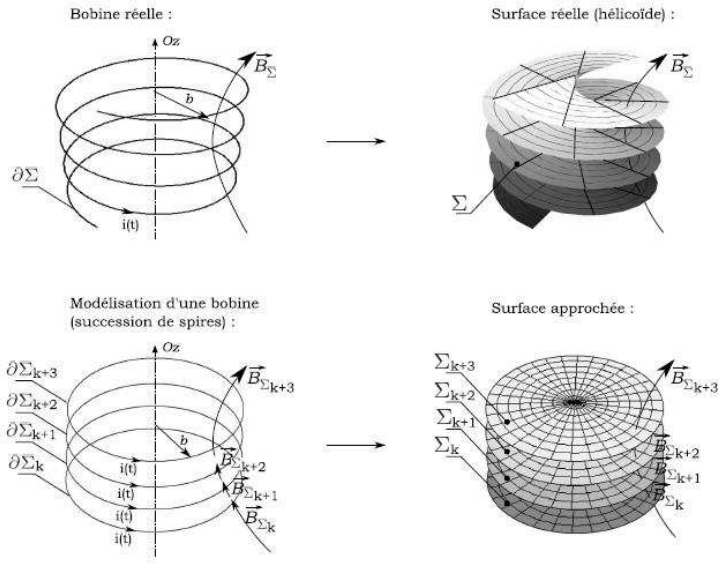

Figure 1.3: A real voice-coil is an helix or a solenoid whose surface Σ is an helicoid. To simplify the calculations, the voice-coil is often seen as a pile of circular turns, whose surface is then the sum of the surfaces Σ_S of each turn. [14]

A traditional loudspeaker voice-coil is a solenoid, and the integrals of (1.10) are difficult to calculate because they are applied on the helical surface Σ or on its contour $\partial\Sigma$. However, coil dimensions, in particular the wire section S_b, are such that it is possible to

consider the voice-coil as a perfect solenoid, that is to say as a pileup of N circular turns of equal radius b, in which the same current $i(t)$ runs, as shown in Fig. 1.3. Taking into account this assumption, it is possible to simplify the calculation of eq. (1.10) [14]. Thus, eq. (1.10) becomes:

$$e_{mf}(t) = -\frac{\partial}{\partial t}\iint_{\Sigma} B_{\Sigma_z}(t)d\Sigma - \int_{\partial\Sigma} v(t)B_{\partial\Sigma_r}(t).dl, \tag{1.13}$$

where $B_{\Sigma_z}(t) = \vec{B}_{\Sigma}(t).\vec{e}_z$ and $B_{\partial\Sigma_r}(t) = \vec{B}_{\partial\Sigma}(t).\vec{e}_r$. Thus, eq. (1.11) expressing the total magnetic flux going across the voice-coil surface Σ becomes:

$$\phi_t(t) = \iint_{\Sigma} B_{\Sigma}(t).d\Sigma, \tag{1.14}$$

and eq. (1.12) giving the total voltage at the coil terminals can be simplified as:

$$u(t) = R_{dc}i(t) + \frac{d\phi_t(t)}{dt} + \int_{\partial\Sigma} v(t)B_{\partial\Sigma_r}(t)dl. \tag{1.15}$$

Due to the geometry of a traditional loudspeaker magnetic circuit, all the equations written previously depend on the voice-coil position in the air gap. That is why, as a first approximation, it is considered that the voice-coil displacement amplitude is small. Moreover, the magnetic field $\vec{b}(t)$ created by the voice-coil is considered to be negligible compared to the static field $\vec{B}$ generated by the magnet, and the effects of the variation of $\vec{b}(t)$ on the magnetic circuit are also neglected, allowing the assumption that $\vec{B}$ does not depend on time. These first three hypotheses permit to express the Laplace force given in eq. (1.2) as:

$$\vec{F}_L(t) = Bl.i(t).\vec{e}_z, \tag{1.16}$$

where the *force factor* is defined as $Bl = B_m.l$ where B_m is the mean value of the radial component B_r of the magnetic field over the voice-coil height. Taking into account all these considerations, the voltage $u(t)$ given in eq. (1.15) can then be written:

$$u(t) = R_{dc}i(t) + \frac{d\phi_t(t)}{dt} + Bl.\frac{dz(t)}{dt}, \tag{1.17}$$

where the coil speed $v(t)$ as been replaced by the time derivative of its displacement $z(t)$ on its axis.

The second term of the right member in eq. (1.17) represents, taking into account all the assumptions above-mentioned, the variation of the total magnetic flux in which the variation of the field generated by the permanent magnet $\vec{B}$ is considered to be negligible. Thus, $\phi_t(t)$ is given by [14]:

$$\phi_t(t) = L_e.i(t), \tag{1.18}$$

where L_e is the inductance of the coil at a given position in the air gap. As a first approximation, the coil inductance is considered to be constant and independent of its position, which gives:

$$\frac{d\phi_t(t)}{dt} = L_e\frac{di(t)}{dt}. \tag{1.19}$$

Finally, the flux expression (1.19) brought back in eq. (1.17) gives the linear expression of the coil voltage $u(t)$ as:

$$u(t) = R_{dc}i(t) + L_e\frac{di(t)}{dt} + Bl.\frac{dz(t)}{dt}. \tag{1.20}$$

1.3.3 Equivalent electrical circuit

In order to define a global model that integrates the whole energy conversion between the electrical signal and the radiated acoustic signal, it is practical to identify the equivalent electrical circuits, or analogous circuits, by using the unidimensional electro-acoustic and electro-mechanical analogies, also called lumped parameters. These methods have been initiated by Olson [15, 16], then reused by Beranek [17] and systematized by Thiele [18, 19] and Small [20]. Equation (1.20) needs the expression of the coil displacement $z(t)$ to be solved. As a first approximation, the loudspeaker moving mass is considered to be a mass-spring-damper system as shown in Fig. 1.4. The mass $M_{ms'}$ includes the diaphragm, the voice-coil and its former as well as the radiating mass of the diaphragm in the air [21]. The spring stiffness K_{ms} and the damper viscous damping coefficient $R_{ms'}$ represent the speaker suspensions, taking into account the radiating resistance of the diaphragm in the air [10].
All the equations are written in the harmonic domain, in which all the variables are complex. Thus, the voltage at the voice-coil's terminals $u(t) = u = U.e^{j\omega t}$, the current flowing through the coil $i(t) = i = I.e^{j\omega t}$ and the displacement of the coil $z(t) = z = Z.e^{j\omega t}$, where ω is the signal pulsation.

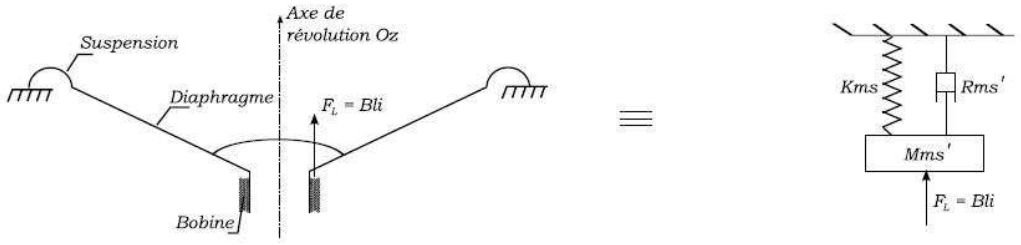

Figure 1.4: The moving mass of a loudspeaker is equivalent, as a first approximation, to a mass-spring-damper system. [14]

This mass-spring-damper system is subject to Laplace force, and the use of the fundamental principle of dynamics, associated with eq. (1.20), permits one to describe the linear functioning of an ideal loudspeaker with a two equation system, coupled by the force factor:

$$\begin{cases} u = R_{dc}.i + L_e.j\omega i + Bl.j\omega z. \\ \\ M_{ms'}.(j\omega)^2 z + R_{ms'}.j\omega z + K_{ms}.z = Bl.i \end{cases} \tag{1.21}$$

Thiele [19] then Small [20] used this equation system (1.21) to represent the loudspeaker with the equivalent electrical circuit shown in Fig. 1.5 [10]. This diagram presents the three coupled domains of the loudspeaker:

- the electrical domain is represented by the blocked electrical impedance Z_e including the voice-coil resistance R_e and inductance L_e. The resistance R_e is assumed to be equal to the direct current resistance R_{dc}. When the moving mass moves, this domain is coupled to the next one via the force factor Bl,

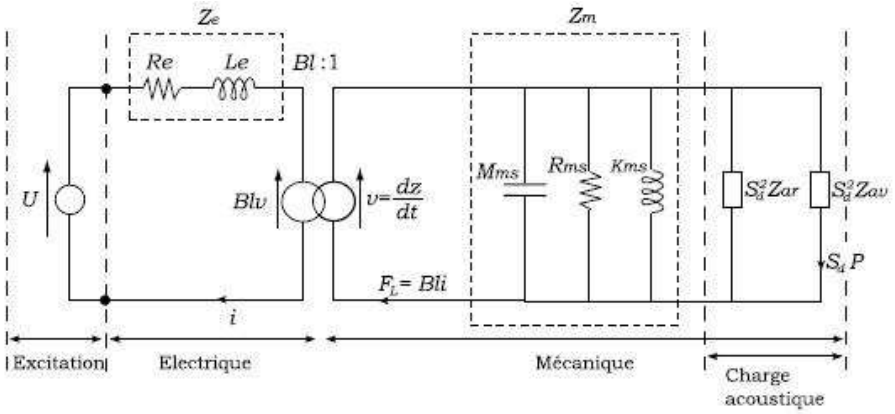

Figure 1.5: Circuit equivalent to a theoretically perfect loudspeaker. [14]

- the mechanical domain is represented by the mechanical impedance Z_m that includes the moving part mass M_{ms}, damping R_{ms} and stiffness K_{ms}. The coupling to the acoustic domain is realized thanks to the radiating surface S_d of the diaphragm,

- the acoustic domain is represented by the front Z_{af} and back Z_{ab} radiating impedances of the speaker diaphragm. In a standard configuration, the loudspeaker is mounted on a cabinet. In this case, Z_{af} is linked to the diaphragm radiation in the listening space whereas Z_{ab} is linked to the diaphragm radiation inside the cabinet. However, if a driver is mounted in an enclosure whose internal volume is large enough so that the air enclosed does not change the effective spring constant of the diaphragm suspension K_{ms}, the enclosure is often said to be an infinite baffle.

The use of the equivalent electrical circuit presented in Fig. 1.5 allows one to easily convert all the parameters to only one domain, that is either electrical, mechanical or acoustic. Expressing these parameters in the electrical domain permits one to write the loudspeaker electrical impedance Z_{HP} as:

$$Z_{HP} = Z_e + Z_{mot} = Z_e + \frac{(Bl)^2}{Z_m + S_d^2 Z_a}, \tag{1.22}$$

where Z_e is the blocked impedance, given by:

$$Z_e = R_e + j\omega Le, \tag{1.23}$$

Z_m is the mechanical impedance, given by:

$$Z_m = R_{ms} + j\omega M_{ms} + \frac{1}{j\omega C_{ms}}, \tag{1.24}$$

where C_{ms} is the mechanical compliance and is equal to $1/K_{ms}$. Z_a is the acoustic impedance, given by:

$$Z_a = Z_{af} + Z_{ab}, \tag{1.25}$$

and finally Z_{mot} is the motional impedance, defined as:

$$Z_{mot} = \frac{(Bl)^2}{\left(R_{ms} + j\omega M_{ms} + \frac{1}{j\omega C_{ms}}\right) + S_d^2(Z_{af} + Z_{ab})}. \tag{1.26}$$

Most of the time, when the diaphragm is approximated by a flat piston whose surface would be identical to S_d, the impedance Z_{af} is written [10, 21]:

$$Z_{af} = R_{af} + jX_{af}, \tag{1.27}$$

where R_{af} is the radiation resistance and X_{af} the radiation reactance, modeling the inductive behavior of the air on which relies the diaphragm. The resistive part R_{af} represents the various loss mechanisms an acoustic wave experiences such as random thermal motion. For resistive effects, energy is removed from the wave and converted into other forms. This energy is said to be 'lost from the system'. The reactive part X_{af} represents the ability of air to store the kinetic energy of the wave as potential energy since air is a compressible medium. It does so by compression and rarefaction. For reactive effects, energy is not lost from the system but converted between kinetic and potential forms.
Thus, the reactance X_{af} acts as a mass adding up to the mechanical moving mass M_{ms}. This mass is noted M_{af} for the front of the diaphragm and is given by [10]:

$$M_{af} = \frac{\rho_0 c_0}{\omega} S_d.X_{af}, \tag{1.28}$$

where ρ_0 is the air density and c_0 the speed of sound in the air. Similarly, an acoustic mass M_{ab} exists for the back of the diaphragm. Thus, the total moving mass $M_{ms'}$ is given by [22]:

$$M_{ms'} = M_{ms} + S_d^2(M_{af} + M_{ab}). \tag{1.29}$$

In the case of an infinite baffle, $M_{af} = M_{ab}$ and $M_{ms'}$ becomes:

$$M_{ms'} = M_{ms} + 2S_d^2 M_{af}. \tag{1.30}$$

At low frequencies, $M_{ms'}$ is given by:

$$M_{ms'} = M_{ms} + 2S_d^2 \frac{8\rho_0}{3\pi^2 a}, \tag{1.31}$$

where a the piston radius of the diaphragm.
In the same manner, the total viscous damping coefficient $R_{ms'}$ is given by:

$$R_{ms'} = R_{ms} + 2S_d^2 R_{af} = R_{ms} + 2R_{ma}, \tag{1.32}$$

where $R_{ma} = S_d^2.R_{af}$ is the front (or back) acoustic resistance, transposed in the mechanical domain.

1.3.4 Low-frequency solution for V_d

The diaphragm velocity v_d is given by:

$$v_d = \frac{V_d}{S_d} = \frac{F_L - F_a}{Z_m} = \frac{Bli - S_d p_d}{Z_m}, \tag{1.33}$$

where where $F_L = Bli$ represents the Laplace force, $F_a = S_d p_d$ represents the acoustic force on the diaphragm generated by the difference in pressure between its front and back, with p_d the pressure difference between the front and back of the diaphragm given by $p_d = V_d(Z_{af} + Z_{ab})$, and $V_d = S_d v_d$ represents the volume velocity emitted by the diaphragm.
After several calculations and approximations [22], the volume velocity emitted by the diaphragm at low frequencies can be expressed as:

$$V_d = u.\frac{Bl.S_d}{(Bl)^2 + R_{ms'}R_e} \cdot \frac{(1/Q_{ts})(j\omega/\omega_s)}{(j\omega/\omega_s)^2 + (1/Q_{ts})(j\omega/\omega_s) + 1}, \tag{1.34}$$

where the fundamental resonant pulsation ω_s of the mass-spring system is given by:

$$\omega_s = 2\pi f_s = \sqrt{\frac{K_{ms}}{M_{ms'}}}, \tag{1.35}$$

and the total quality factor Q_{ts} by:

$$Q_{ts} = \frac{\sqrt{K_{ms}M_{ms'}}}{[(Bl)^2/R_e] + R_{ms'}}. \tag{1.36}$$

Although these are strictly valid only for frequencies that are less than one-half the upper piston frequency limit, they are commonly used to predict the response for the entire piston range.

1.3.5 Small-signal parameters

There are five driver parameters referred to as the small-signal parameters. These are the velocity resonant frequency f_s, the total quality factor Q_{ts}, the electrical quality factor Q_{es}, the mechanical quality factor Q_{ms} and the volume compliance V_{as}. The first two are defined in eqs. (1.35) and (1.36). The other three are defined in this section. These parameters are called small-signal parameters because it is assumed that the driver diaphragm displacement is small enough so that non-linear effects can be neglected.
The total quality factor Q_{ts} can be decomposed into two parts, one that is a function of the electrical losses and the other that is a function of the mechanical losses. The mechanical quality factor Q_{ms} and the electrical quality factor Q_{es} are defined as follows:

$$Q_{ms} = \frac{1}{R_{ms'}}\sqrt{K_{ms}M_{ms'}}, \tag{1.37}$$

and

$$Q_{es} = \frac{R_e}{(Bl)^2}\sqrt{K_{ms}M_{ms'}}. \tag{1.38}$$

The total quality factor is related to the mechanical and the electrical quality factor by:

$$Q_{ts} = \frac{Q_{ms}Q_{es}}{Q_{ms} + Q_{es}}. \tag{1.39}$$

The fifth small-signal parameter is the volume compliance V_{as}. This is the equivalent volume of air which, when compressed by a piston having the same piston area as the driver diaphragm, exhibits the same compliance or stiffness as the driver suspension. The volume compliance is related to K_{ms} by:

$$V_{as} = \rho_0 c_0^2 S_d^2 C_{ms} = \frac{\rho_0 c_0^2 S_d^2}{K_{ms}}. \tag{1.40}$$

1.3.6 High-frequency solution for V_d

The high-frequency modeling of a loudspeaker driver is not as accurate as the low-frequency modeling because the diaphragm can cease to vibrate as a unit above its piston frequency range. When this happens, mechanical standing waves are set up on the diaphragm that cause its velocity distribution to be nonuniform. These effects cannot be modeled with analogous circuits. However, some understanding of the high-frequency behavior can be gained from the analogous circuits.
The high-frequency effects can be approximately accounted for in eq. (1.34) by multiplying by the low-pass transfer function [22]:

$$T_{u1}(j\omega) = \frac{1}{1 + j\omega/\omega_{u1}}, \tag{1.41}$$

where

$$\omega_{u1} = 2\pi f_{u1} = \frac{M_{ms'} R_e}{M_{ms} L_e}. \tag{1.42}$$

where f_{u1} is the frequency which divides the low and high-frequency approximations. Thus, the volume velocity transfer function becomes:

$$V_d = u.\frac{Bl.S_d}{(Bl)^2 + R_{ms'}R_e} \cdot \frac{(1/Q_{ts})(j\omega/\omega_s)}{(j\omega/\omega_s)^2 + (1/Q_{ts})(j\omega/\omega_s) + 1} \cdot \frac{1}{1 + j\omega/\omega_{u1}}. \tag{1.43}$$

The analysis must be considered somewhat qualitative because we have only predicted the ultimate high-frequency asymptote of the Bode plot. The shape of the actual plot between the low-frequency range and the high-frequency range has not been predicted. However, the result predicts that the high-frequency volume velocity is decreased by a pole in the transfer function that is inversely proportional to the voice-coil inductance. If the inductance is increased, this pole frequency decreases.

1.3.7 On-axis pressure

The on-axis pressure radiated by a flat circular piston in an infinite baffle is given by [21, 22]:

$$p(r) = j\omega\rho_0 V_d \frac{e^{-jkr}}{2\pi r}, \tag{1.44}$$

where r is the distance from the piston to the observation point and $k = \omega/c$. For this expression to be valid, the observation point must be in the far field region. This condition requires $r \geq 8a^2/\lambda$, where a is the piston radius and λ the wavelength. At closer distances, Fresnel diffraction effects can cause the pressure to deviate from the value predicted by this equation.
The distance r in the denominator of eq. (1.44) causes the pressure to drop by a factor of 2 (or by $6dB$) each time the distance is doubled. For purposes of defining a transfer function, we will assume $r = 1$ m, even though the distance to the far field may be greater than this at high frequencies. The complex exponential in the equation represents the phase delay caused by the propagation time delay from the piston to the observation point. Because the complex exponential has a magnitude of unity, we omit it in defining the pressure transfer function. Thus we write the normalized on-axis pressure as:

$$p = \frac{\rho_0}{2\pi} j\omega V_d. \tag{1.45}$$

We see from this equation that the on-axis pressure is proportional to $j\omega V_d$. In the frequency domain, a multiplication by the complex frequency $j\omega$ is equivalent to a time derivative in the time domain. Therefore, the on-axis pressure is proportional to the time derivative of the volume velocity, which is proportional to the piston acceleration. We conclude that in the far field we hear the acceleration of the piston. For a constant sound pressure level (SPL) to be radiated, the acceleration must be constant with frequency. Thus, the displacement must be inversely proportional to the frequency squared. This means, for example, that the piston must move 100 times as far to radiate the same sound pressure level at 20 Hz as it does at 200 Hz.

1.3.8 Pressure transfer function

To obtain the low-frequency on-axis pressure transfer function, we substitute the low-frequency transfer function for V_d given by eq. (1.34) into eq. (1.45) to obtain:

$$p = u.\frac{\rho_0}{2\pi} \cdot \frac{Bl.S_d}{R_e M_{ms'}} \cdot \frac{(j\omega/\omega_s)^2}{(j\omega/\omega_s)^2 + (1/Q_{ts})(j\omega/\omega_s) + 1} = u.\frac{\rho_0}{2\pi} \cdot \frac{Bl.S_d}{R_e M_{ms'}} \cdot G(j\omega), \tag{1.46}$$

where $G(j\omega)$ is the second-order high-pass transfer function given by:

$$G(j\omega) = \frac{(j\omega/\omega_s)^2}{(j\omega/\omega_s)^2 + (1/Q_{ts})(j\omega/\omega_s) + 1}. \tag{1.47}$$

At high frequencies, the response can be modeled approximately by multiplying the pressure transfer function by the low-pass function $T_{u1}(j\omega)$ given by eq. (1.41). Thus, the pressure transfer function becomes:

$$p = u.\frac{\rho_0}{2\pi} \cdot \frac{Bl.S_d}{R_e M_{ms'}} \cdot G(j\omega) T_{u1}(j\omega). \tag{1.48}$$

This expression shows that the on-axis pressure is proportional to the product of two transfer functions. $G(j\omega)$ models the low-frequency behavior and $T_{u1}(j\omega)$ models the

high-frequency behavior. The high-frequency modeling is only approximate in the sense that it does not model the effects of mechanical resonances in the diaphragm structure. Despite this limitation, the high-frequency model does provide useful information about the response of the driver. Thus, the loudspeaker is a bandpass filter, limited at low frequencies by the mass-spring mechanical resonance of its moving mass, and limited at high frequencies by the dimensions and mechanical modes of its diaphragm. The frequency zone in between the low and high-frequency limits is called the bandwidth of the loudspeaker.

1.3.9 Acoustic power response

The power output of a driver in an infinite baffle is defined as the acoustic power radiated to the front of the baffle. It is calculated as the power dissipated in the front air load impedance Z_{af} and is given by:

$$P_{ar} = \frac{1}{2} |V_d|^2 \Re\mathrm{e}[Z_{af}(j\omega)] = \frac{1}{2} |V_d|^2 R_{af} = \frac{1}{2} |v_d|^2 R_{ma}. \tag{1.49}$$

First, we calculate the low-frequency power. At low frequencies, eq. (1.34) predicts that $|V_d|^2 \propto \omega^2$ for $\omega < \omega_s$ and $|V_d|^2 \propto 1/\omega^2$ for $\omega > \omega_s$. The low-frequency approximation to $\Re\mathrm{e}[Z_{af}(j\omega)]$ is [22]:

$$\Re\mathrm{e}[Z_{af}(j\omega)] = R_{af} = \frac{\omega^2 \rho_0}{2\pi c_0}. \tag{1.50}$$

It follows that $P_{ar} \propto \omega^4$ for $\omega < \omega_s$ and P_{ar} is constant for $\omega > \omega_s$.
To solve the complete expression for the low-frequency power, we use the low-frequency approximation for $\Re\mathrm{e}[Z_{af}(j\omega)]$ and eq. (1.34) for V_d in the expression for P_{ar}. After some algebraic manipulations, the power can be expressed in terms of the transfer function $G(j\omega)$ defined in eq. (1.47). The result is:

$$P_{ar} = \frac{1}{2} |u|^2 \frac{\rho_0}{2\pi c_0} \cdot \frac{(Bl)^2 S_d^2}{R_e^2 M_{ms'}^2} |G(j\omega)|^2 . \tag{1.51}$$

As the frequency is increased, the voice-coil inductance causes the volume velocity to decrease with increasing frequency. We model the effect of this on the power by multiplying $G(j\omega)$ in this equation by $T_{u1}(j\omega)$ in eq. (1.41) to obtain:

$$P_{ar} = \frac{1}{2} |u|^2 \frac{\rho_0}{2\pi c_0} \cdot \frac{(Bl)^2 S_d^2}{R_e^2 M_{ms'}^2} |G(j\omega) T_{u1}(j\omega)|^2 . \tag{1.52}$$

As frequency is increased, $|G(j\omega)| \to 1$ and $|T_{u1}(j\omega)| \to \omega_{u1}/\omega$. Thus, P_{ar} approaches the value:

$$P_{ar} = \frac{1}{2} |u|^2 \frac{\rho_0}{2\pi c_0} \cdot \frac{(Bl)^2 S_d^2}{R_e^2 M_{ms'}^2} \cdot \frac{\omega_{u1}^2}{\omega^2}. \tag{1.53}$$

This predicts that the high-frequency power is proportional to $1/\omega^2$. However, this is not correct, because we have not accounted for diffraction effects which cause the radiation pattern to narrow at high frequencies. It is shown that the high-frequency power must be proportional to $1/\omega^4$ [22]. It follows that there must be another break frequency in the

Bode plot to account for an additional factor of $1/\omega^2$. We denote this frequency by ω_{u2}. It is given by [22]:

$$\omega_{u2} = 2\pi f_{u2} = \frac{a}{c_0}\sqrt{2}. \tag{1.54}$$

This is the frequency at which the circumference of the diaphragm is equal to $\sqrt{2}\lambda$.
We conclude that there are two break frequencies which model the high-frequency power roll-off. The break at ω_{u1} is caused by the voice-coil inductance. The break at ω_{u2} is caused by diffraction which causes the pressure to be radiated in a beam that becomes narrower as the frequency is increased, thus decreasing the output power. Let us define a second high-frequency transfer function which models the power rolloff above ω_{u2} by:

$$T_{u2}(j\omega) = \frac{1}{1 + j\omega/\omega_{u2}}. \tag{1.55}$$

Thus, the complete power transfer function can be written:

$$P_{ar} = \frac{1}{2}|u|^2 \frac{\rho_0}{2\pi c_0} \cdot \frac{(Bl)^2 S_d^2}{R_e^2 M_{ms'}^2} \left|G(j\omega)T_{u1}(j\omega)T_{u2}(j\omega)\right|^2. \tag{1.56}$$

This expression is only approximate. It does not take into account the effects of mechanical standing waves on the diaphragm which cause the diaphragm velocity distribution to be nonuniform. It assumes that the diaphragm can be modeled as a flat piston, an assumption that fails above the piston range for most drivers. Despite these limitations, the expression provides a basis for calculating the total power output to one side of an idealized driver as a function of frequency.

1.3.10 Reference efficiency

The efficiency η of a driver is defined by:

$$\eta = \frac{P_{ar}}{P_e}, \tag{1.57}$$

where P_{ar} is the acoustic power radiated to the front of the diaphragm and P_e is the electrical input power to the voice-coil. A global power assessment realized on the equations system (1.21) gives the power supplied to the loudspeaker as:

$$\begin{aligned} P_e =< u.i > = < R_e.i^2 > + < R_{ms'}.v_d^2 > \\ + \frac{d}{dt}\left(\frac{1}{2} < L_e.i^2 > + \frac{1}{2} < M_{ms'}.v_d^2 > + \frac{1}{2} < K_{ms}.z_d^2 >\right), \end{aligned} \tag{1.58}$$

where

$$v_d = \frac{dz_d}{dt}. \tag{1.59}$$

In sinusoidal steady state, for which the mean value of a total derivative is equal to zero, the power supplied to the loudspeaker can be written:

$$P_e =< u.i >=< R_e.i^2 > + < R_{ms'}.v_d^2 >= \frac{1}{2}(R_e|i|^2 + R_{ms'}|v_d|^2). \tag{1.60}$$

We substitute the acoustic power given by eq. (1.49) and the electrical power given by eq. (1.60) into eq. (1.57) to obtain:

$$\eta = \frac{R_{ma} \left|v_d\right|^2}{R_e \left|i\right|^2 + R_{ms'} \left|v_d\right|^2}. \tag{1.61}$$

This expression is a function of frequency. If the frequency is chosen to be in the midband region (i.e. $\omega > \omega_0$ and $ka << 1$) where the power radiated is flat, the voice-coil impedance can be approximated by R_e and the acoustic power radiated is given by eq. (1.49) with $|G(j\omega)T_{u1}(j\omega)T_{u2}(j\omega)| = 1$. Furthermore, the efficiency of a loudspeaker is generally very small, most of the time below 5%. This means that most of the power supplied to the loudspeaker is dissipated by Joule effect. This remark leads us to neglect the term linked to the power radiated $R_{ms'} \left|v_d\right|^2$ in the denominator of eq. (1.61) compared to the Joule effect dissipated power term $R_e \left|i\right|^2$. Taking into account all these considerations, a frequency independent ratio is obtained that is defined as the reference efficiency η_0 given by [22]:

$$\eta_0 = \frac{\rho_0}{2\pi c_0} \cdot \frac{(Bl)^2 S_d^2}{R_e M_{ms'}^2} = \frac{4\pi^2}{c^3} \cdot \frac{f_s^3 V_{as}}{Q_{es}}. \tag{1.62}$$

It is important to emphasize on the fact that this reference efficiency, given by eq. (1.62), is only valid in the bandwidth of the loudspeaker and for small amplitude sinusoidal steady state, assuring linear operation of the loudspeaker.

Chapter 2

Evolution of loudspeaker motors

2.1 Magnetic circuit

It is important to be aware that the magnetic field was created in the first loudspeakers by a DC powered coil wound on the stator. Figure 2.1 shows a cross section of an electrodynamic speaker. To make this simpler, the supporting frame or basket which holds everything in correct alignment and the speaker cone center suspension have been left out. In operation, a steady direct current flows through the field coil, magnetizing the field structure as shown. The audio signal is applied to a small coil of wire, called the voice-coil, wrapped on an insulated tube, called the voice-coil former, which is an extension of the speaker cone at the center as shown. The arrangement is such that the voice coil lies in the gap between the north and south magnet poles. When current flows in one direction through the voice coil, it creates a magnetic field that interacts with the field in the gap and makes the cone move slightly to the right or left. When the audio signal current sign changes, it makes the cone move in the other direction. The audio signal is always an alternating current, so as the current fluctuates in response to the power amplifier's output signal, the speaker cone faithfully reproduces the variations of the audio signal as mechanical motion, and the large surface area of the cone effectively generates a sound wave which is a replica of the audio AC signal, as long as we assume a linear behavior. The problem with these speakers using a field coil was that even the slightest amount of $50Hz$ ($60Hz$ in the US) AC power ripple in the DC that is applied to the field coil would react with the voice coil and produce a slight $100Hz$ ($120Hz$) hum in the audio output of the speaker. In order to keep this from happening, there is a small coil of wire right behind the speaker field coil that is in series with the voice coil. If there is any AC "ripple" in the speaker field current , this will, by transformer principle, induce a corresponding ripple current in this "hum-bucking coil". The hum-bucking coil is wired so that its output is applied to the voice coil in opposition to any speaker cone motion that might be induced by AC ripple in the field current. This effectively cancels the action of the slight field current ripple voltage and eliminates the otherwise noticeable resulting AC power line hum from the speaker.

Then, progressively, the DC powered coil wound on the stator got replaced by a permanent magnet. In a magnetic circuit the greatest efficiency BH_{max} is where the external reluctance matches the internal reluctance. Working at some other point requires a larger

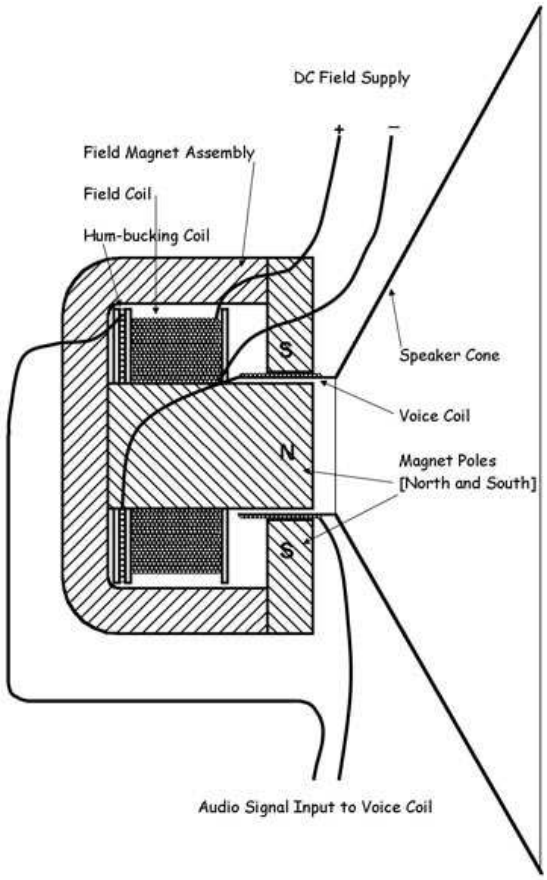

Figure 2.1: Electrodynamic loudspeaker using a DC powered coil, or field coil.

and more expensive magnet. The BH_{max} parameter is used to compare the power of magnetic materials. The units are kiloJoules per cubic meter. At the turn of the twentieth century, the primary permanent magnetic material was glass-hard carbon steel which offered about $1.6kJ/m^3$. In 1920, Honda and Takei discovered cobalt steels [23]. In 1934, Horsburgh and Tetley developed the cobalt-iron-nickel-aluminum system, later further improved with copper. This went by the name of Alnico and offered $12.8kJ/m^3$. In 1938, Oliver and Shedden discovered that cooling the material from above its Curie temperature[1] in a magnetic field dramatically increased the BH product. By 1948, BH products of $60kJ/m^3$ were available at moderate cost and were widely used in loudspeakers under the name of Alcomax. Another material popular in loudspeakers is Ticonal which contains titanium, cobalt, nickel, iron, aluminum and copper.
Around 1930, the telephone industry was looking for non-conductive magnetically soft materials to reduce eddy current losses in transformers. This led to the discovery of the ferrites. The most common of these is barium ferrite which is made by replacing the ferrous ion in ferrous ferrite with a barium ion. The BH product of barium ferrite is rela-

[1]Above a certain temperature, known as the Curie temperature of the material concerned, permanent magnetism is lost

tively poor at only about $30kJ/m^3$, but it is incredibly cheap. Strontium ferrite magnets are also used and permit to obtain BH_{max} around $40kJ/m^3$. In the 1970s, the price of cobalt went up by a factor of twenty because of political problems in Zaire, the principal source. This basically priced magnets using cobalt out of the mass loudspeaker market, forcing commodity speaker manufacturers to adopt ferrite. The hurried conversion to ferrite resulted in some poor magnetic circuit design, a tradition which persists to this day. Ferrite has such a low remanent magnetization that a large area magnet is needed. When a replacement was needed for cobalt-based magnets, most manufacturers chose to retain the same cone and coil dimensions. This meant that the ferrite magnet had to be fitted outside the coil, a suboptimal configuration creating a large leakage area. Consequently, traditional ferrite loudspeakers attract anything ferrous nearby and distort the picture of CRTs. Subsequently, magnet technology continued to improve with the development of samarium cobalt magnets offering up to about $250kJ/m^3$ and then followed in the 1980s by the neodymium iron boron (NdFeB) magnets offering nowadays remarkable $500kJ/m^3$. A magnet of this kind requires 10% of the volume of a ferrite magnet to provide the same field. The rare earth magnets are very powerful but their price has tended to rise exponentially the last few years.
The goal of the magnet and magnetic circuit is to create a radial magnetic field in an annular gap in which the coil moves, called the air gap. The field in the gap has to be paid for. The gap has a finite volume due to its radial spacing and its length along the coil axis. If the gap spacing is increased, the reluctance goes up and the length of the magnet has to be increased to drive the same amount of flux through the gap. If the gap length is increased, the flux density B goes down unless a magnet of larger cross-sectional area is used. Thus, the magnet volume tends to be proportional to the gap volume.

The evolution of loudspeaker motors followed the development of magnet technologies. Therefore, the first evolution occurred when the coil of the motor stator was replaced by an Alnico permanent magnet. Permanent magnet or PM speakers use a permanent magnet and allow us to get rid of the field coil as well as the hum-bucking coil. In the newer PM speakers, there is no ripple in the field of a permanent magnet and thus no need for a hum-bucking coil. Because of the properties of the Alnico, the magnet had to be rather long. Indeed, the demagnetization curve of Alnico magnets requires their load line to have a large slope. Therefore, the magnet was an axially polarized rod located in the center of the device. Consequently, these loudspeakers were still quite long and cumbersome devices. One had to wait for the sixties to see the first decrease in height of the electrodynamic loudspeaker with the use of the hard ferrite magnets. Indeed, the $B(\mu_0 H)$ loop is a straight line in the demagnetization quadrant, with a slope value almost equal to one with the SI units [24]. So, the maximum energy product point, BH_{max}, is on the bisector of the demagnetization quadrant and this line has to be the magnet load line (Fig. 2.3).
Then, the magnet working point is set to the BH_{max} point for characteristic dimensions of the magnet section of the same order as the magnet length. That is the reason for the change in shape of the loudspeaker motors: the long and rather thin cylinder becomes flat and wide. Hard ferrites are the reason why loudspeaker became more accessible. Besides, the magnetic circuit is designed to reach flux density values on the order of $1.5T$ in the

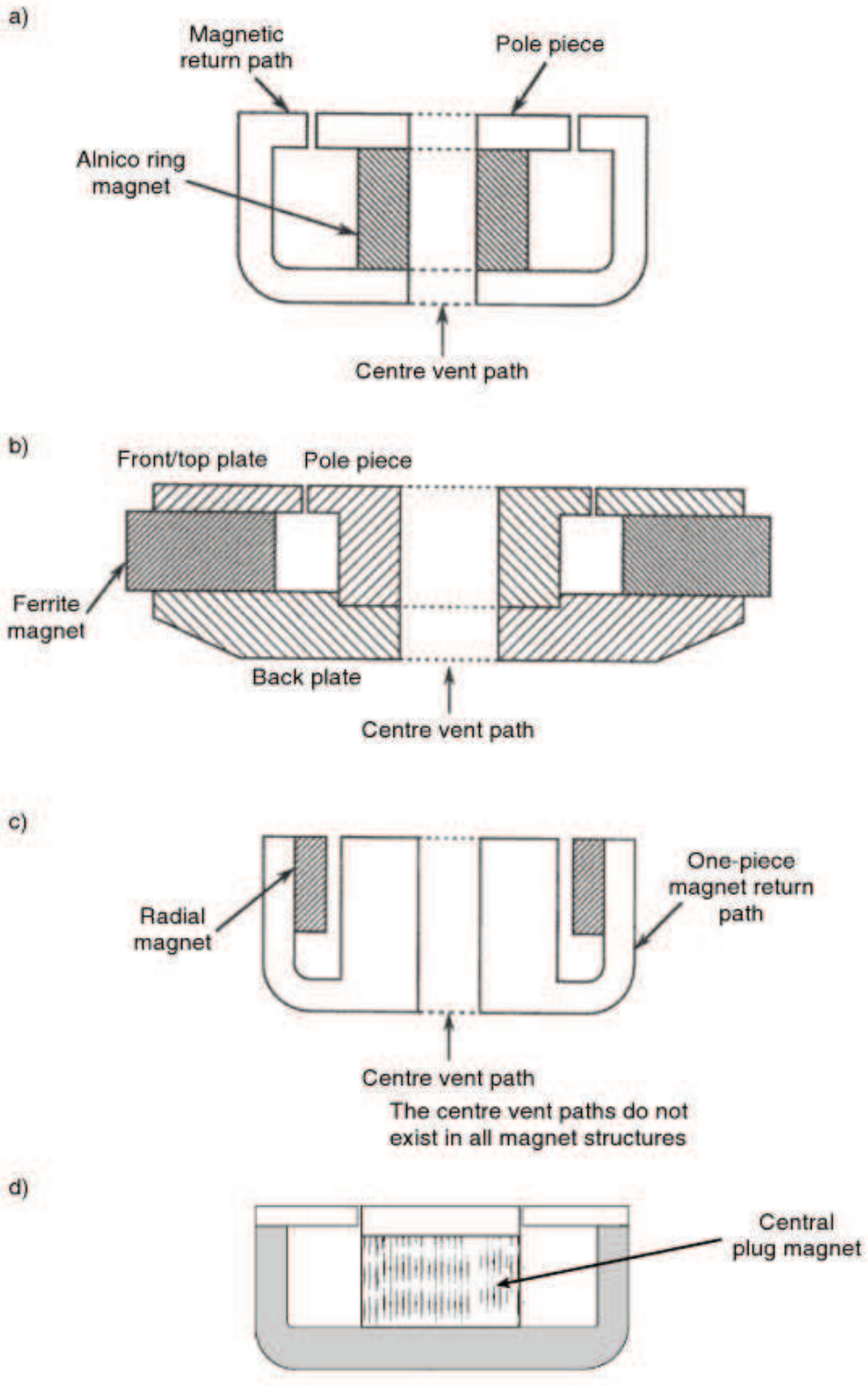

Figure 2.2: Basic magnet structures. a) Alnico ring magnet. b) Ferrite ring magnet. c) Radial, high energy magnet (neodymium). d) Alcomax plug magnet.

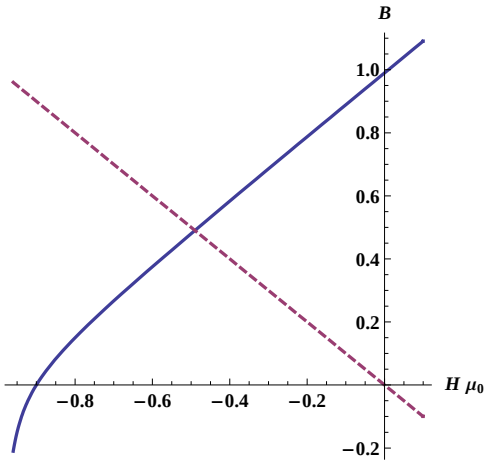

Figure 2.3: Load line (dashed) in the demagnetization quadrant of the B(μ_0 H) loop for a normalized (remanence equal to 1T) rigid permanent magnet.

air gap, corresponding to the magnetic saturation of iron.
The next step forward came in the 1970s with the Samarium-Cobalt permanent magnets. As the maximum energy product point, BH_{max} , is still on the bisector of the $B(\mu_0 H)$ loop in the demagnetization quadrant, the shapes did not really change, the size simply shrank. The appearance in the eighties of neodymium permanent magnets is the last step linked to the progress in permanent magnet materials. With such NdFeB permanent magnets, the size and weight of the devices decreased dramatically: they led the way to miniaturization. The phenomenon is enhanced by the fact that these magnets are so powerful that it is sufficient to have cylindrical flat magnets located in the device center. Several examples of motor topologies are given in Fig. 2.2.
One may emphasize here that the structure of the electrodynamic loudspeaker did not change during the last century except for the replacement of a kind of permanent magnet by a better one. It is also well-known that this structure has drawbacks leading to non-linearities in the behavior and distortion in the sound reproduction.
Indeed, voice-coil motors, such as those used in traditional electrodynamic loudspeakers, present a number of well-known drawbacks [25, 26, 14]. The presence of iron in such motors leads to several kinds of nonlinearities. These include Eddy currents, the magnetic saturation of the iron and the variation of the coil inductance with its position causing a reluctant effect. However, it is desirable for the force applied on the moving part to be an image of the driving current. The driving forces applied on the moving part of the loudspeaker can be written as

$$F_{driv} = F_L + F_r = Bli + \frac{1}{2}\frac{dL_e}{dz}i^2 \tag{2.1}$$

where F_L is the Laplace force, F_r the reluctant force, B the induction seen by the voice-coil, l the length of the coil, i the driving current flowing through the coil, L_e the inductance of the coil and z the displacement of the coil. Thus, (2.1) shows that if the inductance of the coil varies with its position, a reluctant force, proportional to i^2, occurs and interferes with the Laplace force. This reluctant force creates a force distortion resulting directly in

an audible acoustical distortion. It can be compared to the reluctant torque in brushless motors, arising from a reluctant effect, which prevents a smooth rotation of the motor and results in undesirable vibration and noise [27, 28].

Using ironless motors, made totally out of permanent magnets, can help solve most of these defects. Indeed, we know that a magnet, as a hard ferromagnetic material and used in normal conditions, is characterized by a linear relation between the magnetic induction B_a and the magnetic excitation H_a[14]:

$$B_a = J + \mu_0 \mu_a H_a. \tag{2.2}$$

The linearity of the relation implies that the magnetic field created by the voice-coil becomes a linear function of the current flowing through the coil. Furthermore, in comparison with soft ferromagnetic materials generally used in traditional loudspeakers, the magnetic relative permeability of magnets, μ_a, is very low, near 1. This implies that the voice-coil inductance of an ironless motor is weak. Thus, the electrical impedance rise at high frequencies is substantially diminished. The other advantage of the magnets' low permeability is that the geometry of the motor does not affect the magnetic environment seen by the coil during its displacement, leading to a constant inductance, as for an air core inductor.

Concerning the Eddy currents, permanent magnets have an electrical conductivity that is much smaller than the one of the soft ferromagnetic materials, such as iron. For instance, NdFeB magnets offer an electrical resistivity approximately equal to $130.10^{-8}\Omega.m$, compared to the iron resistivity that is about $11.10^{-8}\Omega.m$. Thus, these magnets are really poor electrical conductors, resulting in small losses such as Eddy currents.

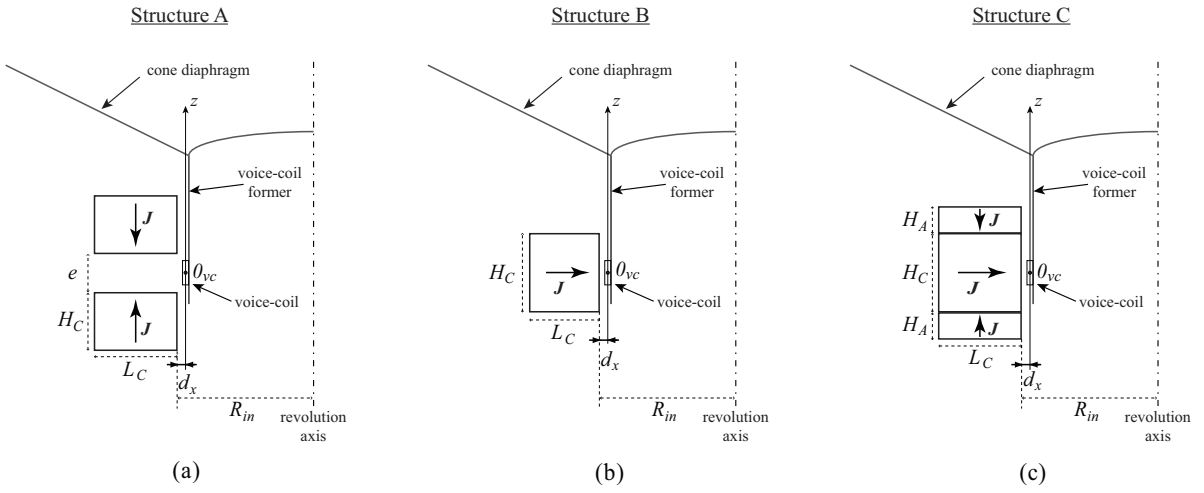

Figure 2.4: Cross sections of the first three ironless structures. (a) Structure A: two axially polarized rings in repulsion [29]. (b) Structure B: one radially polarized ring [30, 31]. (c) Structure C: one radially polarized ring and two axially polarized adjacent rings in repulsion [32].

Despite some advantages from a performance point of view, the use of ironless motors is still really rare in loudspeakers, because of cost and knowledge of the technology. The

knowledge concerns the fabrication and the magnetization of the most powerful magnets, as well as the calculation of the magnetic field created by a multiple magnet assembly. Most of the time, finite element methods are used for these computations, thanks to software such as Flux, Maxwell, OPERA or FEMM. The first ironless loudspeaker motor structure was proposed and patented by House in 1992 [29]. This structure uses two magnet rings axially magnetized in repulsion as shown in Fig. 2.4.a. This structure is adapted to high frequencies because of its intense but rather narrow force factor. Thanks to the advances made in this field of knowledge, radially magnetized rings or ring sections start to appear in the mid-nineties. Then, Geisenberger and Krump [30, 31] present in 1997 a structure composed of a simple magnet ring radially magnetized placed within the voice-coil former (Fig. 2.4.b). This magnet is fixed to the loudspeaker basket using materials that do not conduct either electricity or magnetic flux. Several years later, in 2005, Ohashi [32] uses both previous structures to propose a new structure that is composed of a radially magnetized ring placed between two axially magnetized rings in repulsion as presented in Fig. 2.4.c. With this structure, the linearity range of the magnetic field is enhanced, allowing a increase of the bandwidth toward low frequencies. Following this invention, Lemarquand et al. [33] present in 2006 a wide variety of ironless structures using different magnet ring assemblies in order to create a magnetic induction seen by the voice-coil as intense as possible and to reduce the magnetic field leakage out of the voice-coil path as much as possible; this is the type of structures on which Berkouk had already worked a couple of years earlier [34, 35]. These assemblages sometimes require the use of magnet rings having a triangular section that are difficult and expensive to fabricate, such as the one shown in Fig. 2.5. These leakage free structures will be studied in more details in Chapter 3.

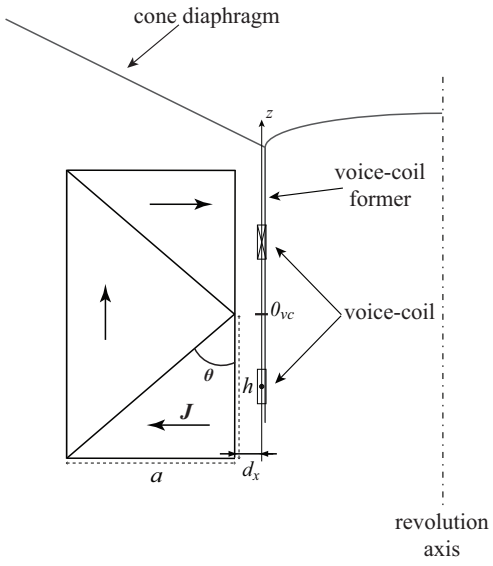

Figure 2.5: Cross section of the three triangular rings structure [33]: two radially polarized rings and one axially polarized ring.

All the structures presented above are able to produce magnetic fields at least as intense

as those created by traditional loudspeaker motors using soft ferromagnetic materials. However, the use of these rather new ironless structures is still almost nonexistent and one had to wait until 2009 when Mowry [36] published his study on an ironless magnetic structure in a very influential specialized journal in the loudspeaker domain. The proposed structure is an improvement of the structure presented by House in 1992, using four axially magnetized magnet rings. In the same manner as House's structure, it is well suited only for high frequency reproduction, but offers a real opportunity to loudspeaker designers. Then, in 2010, Merit patented [37] and presented [14] two new ironless structures. The first one, that he called the *High Induction* (*HI*) structure, was inspired by the one proposed by Ohashi (Fig. 2.4.c), in which the remanent magnetization J_A of the adjacent magnets becomes a variable parameter and is not necessarily the same as the remanent magnetization J of the main magnet (Fig. 2.6). The second one, called *Compact with Constant Induction* (*CCI*) structure, uses as well a pair of magnets adjacent to the main magnet. The difference is that in this case, the polarization of these adjacent magnets is not axial anymore but radial, in the same direction as the main magnet polarization (Fig. 2.7).

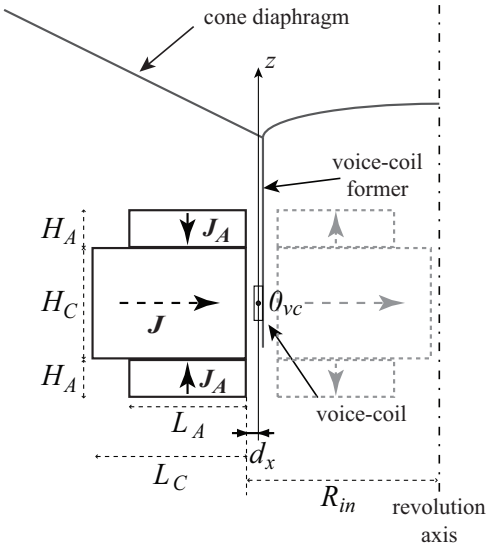

Figure 2.6: Cross section of the *HI* structure [37]: one radially polarized ring and two axially polarized adjacent rings in repulsion. This structure can be outside the voice-coil (solid line), inside the voice-coil (dashed line) or both.

2.2 Theoretical Model

2.2.1 3D Analytical Model

An hexahedral magnet is defined in space by the coordinates of the eight points defining its surfaces. The analytical calculation of the magnetic field created by an hexahedral magnet allows us to generalize the formulation published by Bancel and Lemarquand [38] to any straight magnet having at least two pairs of parallel facets. These four facets are called

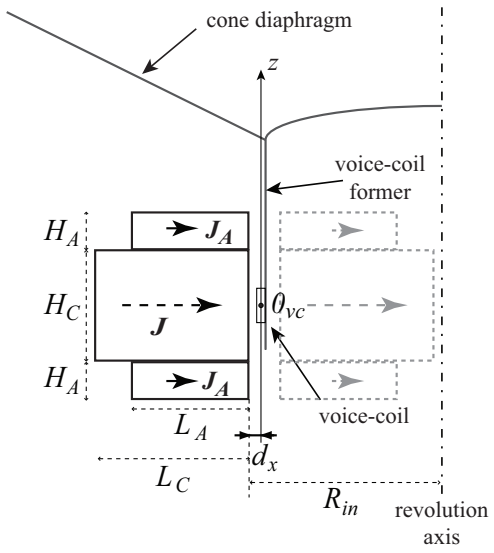

Figure 2.7: Cross section of the *CCI* structure [37]: one central ring and two adjacent rings, all of them being radially polarized in the same direction. This structure can be outside the voice-coil (solid line), inside the voice-coil (dashed line) or both.

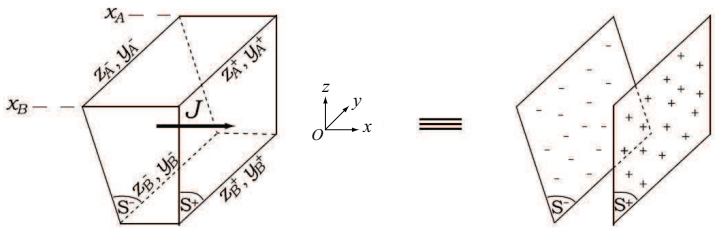

Figure 2.8: Hexahedral magnet.

neutral facets. The two remaining facets are noted S^+ and S^-. The magnet of volume V_m is located in the Cartesian coordinate system $(0, \vec{x}, \vec{y}, \vec{z})$ as represented in Fig. 2.8. This magnet is characterized by its magnetic polarization $\vec{J}$, assumed to be uniform and in the parallel direction of the four neutral facets. The Coulombian approach is used to calculate analytically the magnetic field created by a magnet [39, 40, 41, 42, 43, 38, 44]. In this model, the magnetic field $\vec{B}$ created at any point $M(x, y, z)$ by a magnet of volume V_m closed by a surface S_m is written in the general case as:

$$\vec{B} = -\nabla \left[\frac{1}{4\pi} \iint \frac{\vec{J}.d\vec{S}_m}{\left|\overrightarrow{PM}\right|} + \iiint \frac{div\vec{J}}{\left|\overrightarrow{PM}\right|} dV_m \right], \tag{2.3}$$

where $P(x, y, z)$ is a point belonging to the magnet. For each magnet surface, the surface charge density σ_i^* is defined by:

$$\sigma_i^* = \vec{J}.\vec{n_i}, \tag{2.4}$$

where $\vec{J}$ is the magnetic polarization vector and $\vec{n_i}$ is the outwards surface normal vector. In an hexahedral magnet whose polarization is uniform and parallel to the neutral facets,

the surface charges are only located on the facets S^+ and S^-, whose signs + or − are defined by the scalar product given in eq. (2.4). Then, the volume charge density ρ^* is given by:

$$\rho^* = div\vec{J}. \tag{2.5}$$

If the magnetic polarization is invariant in the magnet, we get:

$$\rho^* = div\vec{J} = 0. \tag{2.6}$$

Using the fact that

$$-\nabla\left(\frac{1}{\left|\overrightarrow{PM}\right|}\right) = \frac{\overrightarrow{PM}}{\left|\overrightarrow{PM}\right|^3} \tag{2.7}$$

permits us to write the magnetic field created by a uniformly magnetized magnet as:

$$\vec{B} = \frac{J}{4\pi}\iint \frac{\overrightarrow{PM}}{\left|\overrightarrow{PM}\right|^3} dS^+ - \frac{J}{4\pi}\iint \frac{\overrightarrow{PM}}{\left|\overrightarrow{PM}\right|^3} dS^-. \tag{2.8}$$

Equation (2.8) shows that the calculation of the magnetic field created by a hexahedral magnet boils down to calculate the magnetic field generated by the two facets secant to the polarization vector $\vec{J}$. The analytical calculation of this magnetic field then gives components B_x, B_y and B_z of the magnetic induction field $\vec{B}$ on the three axis Ox, Oy and Oz.

Thus, writing the three components of the magnetic field created by a plane surface as a function of its coordinates in space permits the calculation of any type of magnet in which the polarization vector $\vec{J}$ is invariant. However, for structures whose the polarization vector is not invariant, these formulas can only be used as an indication. Indeed, when the polarization direction varies in the magnet volume, the volume charges bring a non negligible contribution to the total magnetic field created by the magnet. These charges are not taken into account in the simple approximation of the magnet by its facets. A calculation of the true magnetic field created by a magnet in which the direction of polarization varies, using [40] for instance, is necessary to finalize the design of an ironless magnet structure. Ravaud [45] compared, using a radially polarized magnet ring, the calculation results of the magnetic field created by the ring when the volume charges are taken into account and when they are not. He shows that the smaller the radius of the studied structures is, the bigger is the difference between both calculations. He shows as well that the difference is smaller close to the magnet surface than far from it. However, the difference between these two results impacts mostly the absolute intensity of the magnetic field. The variation of the magnetic field over the observation axis $O_{vc}z$ is comparable.

2.3 Analysis of the existing ironless structures

Then, using the calculation formulas given in [40] or [45], it is possible to calculate the exact magnetic field created by the structures described in [29, 30, 32, 37] that we presented above. In the case of a straight magnet, the component B_x, in the convention shown in

Fig. 2.8 is equivalent to the radial component B_r in the case of a magnet ring. In the following, for simplicity reasons, the notation B_r is used to designate this component orthogonal to the voice-coil displacement, for a straight magnet as well as for a magnet ring.
For the first three structures, A, B and C, the remanent magnetization of the magnets is normalized to $J = 1T$. This only affects the absolute intensity of the magnetic field but not its shape over the observation axis. The point O_{vc} represents the center of the loudspeaker voice-coil at rest position. This voice-coil oscillates around this position in the $O_{vc}z$ direction, parallel to the revolution axis of the loudspeaker, and thus, parallel to the inner surface of the magnet ring. Over the three components of the magnetic field in space, only the component B_r, orthogonal to the voice-coil displacement is studied, since it is the only component creating the Laplace force. This induction field B_r is calculated on the axis $O_{vc}z$ at a distance d_x away from the inner facet of the magnet ring.
Merit [14] defined a parameter called z_{uni}, representing the distance, on the $O_{vc}z$ axis and centered on the point O_{vc}, on which the induction B_r seen by the voice-coil shows a maximum variation of 1%. The aim of this constant induction B_r is to get a force factor Bl that is as constant as possible, the latter being a function of the voice-coil height. This constant force factor allows a good linearity of the loudspeaker motor and thus, an accurate reproduction of the input signal.
The criterion z_{uni} can only be strictly associated to the notion of motor linearity when the voice-coil, over its displacement, stays entirely in the interval defined by z_{uni}. In this case, the distance z_{uni} defines the interval on which the voice-coil displacement can be linear. When this displacement can be large, thanks to a large distance z_{uni}, the associated magnetic structure can be integrated into a loudspeaker designed for a linear reproduction of low frequencies. Conversely, a structure having a small distance z_{uni} is limited to high frequency reproduction, at least as long as the linearity is a major criterion.

2.3.1 Structure A

Structure A (Fig. 2.4.a) is today the easiest to fabricate since it is composed of two axially polarized magnet rings, which are the same as those used in traditional loudspeaker motors. These rings, of height H_C and width L_C, are concentric and separated by an air gap of thickness e. They are set to be in repulsion, which means that the poles of the rings facing each other have the same sign, either both positives or both negatives. The magnetic field lines produced by each magnet of this structure reject each other in the air gap and the magnetic flux flowing through the voice-coil placed in front of this air gap is radial. The magnets dimensions affect only the intensity of the radial magnetic field B_r and, for a given observation distance d_x, the variation of B_r over the observation axis $O_{vc}z$ is mainly affected by the thickness e of the air gap. Figure 2.9 shows the global behavior of this induction B_r depending on the distance e between the magnet rings.

The possible linear displacement of the voice-coil z_uni grows when the interval e increases, to the detriment of B_r intensity. However, this uniformity distance remains really poor, so that it is not possible to make it visible on the curves.

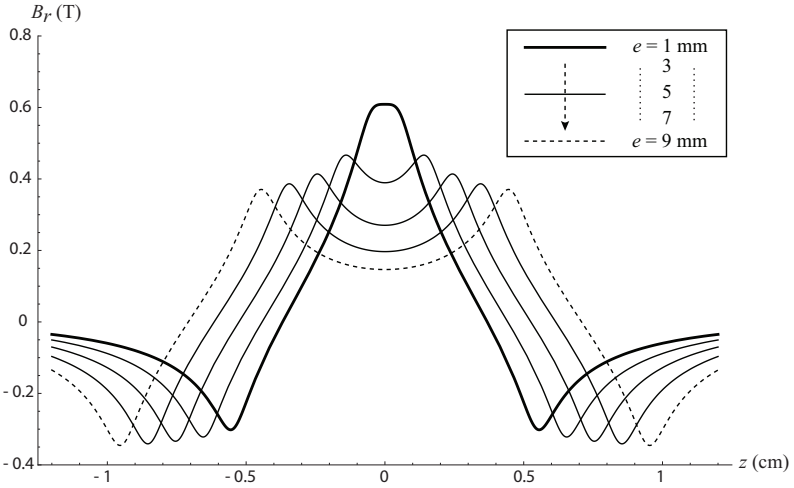

Figure 2.9: Radial component B_r of the magnetic field created by structure A along the observation axis $O_{vc}z$ at a distance $d_x = 0.5mm$, with $J = 1T$, $R_{in} = 20mm$, $H_C = 5mm$, $L_C = 10mm$, and for different air gap thicknesses e between the rings: $1mm$ (bold solid line) then, from top to bottom, $3mm$, $5mm$, $7mm$ and $9mm$ (dashed line).

2.3.2 Structure B

Structure B (Fig. 2.4.b) is composed of only one magnet ring with a rectangular cross section whose polarization is radial. At rest position, the voice-coil is situated halfway up the magnet height H_C. Lemarquand [46] showed in a previous study that a plane-parallel magnet, for a given observation distance, can always generate a uniform magnetic field when its dimensions are chosen correctly. In this case, the distance z_{uni} in which the magnetic field is uniform represents at best 65% of the magnet height H_C. These conclusions are also applicable to a magnet ring with a rectangular cross section, whose inner and outer radii are part of the design constraints. Figure 2.10 shows several calculation results of the magnetic field created by structure B with a constant width L_C and different heights H_C. The dashed line ($H_C = 10mm$ illustrates the ideal case where the magnet dimensions are such that magnetic field created at the observation distance $d_x = 0.5mm$ is the as uniform as possible, with z_{uni} that is almost equal to 60% of the magnet height H_C. For the same observation distance and a equivalent magnet volume as structure A, structure B generates a magnetic field that is less intense but more uniform.

Thanks to its potential to create a uniform magnetic field B_r of a satisfying height, the use of this structure can be considered, from a motor linearity point of view, either for high frequency or low frequency applications. However, it is important to point out that in structure B, the magnet is the only element of the magnetic circuit in the air. Thus, the air, having a low permeability μ_0, is a poor magnetic flux conductor. This means that the induction B_r that flows through the voice-coil is weak and, since the magnetic flux follows the path having the lowest reluctance, the magnetic field turns quickly around the magnet. Notably, the field lines quitting the magnet from its inferior (around $z = -H_C/2$) and superior (around $z = H_C/2$) extremities of the positive pole turns around immediately to close on the respective extremities of the negatively charged pole (Fig. 2.11). Thus, in front of these extremities, the radial component of the magnetic field is highly diminished.

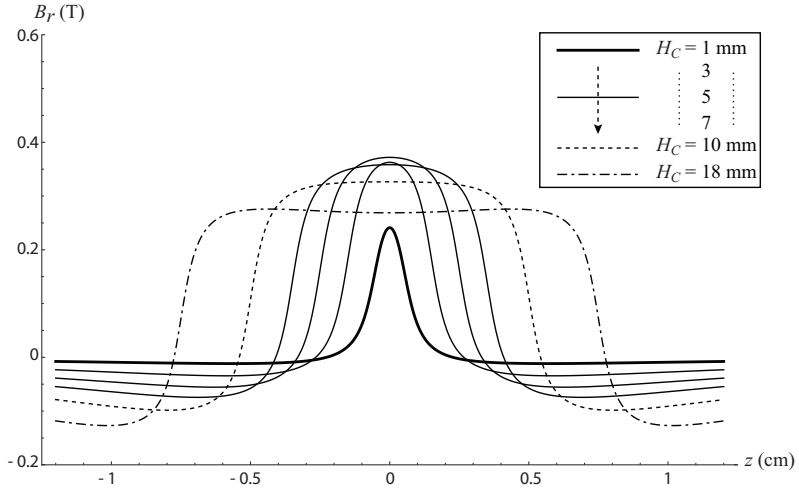

Figure 2.10: Radial component B_r of the magnetic field created by structure B along the observation axis $O_{vc}z$ at a distance $d_x = 0.5mm$, with $J = 1T$, $R_{in} = 20mm$, $L_C = 10mm$, and for different values of H_C: $1mm$ (bold solid line) then, from top to bottom, $3mm$, $5mm$, $7mm$, $10mm$ (dashed line) and $18mm$ (mixed line).

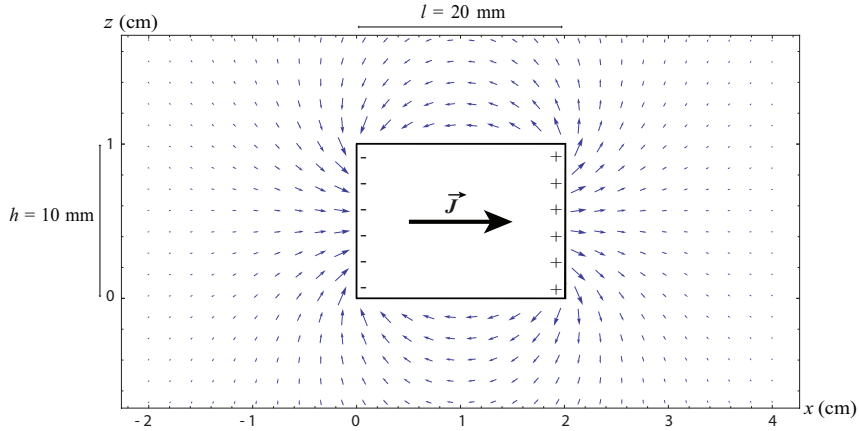

Figure 2.11: Magnetic field lines (vector field) in the plane (x, z) of a magnetic bar of height $h = 10\ mm$, width $l = 20\ mm$, infinitely long along y and uniformly magnetized in the x direction

This effect is called the *edge effect*. For the rectangular cross section magnet, this edge effect is responsible for the fact that distance z_{uni} cannot be greater than 65% of the magnet height H_C.

2.3.3 Structure C

Structure C (Fig. 2.4.c) uses one central radially magnetized annular magnet and two adjacent axially polarized magnet rings. The radial component of the magnetic field created by the adjacent magnets is maximum at the superior and inferior extremities of each magnet (as shown in Fig. 2.9 with structure A). Then, the aim of this structure is to compensate for the edge effect of the central magnet by using the magnetic field created

by the adjacent magnets, as well as to benefit of the magnetic field intensity that can be generated by these magnets in repulsion.
The dimensions of the magnets are chosen in order to have the same volume of magnetic matter as the structures A and B. Therefore, the following dimensions are used: $H_C = 5mm$, $H_A = 2.5mm$, $L_C = 10mm$ and $R_{in} = 20mm$. Figure 2.12 shows the radial component of the magnetic field B_r (bold solid line) created by this structure as well as the contribution of each magnet to this total magnetic field.

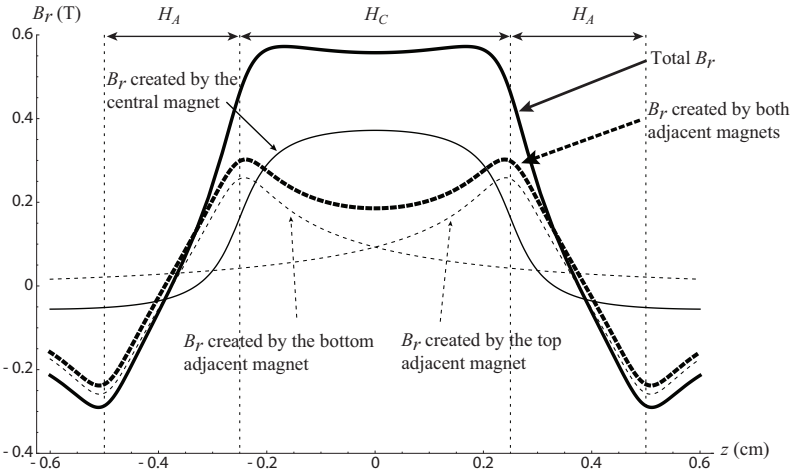

Figure 2.12: Radial component B_r of the magnetic field created by structure C along the observation axis $O_{vc}z$ at a distance $d_x = 0.5mm$ (bold solid line), with $R_{in} = 20mm$. It uses a central magnet with $H_C = 5mm$, $L_C = 10mm$ (thin solid line), and two adjacent magnets with $H_A = 2.5mm$, $L_C = 10mm$ (dashed lines).

2.3.4 Structure *HI*: *High Induction*

After studying these three structures, Merit [14] developed and patented two new structures that have been presented earlier. The first one, called structure *HI* (*High Induction*), is an adaptation of Ohashi's structure ((Fig. 2.4.c)). It is composed of one radially magnetized central magnet ring and two axially magnetized adjacent magnet rings but contrary to structure C where the magnetization J and the width L_C were the same for all magnets, in this case, they can be different for the central magnet and the adjacent magnets. Indeed, Fig. 2.6 shows that the adjacent magnets have a width L_A that is smaller than the width L_C of the central magnet. In the same manner, the magnetization J_A of the adjacent magnets is not the same as the magnetization J of the central magnet. Merit shows that thanks to this optimization, the height z_{uni} of uniformity of B_r along the voice-coil path can be increased by about 170% compared to Ohashi's structure, with a structure that has the same overall dimensions. This allows us to avoid the bumps that are present at the inferior and superior borders of the central magnet and thus, have a much flatter magnetic induction.
When the magnetization J_A and the dimensions of each magnet are optimized in order to favor the magnetic field uniformity rather than its intensity, the height z_{uni} can reach

up to 60% of the total height of structure *HI*. The potential of this structure is then its capacity to generate a uniform and intense field over a satisfying height despite its relative compactedness.
This structure can also be designed for bigger structures that are able to create a constant radial induction over a rather large distance. As given by Merit [14], the biggest size that makes this structure useful is a total height of $24mm$. The radial component of the induction B_r created by this structure is shown in Fig. 2.13.a. The internal diameter is equal to $80mm$ and the other dimensions and the magnetizations have been tuned in order to optimize the compromise between the uniformity distance z_{uni} and the intensity of the field B_r. With a total height of $24mm$, the distance z_{uni} reaches $14mm$ with a magnetic induction of $0.57T$.

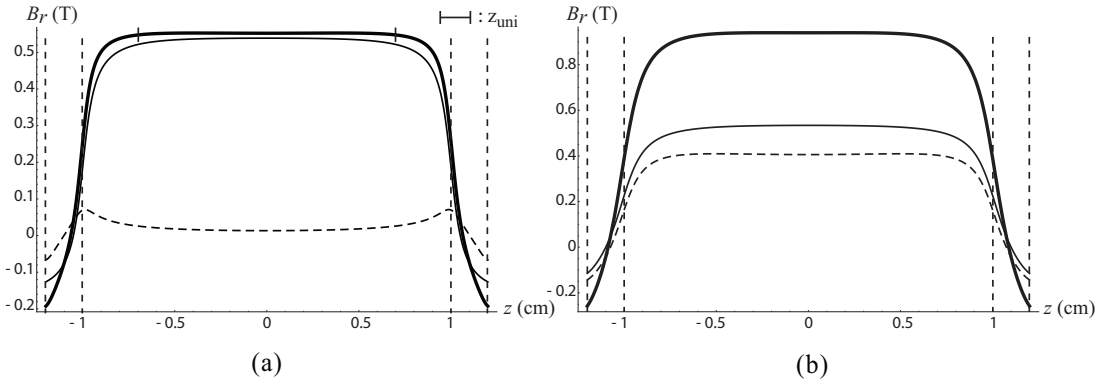

Figure 2.13: (a) Radial component B_r of the magnetic field created by structure *HI* along the observation axis $O_{vc}z$ at a distance $d_x = 0.5mm$ (bold solid line), with $R_{in} = 80mm$. It uses a central magnet with an internal diameter of $80mm$, $L_C = 25mm$ and $J = 1.48T$ (thin solid line), and two adjacent magnets with $H_A = 2mm$, $L_A = 25mm$ and $J_A = 0.8T$ (dashed lines); (b) Radial component B_r of the magnetic field created by structure *HI* along the observation axis $O_{vc}z$ (bold solid line) when the external structure (thin solid line) is coupled to an internal structure (dashed lines)with an external diameter of $78mm$. It uses a central magnet with $H_C = 20mm$, $L_C = 30mm$ and $J = 1.48T$, and two adjacent magnets with $H_A = 2mm$, $L_A = 30mm$ and $J_A = 0.8T$.

Even though the intensity of this field seems to be rather weak compared to the magnetic inductions created by traditional loudspeaker motors, by using the equivalent structure whose external diameter is smaller than the voice-coil diameter (as represented in dashed line in Fig. 2.6), it is possible to almost double the intensity of the magnetic field. It is not quite doubled because the magnetic field created outside the internal structure is slightly lower than the one created inside the external structure, due to the influence of volume charges. Thanks to this double structure, it is possible to obtain really intense magnetic fields over distances much bigger than the ones typically seen in traditional loudspeaker magnetic structures. Nevertheless, structure *HI* cannot create induction fields whose distance z_{uni} is higher than 60%. Therefore, when the height of the central magnet is bigger than $H_C = 20mm$, the adjacent magnets are too outspread to both compensate the border effect and increase the total intensity of the field going through the voice-coil. Thus, beyond this gap H_C between the two adjacent magnets, structure *HI* is not more efficient than the simple magnet ring of structure B. Moreover, it can be useful

or necessary in some cases to have a magnetic structure that is as compact as possible, without deteriorating the distance z_{uni}. The second structure proposed and patented by Merit [37] allows us to fulfil this condition by improving the ratio z_{uni}/H_C.

2.3.5 Structure *CCI*: *Compact with Constant Induction*

This structure also uses magnets that are adjacent to the central magnet. However, the polarization of the adjacent magnets is not axial anymore, as it was the case in structure *HI*, but radial, in the same direction as the central magnet polarization, as shown in Fig. 2.7. By tuning separately the magnetization and the width of the central and the adjacent magnets, it is possible to obtain the same performance as structure B but with a total volume of magnet that is significantly smaller. The structure *CCI* optimized to get the induction B_r presented in Fig. 2.14 has a total magnet volume more than 35% smaller than structure B with $H_C = 10mm$ (dashed line in Fig. 2.10) for the same field intensity and distance z_{uni}. The distance z_{uni} now represents 75% of this optimized structure whose total height is $8mm$. Thus, the main advantage of structure *CCI* is to create fields B_r with a medium intensity but a great uniformity with a reduced total magnet volume. Therefore, when the height limit of structure *HI* is exceeded, structure *CCI* becomes more efficient than the simple structure B.

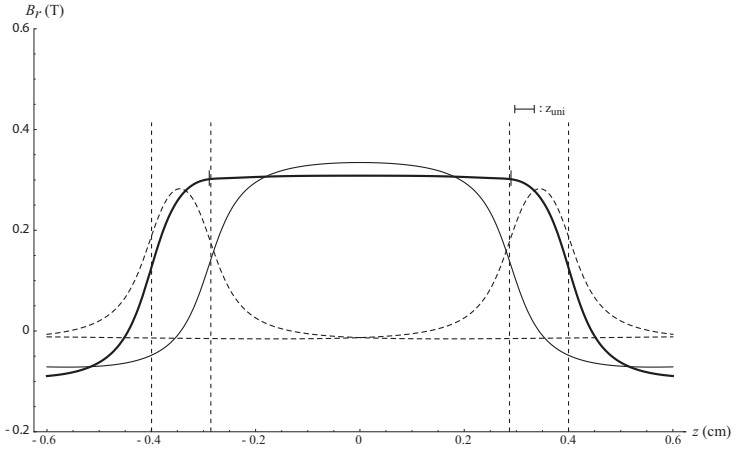

Figure 2.14: Radial component B_r of the magnetic field created by structure *CCI* along the observation axis $O_{vc}z$ at a distance $d_x = 0.5mm$ (bold solid line), with $R_{in} = 20mm$. It uses a central magnet with $H_C = 5.8mm$, $L_C = 7mm$ and $J = 1T$ (thin solid line), and two adjacent magnets with $H_A = 1.1mm$, $L_A = 8.5mm$ and $J_A = 1.09T$ (dashed lines).

2.4 Conclusion

Structures *HI* and *CCI* are thus complementary and seem to be really promising as for the uniformity of the magnetic field B_r they can generate.

However, all the structures presented in this Chapter present a rather high leakage magnetic field. In order to try to optimize the magnetic mass as much as possible, several motor structures have been designed to concentrate all the magnetic field on the voice-coil path. Two of these structures, that we call leakage free structures, are studied in detail in the next Chapter.

Chapter 3

Leakage free structures

3.1 The 2D approximation

If we consider that a magnetic structure with a symmetry of revolution around z axis can be approximated by a magnet that has the same cross section and is infinitely long in the y direction [35, 34], it allows us to describe each surface of the magnet in the plane (x, z) as shown in Fig. 3.1.

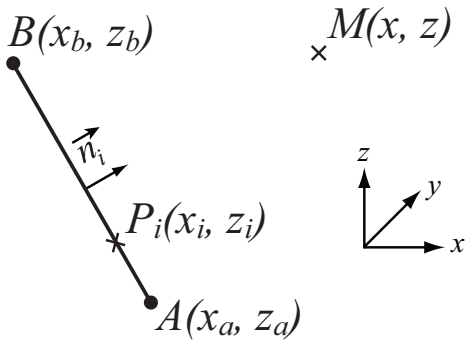

Figure 3.1: Cross section of a plane infinitely long along y defined with its two extremities $A(x_a, z_a)$ and $B(x_b, z_b)$ in the plane (x, z).

Thus, we end up with a 2D Coulombian model and the magnetic field $\vec{B_i}$ created by each magnet surface i at any point $M(x, z)$ is given by:

$$\vec{B_i}(M) = \frac{\sigma_i^*}{4\pi} \int_{y_i=-\infty}^{y_i=+\infty} \int_{z_i} \frac{\overrightarrow{P_iM}}{\left|\overrightarrow{P_iM}\right|^3} dy_i dz_i \tag{3.1}$$

where $P_i(x_i, z_i)$ is a point on the considered surface i. Thus, the magnetic field $\vec{B_i}$ can be expressed as

$$\vec{B_i} = \frac{\sigma_i^*}{4\pi} \int_{z_i} \int_{y_i=-\infty}^{y_i=+\infty} \frac{(x - x_i, y - y_i, z - z_i)}{\left((x - x_i)^2 + (y - y_i)^2 + (z - z_i)^2\right)^{\frac{3}{2}}} dy_i dz_i \tag{3.2}$$

where x_i is expressed as a function of z_i in order to be able to integrate with a surface element $dy_i dz_i$.
We consider a surface of width dy defined with its two extremities $A(x_a, z_a)$ and $B(x_b, z_b)$ in the plane (x, z), as illustrated in Fig. 3.1. The abscissa x_i of a point $P(x_i, z_i)$ belonging to this segment $[AB]$ can be expressed as a function of z_i as follows:

$$x_i = \frac{x_a z_i - x_b z_i + x_b z_a - x_a z_b}{z_a - z_b} \tag{3.3}$$

Each side of a magnet cross section is then defined with its two extremities, $A(x_a, z_a)$ and $B(x_b, z_b)$, in the plane (x, z). The integration lower and upper limits in the y direction are $y_a < 0$ and $y_b > 0$, whose absolute values are considered to be large compared to x and z dimensions of the magnet. Replacing x_i in eq.(3.2) by its value given in eq.(3.3), we obtain the generalized formula:

$$\vec{B_i} = \frac{\sigma_i^*}{4\pi} \int_{z_i=z_a}^{z_i=z_b} \int_{y_i=y_a}^{y_i=y_b} \frac{\left(x - \frac{x_a z_i - x_b z_i + x_b z_a - x_a z_b}{z_a - z_b}, y - y_i, z - z_i\right)}{\left(\left(x - \frac{x_a z_i - x_b z_i + x_b z_a - x_a z_b}{z_a - z_b}\right)^2 + (y - y_i)^2 + (z - z_i)^2\right)^{\frac{3}{2}}} dy_i dz_i \tag{3.4}$$

Using the superposition principle, the total magnetic field created by a magnet is equal to the sum of all the field B_i created by each surface i and is written:

$$\vec{B} = \sum_i \vec{B_i} \tag{3.5}$$

B_x and B_z components of the magnetic field are then respectively defined by:

$$\sum_i B_{ix} = \sum_i \frac{\sigma_i^*}{4\pi} \int_{z_i=z_a}^{z_i=z_b} \int_{y_i=y_a}^{y_i=y_b} \frac{x - \frac{x_a z_i - x_b z_i + x_b z_a - x_a z_b}{z_a - z_b}}{\left(\left(x - \frac{x_a z_i - x_b z_i + x_b z_a - x_a z_b}{z_a - z_b}\right)^2 + (y - y_i)^2 + (z - z_i)^2\right)^{\frac{3}{2}}} dy_i dz_i, \tag{3.6}$$

and

$$\sum_i B_{iz} = \sum_i \frac{\sigma_i^*}{4\pi} \int_{z_i=z_a}^{z_i=z_b} \int_{y_i=y_a}^{y_i=y_b} \frac{z - z_i}{\left((x - x_i)^2 + (y - y_i)^2 + (z - z_i)^2\right)^{\frac{3}{2}}} dy_i dz_i. \tag{3.7}$$

3.1.1 Simple Example

We consider a magnetic bar of height h along z and width l along x, infinitely long along y and uniformly magnetized in the x direction, as shown in Fig. 3.2.

In this case, $\vec{J}$ is oriented along x. Thus, $\sigma_2^* = \vec{J}.\vec{n_2} = \sigma_4^* = \vec{J}.\vec{n_4} = 0$. In the same manner, $\sigma_1^* = \vec{J}.\vec{n_1} = -J$ and $\sigma_3^* = \vec{J}.\vec{n_3} = J$. The magnetic fields created by each surfaces 1 and 3 are then defined as:

$$\vec{B_1} = \frac{-J}{4\pi} \int_{z_1=0}^{z_1=h} \int_{y_1=y_a}^{y_1=y_b} \frac{(x, y - y_1, z - z_1)}{\left(x^2 + (y - y_1)^2 + (z - z_1)^2\right)^{\frac{3}{2}}} dy_1 dz_1 \tag{3.8}$$

$$\vec{B_3} = \frac{J}{4\pi} \int_{z_3=0}^{z_3=h} \int_{y_3=y_a}^{y_3=y_b} \frac{(x - l, y - y_3, z - z_3)}{\left((x - l)^2 + (y - y_3)^2 + (z - z_3)^2\right)^{\frac{3}{2}}} dy_3 dz_3 \tag{3.9}$$

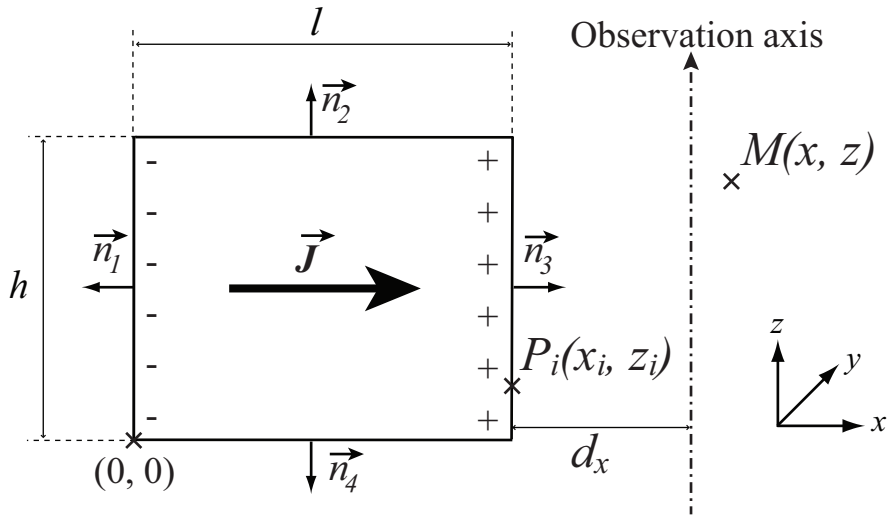

Figure 3.2: Cross section of a magnetic bar, infinitely long along y and uniformly magnetized along x.

Thus, the total magnetic field created by the magnet is given by $\vec{B} = \vec{B_1} + \vec{B_3}$. It is then possible to calculate the integrals and express the x and z components B_x and B_z of the magnetic field $\vec{B}$ as:

$$
\begin{aligned}
B_x \;=\; & \frac{J}{4\pi}\Bigg(- \mathrm{ArcTan}\left[\frac{(y-y_a)(h-z)}{(l-x)\sqrt{(l-x)^2+(y-y_a)^2+(h-z)^2}}\right] \\
& + \mathrm{ArcTan}\left[\frac{(y-y_b)(h-z)}{(l-x)\sqrt{(l-x)^2+(y-y_b)^2+(h-z)^2}}\right] \\
& + \mathrm{ArcTan}\left[\frac{(y-y_a)(-h+z)}{x\sqrt{x^2+(y-y_a)^2+(h-z)^2}}\right] \\
& - \mathrm{ArcTan}\left[\frac{(y-y_b)(-h+z)}{x\sqrt{x^2+(y-y_b)^2+(h-z)^2}}\right] \\
& - \mathrm{ArcTan}\left[\frac{(y-y_a)z}{(l-x)\sqrt{(l-x)^2+(y-y_a)^2+z^2}}\right] \\
& - \mathrm{ArcTan}\left[\frac{(y-y_a)z}{x\sqrt{x^2+(y-y_a)^2+z^2}}\right] \\
& + \mathrm{ArcTan}\left[\frac{(y-y_b)z}{(l-x)\sqrt{(l-x)^2+(y-y_b)^2+z^2}}\right] \\
& + \mathrm{ArcTan}\left[\frac{(y-y_b)z}{x\sqrt{x^2+(y-y_b)^2+z^2}}\right]\Bigg)
\end{aligned}
\tag{3.10}
$$

$$
\begin{aligned}
B_z &= \frac{J}{4\pi}\Bigg(\mathrm{Log}\left[y-y_a+\sqrt{(l-x)^2+(y-y_a)^2+(h-z)^2}\right] \\
&- \mathrm{Log}\left[y-y_a+\sqrt{x^2+(y-y_a)^2+(h-z)^2}\right] \\
&- \mathrm{Log}\left[y-y_b+\sqrt{(l-x)^2+(y-y_b)^2+(h-z)^2}\right] \\
&+ \mathrm{Log}\left[y-y_b+\sqrt{x^2+(y-y_b)^2+(h-z)^2}\right] \\
&- \mathrm{Log}\left[y-y_a+\sqrt{(l-x)^2+(y-y_a)^2+z^2}\right] \\
&+ \mathrm{Log}\left[y-y_a+\sqrt{x^2+(y-y_a)^2+z^2}\right] \\
&+ \mathrm{Log}\left[y-y_b+\sqrt{(l-x)^2+(y-y_b)^2+z^2}\right] \\
&- \mathrm{Log}\left[y-y_b+\sqrt{x^2+(y-y_b)^2+z^2}\right]\Bigg)
\end{aligned}
\tag{3.11}
$$

Using these expressions (3.11) and (3.12), it is possible to draw the vector field in the plane (x, z) around the magnet, as shown in Fig. 2.11.

If we consider that a magnet ring can be approximated by an infinitely long magnet having the same cross section, then the x component of the magnetic field B_x is equivalent to the radial component B_r which would be expressed for a magnet ring in a cylindrical coordinate system.

3.2 Leakage free structures

A significant part of the magnetic field created by most loudspeaker motors does not contribute towards making the membrane move. In addition to a simple loss of magnetic field, this leakage flux can be attracted by any ferromagnetic object placed nearby, leading to a decrease of the device efficiency. Furthermore, this leakage magnetic field can prevent some devices placed nearby from working properly. Therefore, an intended specification of the motor is to have a minimized magnetic field leakage.

An example of ironless and leakage free motor structure made totally of sintered permanent magnets is shown in Fig. 3.3. It is composed of three prismatic magnet rings arranged in such a way that the magnetization is always parallel to the outer edge. Thus, the whole magnetic field created by the motor is focused on the voice-coil path. However, one problem with the structures made of sintered magnets is that it can be difficult to assemble. The structure shown in Fig. 3.3 requires the fabrication of three magnet rings, two of them being radially magnetized which is not easy to achieve.
By using bonded magnets, this problem can be solved and furthermore, better cross section shapes and optimized magnetization of the structure can be realized. The whole structure is directly injected in a mold and no assembly is needed. One possible leakage free structure made of bonded magnets is presented in Fig. 3.4. The structure that we propose has an ellipsoidal cross section. The magnetization is realized when the material is still viscous so that the magnetic particles follow the magnetic field lines created by the

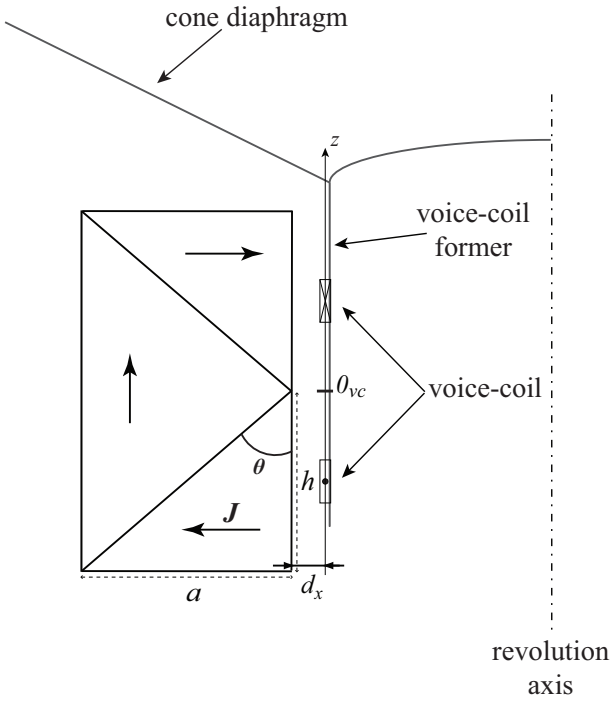

Figure 3.3: Cross section of the three sintered magnets structure (rectangular motor).

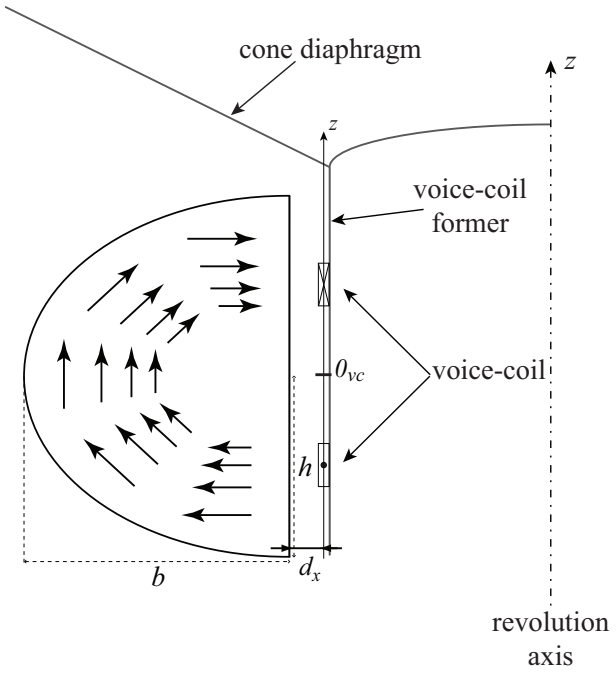

Figure 3.4: Cross section of the bonded magnet structure (ellipsoidal motor).

magnetizer. Once again, the magnetization of the structure is done so that it is always tangent to the outer edge except on the side facing the voice-coil, where it is perpendic-

ular to the edge. The magnetic field created by the motor is then concentrated on the voice-coil path in order to increase the efficiency of the loudspeaker, which is proportional to the square of the force factor Bl.

Another advantage of these structures is that a double coil winding can be used to improve the efficiency. Furthermore, the magnetic field created by these structures presents a high gradient around the semi-height of their inner face. This high magnetic field gradient permits the use of ferrofluid seals to guide the moving part [47]. Ferrofluid seals have also a role of thermal bridge, allowing the heat created by the voice-coil to flow through and be dissipated in the motor. However, in the second case (Fig. 3.4), since the motor is made of bonded magnet (plastic), the thermal dissipation in this latter case is quite poor.

3.2.1 Sintered Magnet Structure

We first start the study of these leakage free structures by the one that has been patented by Lemarquand and al. [33] and that is presented in Fig. 3.3.
This motor structure is composed of three independent magnets. Overall, the magnetic field created by the six surfaces, two for each magnet, has to be calculated independently then summed to obtain the total magnetic field created by the motor structure.
It can be noted that for this structure, if θ equals 45° (i.e. $a = h$), only the two surfaces facing the voice-coil have to be taken into account in the calculation. This is due to the fact that the remaining surface charge density is equal to zero on the two other magnet interfaces.
As we can see in Fig. 3.5, most of the magnetic field created by the motor is concentrated in front of this latter (x positive) and turns around the point $(0, 0)$.

3.2.1.1 Effect of the structure height

Figure 3.6 shows in which manner the modification of the structure height acts on the magnetic field radial component B_r created by the three sintered magnets structure along the observation axis $O_{vc}z$, corresponding to the voice-coil path. In each case, the width a is equal to the semi-height h.

As we can see, not only does the rise of structure height increase the height z_{uni} of uniformity of B_r along the voice-coil path, it does as well increase the absolute maximum value of the radial magnetic induction seen by the voice-coil. For instance, for $h = 1cm$, $z_{uni} = 0.33cm$ and $B_{r_{max}} = 0.459T$, whereas for $h = 2.5cm$, $z_{uni} = 1.1cm$ and $B_{r_{max}} = 0.484T$. We notice as well that the ratio between z_{uni} and h increases when z increases. Indeed, in the first case presented above, $z_{uni}/h = 33\%$ whereas it reaches 44% in the second case. If we take $h = 20cm$ for instance (which is not represented here), the ratio z_{uni}/h goes up to 82%. However, such a big structure, reaching a total height of $40cm$, could not be used in a loudspeaker, but maybe in another linear magnetic actuator.

3.2.1.2 Effect of the structure width

We now take a look at the effect of the ratio between the height and the width of the structure. In order to do that, we set the semi-height h to $1cm$. Then, we make the width

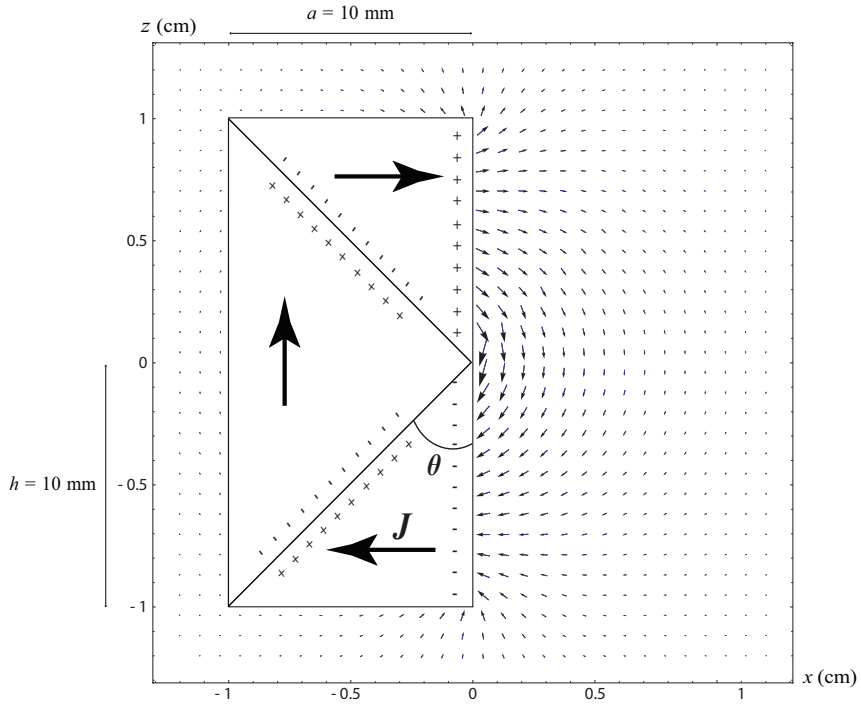

Figure 3.5: Magnetic field lines (vector field) in the plane (x, z) of the leakage free structure of height $2h = 20\ mm$, width $a = 10\ mm$ and infinitely long along y.

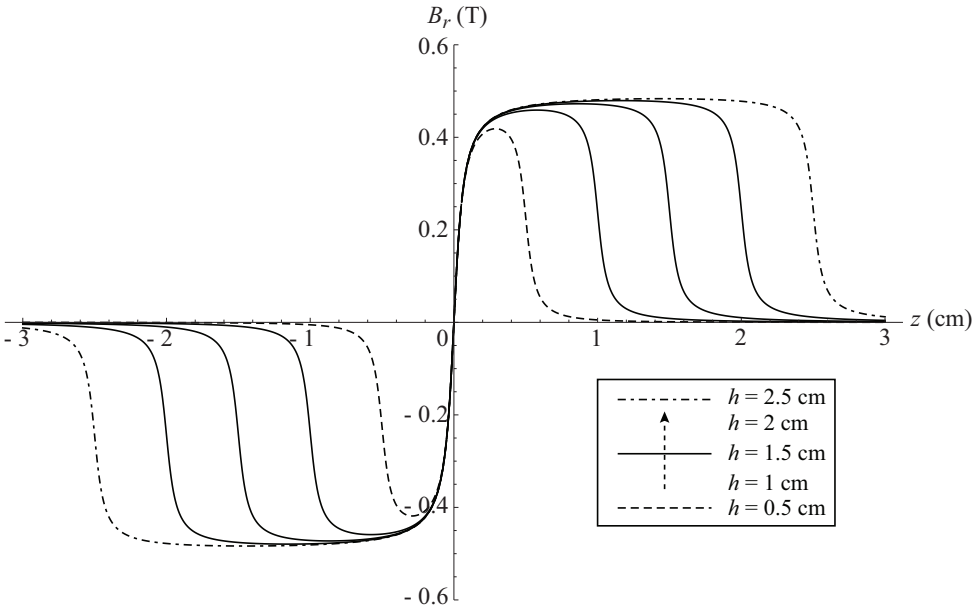

Figure 3.6: Radial component B_r of the magnetic field created by the three sintered magnets structure along the observation axis $O_{vc}z$ at a distance $d_x = 0.5mm$, with $J = 1T$, $a = h$, and for different semi-heights h: $0.5cm$ (dashed line) then, from left to right in the top-right quadrant, $1cm$, $1.5cm$, $2cm$ and $2.5cm$ (mixed line).

a vary from 0 to $4h$, which represents, in our example, 0 to $4cm$.
Figure 3.7 shows the variation of the maximum value of the magnetic field radial component $B_{r_{max}}$ with the variation of the ratio a/h.

We notice that, at the distance where we are looking, $B_{r_{max}}$ reaches a maximum when

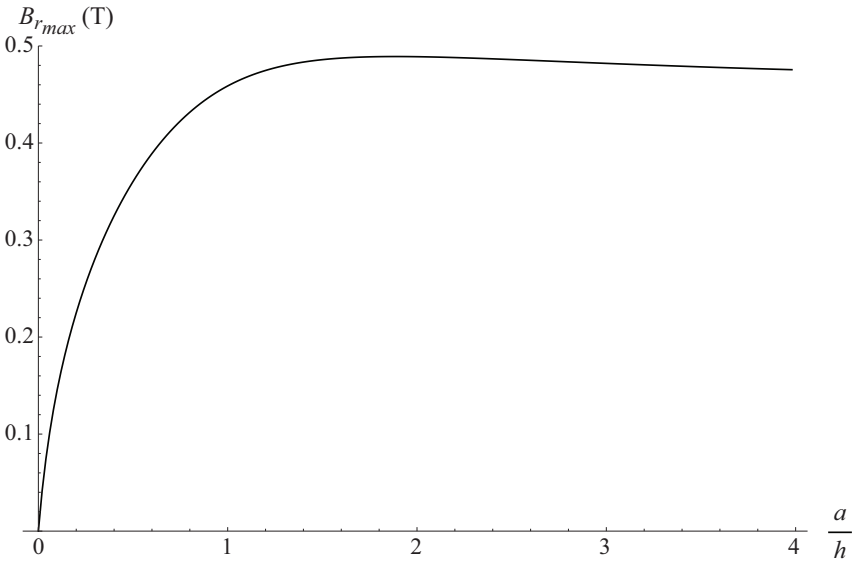

Figure 3.7: Evolution of the radial component maximum value $B_{r_{max}}$ of the magnetic field created by the three sintered magnets structure along the observation axis $O_{vc}z$ at a distance $d_x = 0.5mm$, with $J = 1T$, $h = 1cm$, and the width a varying from 0 to $4cm$.

the ratio a/h is around 2. More precisely, the maximum value of $B_{r_{max}}$ is $0.489T$ when $a/h = 1.89$. Above this ratio, the maximum magnetic induction seen by the voice-coil on its path goes down whereas the magnet volume increases.

Figure 3.8 shows the radial component B_r of the magnetic field created by the three sintered magnets structure along the observation axis $O_{vc}z$ between $z = 0$ and $z = h$ for different ratios a/h. These curves confirm the trend that we observed in Fig. 3.7, which is that we obtain the maximum magnetic induction for a width a two times bigger than the semi-height h. In other words, when the width is equal to the total height of the motor structure. If we now take a look at the evolution of the uniformity distance z_{uni} as a function of the width to height ratio, we see that it is fairly constant. Indeed, the values of $B_{r_{max}}$ and z_{uni} in each case are the following:

- For $a = h$: $B_{r_{max}} = 0.459T$ and $z_{uni} = 3.3mm$,
- For $a = 2h$: $B_{r_{max}} = 0.489T$ and $z_{uni} = 3.2mm$,
- For $a = 3h$: $B_{r_{max}} = 0.482T$ and $z_{uni} = 3.2mm$,
- For $a = 4h$: $B_{r_{max}} = 0.475T$ and $z_{uni} = 3.3mm$.

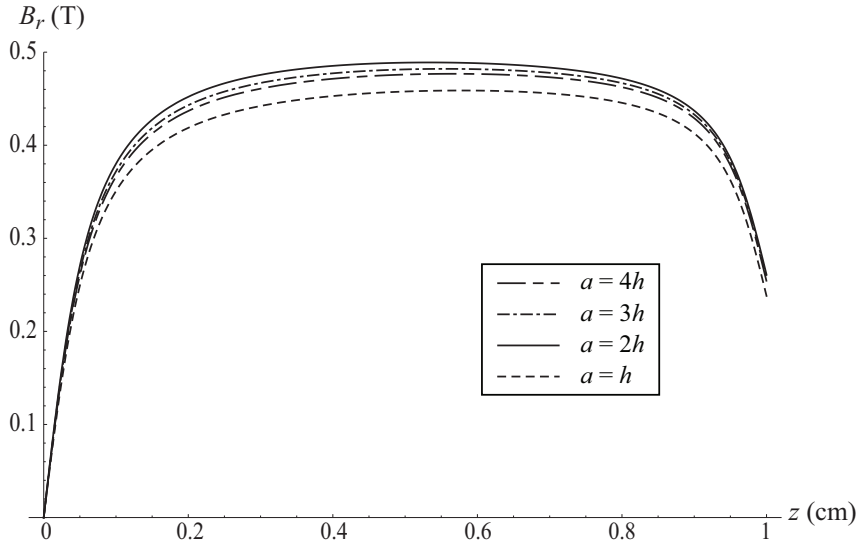

Figure 3.8: Radial component B_r of the magnetic field created by the three sintered magnets structure along the observation axis $O_{vc}z$ at a distance $d_x = 0.5mm$, with $J = 1T$, $h = 1cm$, and for different width a: $1cm$ (dashed line), $2cm$ (solid line), $3cm$ and $4cm$ (mixed lines).

In each case, the uniformity distance z_{uni} represents about one third of the height of the structure, regardless of the ratio between a and h. This ratio between z_{uni} and h only depends on the absolute height of the structure.

All these calculations show that the ratio between a and h does not affect much the uniformity of the magnetic field seen by the voice-coil but acts on the intensity of this latter. Thus, looking at $B_{r_{max}}$, the best ratio seems to be $a = 1.89h$. Furthermore, by increasing the absolute height of the structure, keeping the same ratio a/h, we can augment the ratio z_{uni}/h above 80%.
However, one disadvantage of this structure made of three sintered magnet rings having a triangular cross section is that it can be quite difficult to fabricate. By using bonded magnets, we can think of a leakage free structure that has the same advantages as this one, and even try to optimise it a little bit more, but that is much easier to realise. The cross section of this structure, that we call the ellipsoidal motor, is presented in Fig. 3.4.

3.2.2 Bonded Magnet Structure

The ellipsoidal motor (Fig. 3.4) is discretized in order to enable analytical calculations of the magnetic field to be performed. An example of this discretization, using seven magnets of equal angular section, is shown in Fig. 3.9. All the surfaces between each section are defined in the (x, z) plane.

The same method that we used to calculate the magnetic field created by the three magnets structure is used to calculate this ellipsoidal motor structure. The detailed expressions of each surface coordinate and surface charge density are given in Appendix A. Overall, the magnetic field created by the fourteen surfaces, two for each magnet, has to be calculated

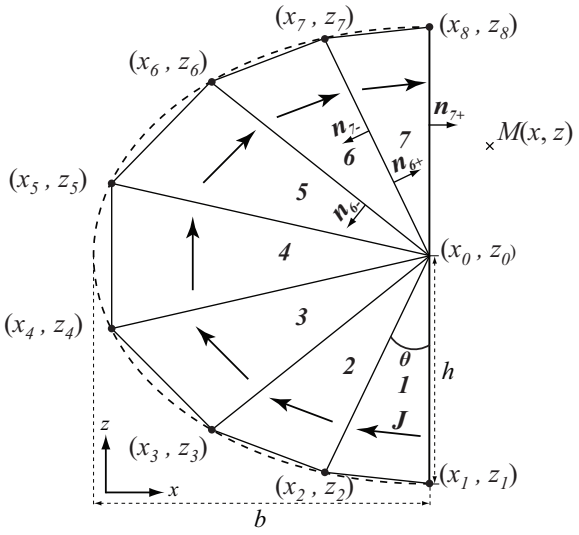

Figure 3.9: Cross section of the discretized bonded magnet structure used for analytical calculations.

independently then summed to obtain the total magnetic field created by the ellipsoidal structure.

3.2.2.1 Discretization of the structure

In order to decide the number of sections that we should use to discretize the semi-ellipsoid, allowing us to get an accurate result but keeping a computation time as small as possible, we calculate two different cases with five different discretizations. In the first case, the width b is equal to the semi-height h, and in the second case, $b = 2h$. Both calculations are run using 3, 5, 7, 9 or 11 sections to discretize the bonded magnet structure. The results of these two calculations are presented in Fig. 3.10 and 3.11.

In the first case, where $b = h$, the difference on the magnetic field induction maximum value $B_{r_{max}}$ between 3 and 11 sections reaches 12.5%, 3.9% between 5 and 11, 1.5% between 7 and 11, and only 0.5% between 9 and 11 sections. In the second case, where $b = 2h$, these differences respectively fall down to 5.7%, 1.4%, 0.5% and 0.1%.
One important point is the fact that no matter how many sections are used to discretize the bonded magnet motor structure, the distance z_{uni} is not affected. If we now look at the distance where B_r is included between 90% and 100% of $B_{r_{max}}$, it is once again not affected by the number of sections that are used to discretize the structure and is equal to $7.2mm$ in this case, which represents 72% of the structure height.
One big difference between the different discretizations is the computation time. Indeed, it is for instance ten times longer to calculate the same example with 11 sections than with 3 sections. All these results are summarized in Table 3.1.
Therefore, it seems that the number of sections only changes the maximum value of the magnetic field radial component and the computation time. We choose to realize all the following calculations with 7 sections to discretize the structure because it appears to be a good compromise between results accuracy and computation time. The difference

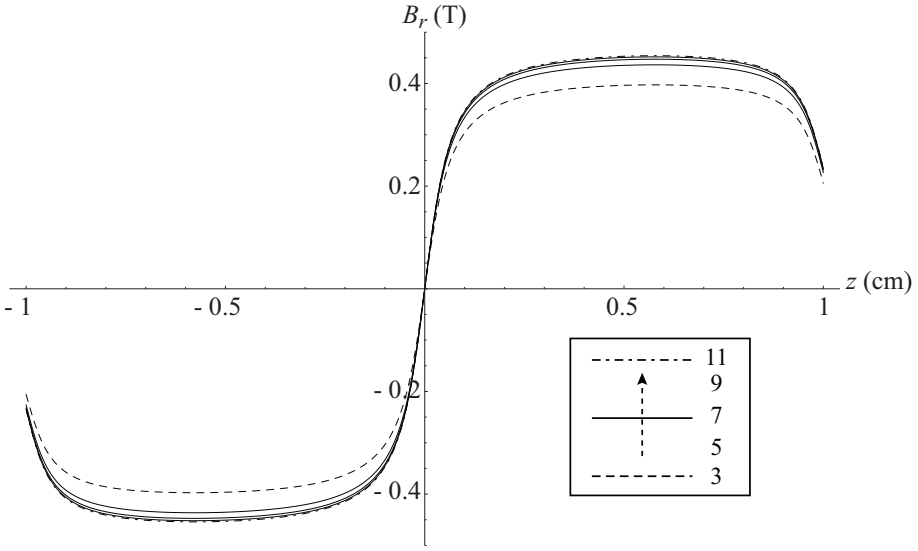

Figure 3.10: Radial component B_r of the magnetic field created by the ellipsoidal bonded magnet structure along the observation axis $O_{vc}z$ at a distance $d_x = 0.5mm$, with $J = 1T$, $h = 1cm$, $b = h = 1cm$ and for several number of discretization sections: 3 (dashed line), 5, 7, 9 (solid lines), and 11 (mixed line).

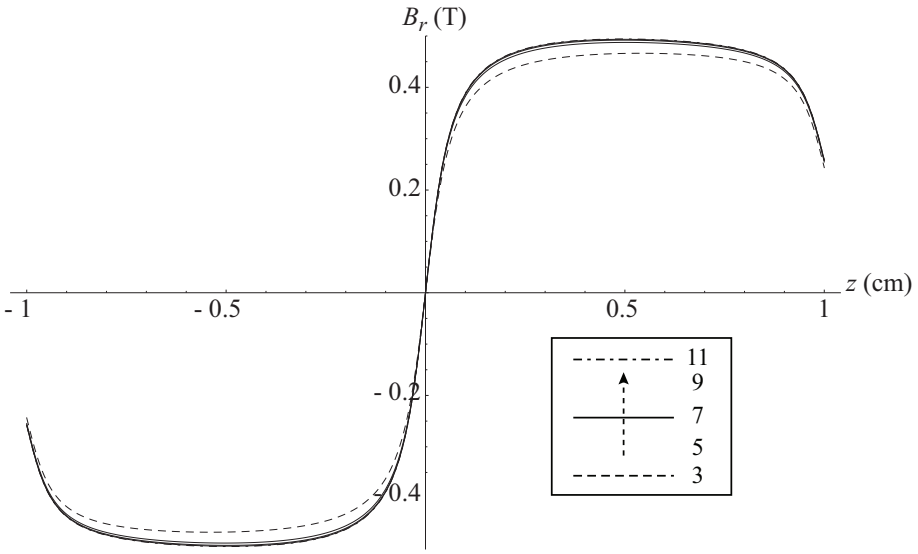

Figure 3.11: Radial component B_r of the magnetic field created by the ellipsoidal bonded magnet structure along the observation axis $O_{vc}z$ at a distance $d_x = 0.5mm$, with $J = 1T$, $h = 1cm$, $b = 2h = 2cm$ and for several number of discretization sections: 3 (dashed line), 5, 7, 9 (solid lines), and 11 (mixed line).

between 7 and 11 sections is only around 1% and it is twice as fast to compute. This difference can be appreciable when doing optimization loops.

3.2.2.2 Effect of the structure height

Figure 3.12 shows in which manner the modification of the structure height acts on the magnetic field radial component B_r created by the ellipsoidal bonded magnet structure

	Number of sections	$B_{r_{max}}$ (T)	$B_{r_{max}}$ difference with 11 sections (%)	z_{uni} (mm)	Computation time (%)
$b = h$	3	0.397	12.5	3.3	10
	5	0.436	3.9	3.3	30
	7	0.447	1.5	3.3	55
	9	0.452	0.5	3.3	65
	11	0.454	0	3.3	100
$b = 2h$	3	0.466	5.6	3.2	10
	5	0.488	1.2	3	30
	7	0.492	0.5	3	55
	9	0.493	0.1	3	65
	11	0.494	0	3	100

Table 3.1: Computation differences

along the observation axis $O_{vc}z$. In each case, the width a is equal to the semi-height h.
As we can see, the trend is really similar to what we already noticed on the three sintered

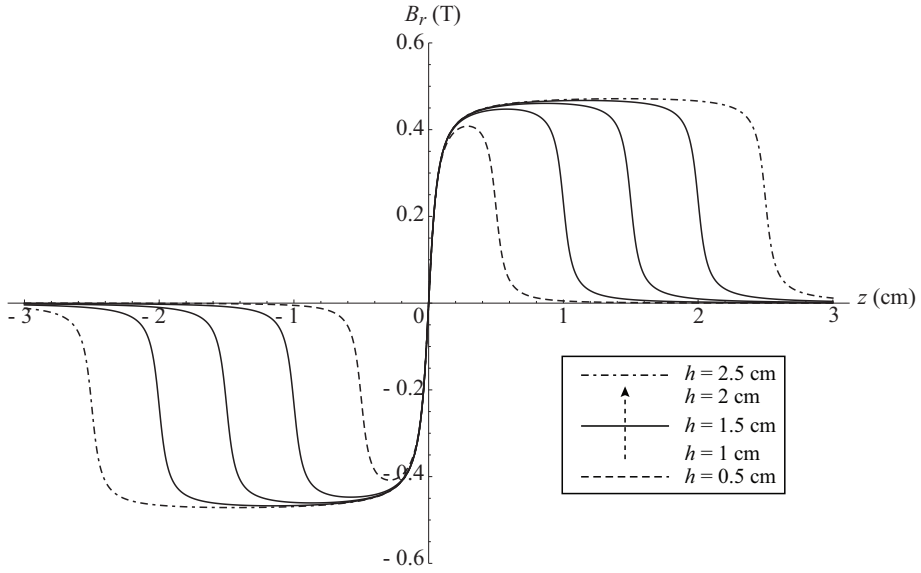

Figure 3.12: Radial component B_r of the magnetic field created by the ellipsoidal bonded magnet structure along the observation axis $O_{vc}z$ at a distance $d_x = 0.5mm$, with $J = 1T$, $b = h$, and for different semi-heights h: $0.5cm$ (dashed line) then, from left to right in the top-right quadrant, $1cm$, $1.5cm$, $2cm$ (solid lines) and $2.5cm$ (mixed line)

magnets motor structure. Not only does the rise of structure height increase the height z_{uni} of uniformity of B_r along the voice-coil path, it does as well increase the absolute maximum value of the radial magnetic induction $B_{r_{max}}$ seen by the voice-coil. For instance, for $h = 1cm$, $z_{uni} = 0.33cm$ and $B_{r_{max}} = 0.447T$, whereas for $h = 2.5cm$, $z_{uni} = 1.2cm$ and $B_{r_{max}} = 0.471T$. In the same way as for the three sintered magnets structure, the

ratio between z_{uni} and h increases when z increases. Indeed, in the first case presented above, $z_{uni}/h = 33\%$ whereas it reaches 48% in the second case. If we take $h = 20cm$, as we did with the other structure, the ratio z_{uni}/h goes up to 72%.

3.2.2.3 Effect of the structure width

We now take a look at the effect of the ratio between the height and the width of the structure. In order to do so, we set once again the semi-height h to $1cm$. Then, we make the width b vary from 0 to $4h$, which represents, in our example, 0 to $4cm$.
Figure 3.13 shows the variation of the maximum value of the magnetic field radial component $B_{r_{max}}$ with the variation of the ratio b/h.

Once again, we notice that $B_{r_{max}}$ reaches a maximum when the ratio b/h is around 2.

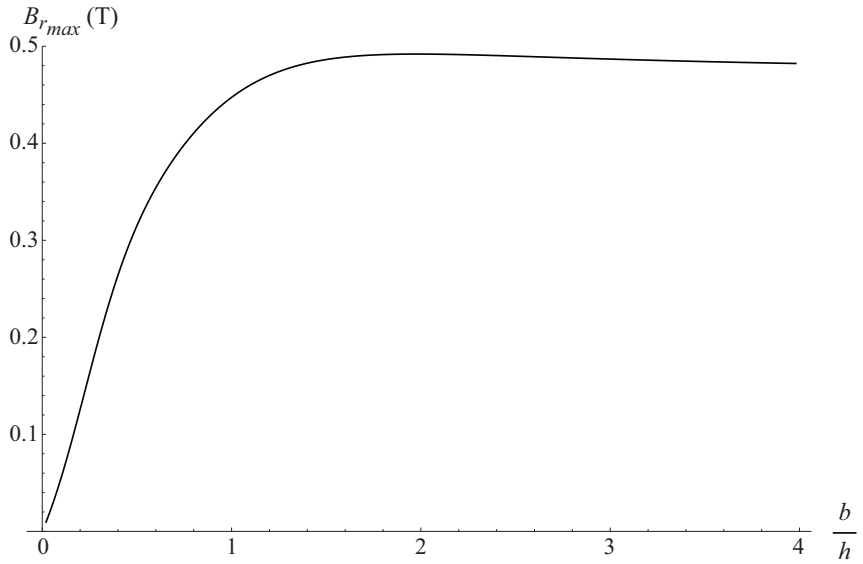

Figure 3.13: Evolution of the radial component maximum value $B_{r_{max}}$ of the magnetic field created by the ellipsoidal bonded magnet structure along the observation axis $O_{vc}z$ at a distance $d_x = 0.5mm$, with $J = 1T$, $h = 1cm$, and the width a varying from 0 to $4cm$.

More precisely, the maximum value of $B_{r_{max}}$ is $0.492T$ when $a/h = 1.97$. Above this ratio, the maximum magnetic induction seen by the voice-coil on its path goes down whereas the magnet volume increases.

Figure 3.14 shows the radial component B_r of the magnetic field created by the ellipsoidal bonded magnet structure along the observation axis $O_{vc}z$ between $z = 0$ and $z = h$ for different ratios b/h. These curves confirm the trend that we observed in Fig. 3.13, which is that we get the maximum magnetic induction for a width b two times bigger than the semi-height h. In other words, when the width is equal to the total height of the motor structure. If we now take a look at the evolution of the uniformity distance z_{uni} as a function of the width to height ratio, we see that it is relatively constant. Indeed, the values of $B_{r_{max}}$ and z_{uni} in each case are the following:

- For $b = h$: $B_{r_{max}} = 0.447T$ and $z_{uni} = 3.3mm$,

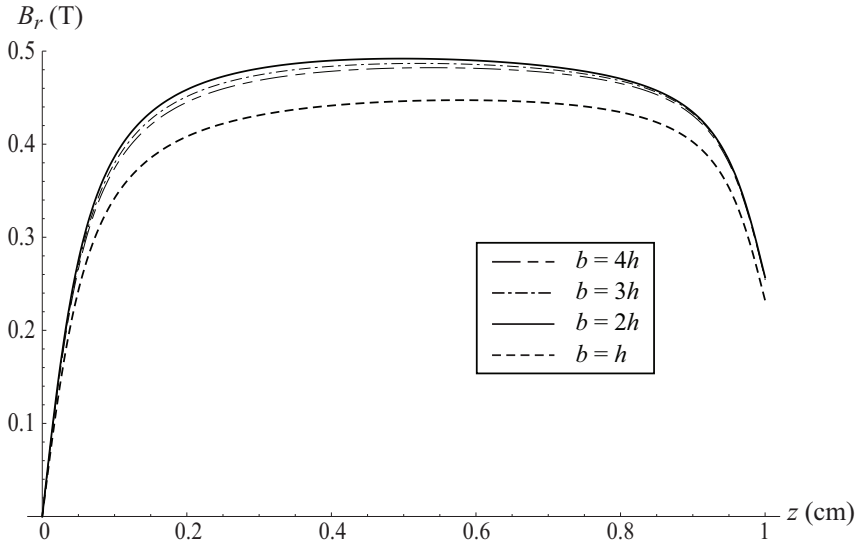

Figure 3.14: Radial component B_r of the magnetic field created by the ellipsoidal bonded magnet structure along the observation axis $O_{vc}z$ at a distance $d_x = 0.5mm$, with $J = 1T$, $h = 1cm$, and for different width b: $1cm$ (dashed line), $2cm$ (solid line), $3cm$ and $4cm$ (mixed lines).

- For $b = 2h$: $B_{r_{max}} = 0.492T$ and $z_{uni} = 3mm$,
- For $b = 3h$: $B_{r_{max}} = 0.487T$ and $z_{uni} = 3.1mm$,
- For $b = 4h$: $B_{r_{max}} = 0.482T$ and $z_{uni} = 3.2mm$.

In each case, the uniformity distance z_{uni} represents about one third of the height of the structure, regardless of the ratio between a and h. This ratio between z_{uni} and h only depends on the absolute height of the structure.
All these calculations show that the ratio between b and h does not greatly affect the uniformity of the magnetic field seen by the voice-coil but acts on the intensity of the latter. The best ratio seems to be $b = 1.97h$. Furthermore, by increasing the absolute height of the structure, keeping the same ratio b/h, we can augment the ratio z_{uni}/h above 70%.

3.2.3 Comparison of the Two Structures Performances

In order to compare the performance of these two ironless structures, presented in Fig. 3.3 and 3.4 and studied in detail in the previous paragraphs, some additional numerical applications are realized. In the following section, the three sintered magnet motor structure is called the rectangular structure, for reasons of simplicity.

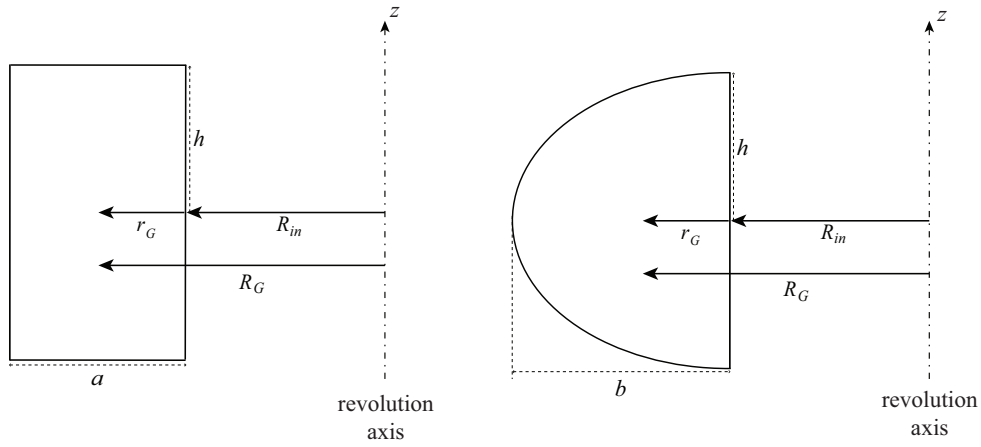

Figure 3.15: Notations used to calculate the volume of both structures

3.2.3.1 Equality of volumes

We decide to compare the magnetic fields created by two structures having the same magnet volume. In order to do so, we have to calculate the width b of the ellipsoidal structure giving the same magnet volume as the rectangular structure with $a = h$. Figure 3.15 represents the two structures and gives the notations used to calculate the respective volumes of these motors.
Using Pappus's centroid theorem, we manage to write the volume of the rectangular structure as a function of its width a, its semi-height h, its revolution radius R_{in} and its geometric centroid radius r_G as follows:

$$V_{rect} = (2a.h)(2\pi.R_G) = 2a.h(2\pi(R_{in} + r_G)) = 4\pi.a.h\left(R_{in} + \frac{a}{2}\right). \tag{3.12}$$

In the same manner, we write the volume of the ellipsoidal magnet structure as:

$$V_{ell} = \left(\frac{1}{2}\pi.b.h\right)(2\pi.R_G) = (\pi.b.h)(\pi(R_{in} + r_G)) = \pi^2.b.h\left(R_{in} + \frac{4}{3\pi}b\right). \tag{3.13}$$

These equations (3.12) and (3.13) permit to find the equality of the volumes by writting:

$$4\pi.R_{in}.a + 2\pi.a^2 = \pi.R_{in}.b + \frac{4}{3}b^2. \tag{3.14}$$

After some manipulations, we finally find the relationship between a and b in order to get the same volume for both structures. This gives:

$$b = \frac{1}{8}\left(-3\pi.R_{in} + \sqrt{3}.\sqrt{32a^2 + 64aR_{in} + 3\pi^2R_{in}^2}\right) \tag{3.15}$$

Depending on the inner radius R_{in} of both structures and the width a of the rectangular motor, b varies between 1.2 and 1.3 times a. If we take for instance $R_{in} = 5cm$ and $a = 1cm$, it leads to $b = 1.26cm$.

3.2.3.2 Numerical examples

In the following calculations, the semi-height h is set to 1 cm and the width a of the rectangular structure is taken equal to h. For the general case, we consider that the magnetization of each magnet is equal to 1 T. Then, it is easy to recalculate for other values of J since all the results are proportional to this former. Actually, with Neodymium-Iron-Boron (Nd-Fe-B) bonded magnets, it is difficult to obtain a magnetization bigger than 0.8 or $0.9T$ whereas Nd-Fe-B sintered magnets can have a magnetization up to about $1.5T$ for the strongest.

Figure 3.16 presents the magnitude isolines of the magnetic field radial component B_r,

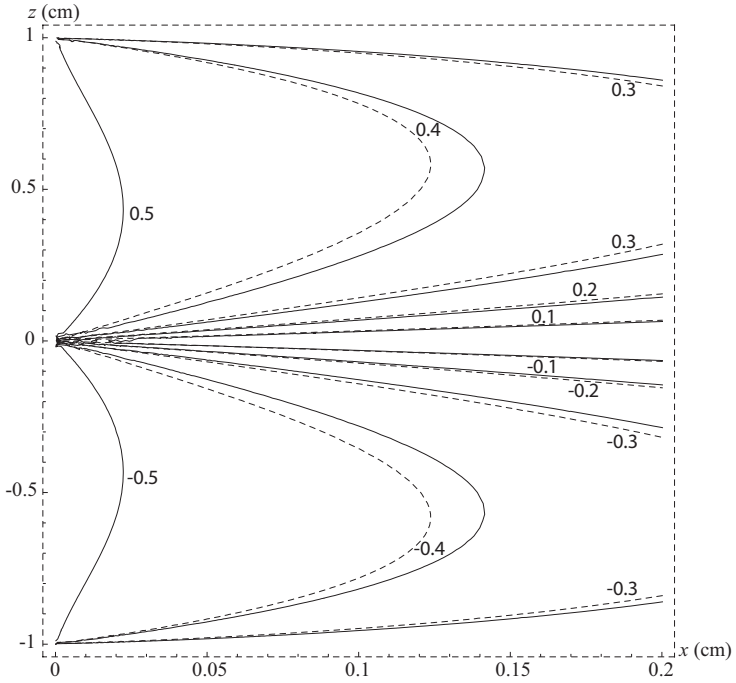

Figure 3.16: Magnitude isolines of the radial component of the magnetic field induction created (in Tesla) by the rectangular section structure (dashed line) and the one created by the ellipsoidal section structure (solid line) of same volume.

created in front of the magnet for both structures having the same volume. It shows that the ellipsoidal structure gives a more intense magnetic field radial component B_r than the rectangular one.

Figure 3.17 compares the evolution of B_r in front of the whole height of both magnet structures (i.e. z equals -1 cm to z equals 1 cm) at a distance d_x from the magnet equal to $0.5mm$, which is a typical distance for loudspeaker applications, with $J = 1T$, $h = 1cm$, $a = 1cm$ and $b = 1.26cm$. Once again, it clearly shows that the ellipsoidal structure gives a more intense magnetic field than the rectangular one of equal magnet volume. The rectangular motor gives $B_{r_{max}} = 0.459T$ whereas the ellipsoidal structure reaches $B_{r_{max}} = 0.475T$. The linearity is about the same for both structures. z_{uni}, corresponding to a 1% variation of the magnetic field, is equal to $3.3mm$ for the rectangular structure and $3mm$ for the ellipsoidal structure. If we look at the 10% decrease of the magnetic induction intensity, we get $7.2mm$ for both structures.

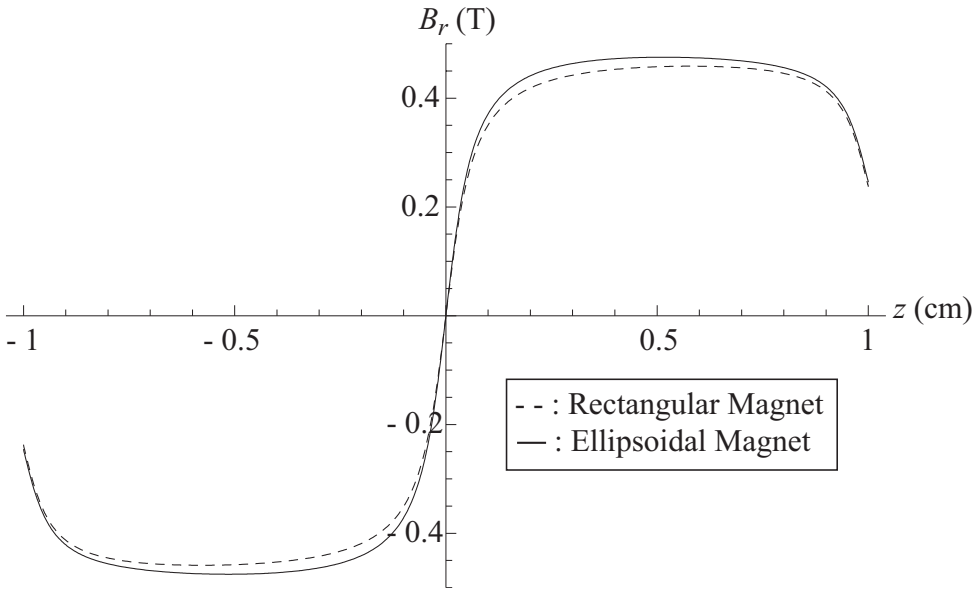

Figure 3.17: Radial component of the magnetic field created by the rectangular motor structure (dashed line) and the one created by the ellipsoidal motor structure (solid line) of same volume along the observation axis $O_{vc}z$ at a distance $d_x = 0.5mm$, with $J = 1T$, $h = 1cm$, $a = 1cm$ and $b = 1.26cm$.

The symmetry around the rest position and the uniformity of the induction across the whole voice-coil trajectory is an important characteristic for an accurate loudspeaker motor. The length of this trajectory is determined by the intended acoustical pressure at low frequencies, giving the maximal needed acoustic flow, and thus, the maximal required excursion for a given radiating surface. For example, to obtain a sound pressure level of $95dB\ SPL$ at $1m$ on axis and at $100Hz$ with a loudspeaker having a $5cm$ radius membrane, the required excursion is $\pm 2mm$. If we consider this oscillation range around the rest position, the magnetic field intensity variation seen by the voice-coil is less than 2% for both structures. This amount of variation is very low and should not create audible distortion. In comparison, with the standard loudspeaker that we used for the measurements presented in Chapter 4, the variation of the magnetic field intensity over the same displacement range is about 20%.

3.2.4 Comparison with 3D FEM calculation

All the results presented in the previous section were obtained with 2D analytical calculations. In order to evaluate the validity of the 2D model for magnet rings, we compare them to FEM 3D calculations. We take the example of an ellipsoidal motor structure with $h = 6mm$, $b = h$ and $R_{in} = 1cm$, corresponding to the prototype that we will study in the next chapter.

Figure 3.18 shows the calculation results of the magnetic field radial component B_r created by the ellipsoidal bonded magnet structure along the observation axis $O_{vc}z$ at a distance $d_x = 0.5mm$ using, in one case, the 2D analytical model that we have been using for all the calculations presented in this chapter and, in another case, a 3D FEM model.

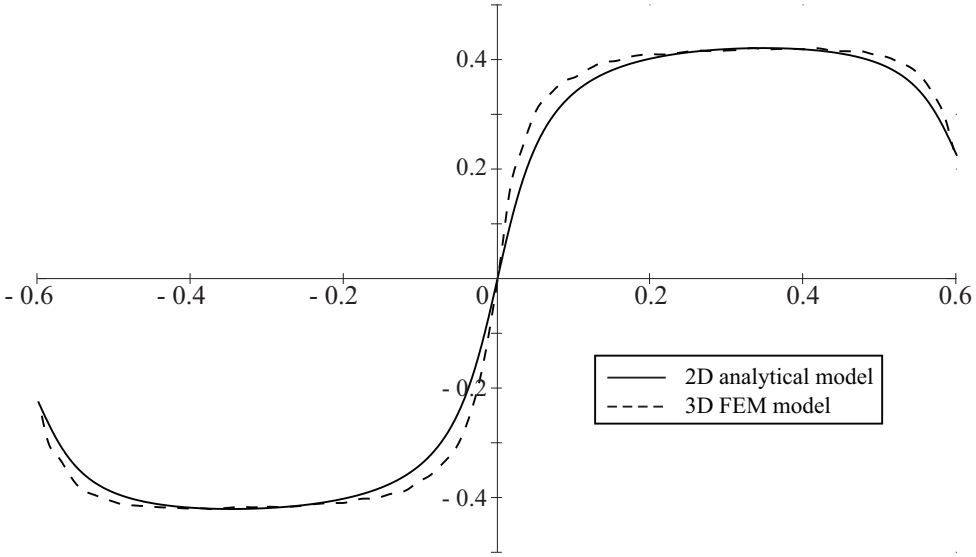

Figure 3.18: Radial component B_r of the magnetic field created by the ellipsoidal bonded magnet structure along the observation axis $O_{vc}z$ at a distance $d_x = 0.5mm$, with $J = 1T$, $h = 6mm$, $b = h$ and $R_{in} = 10mm$, calculated analytically in 2D (solid line) and with a 3D FEM model (dashed line).

We notice that the 2D model gives a good approximation and even underestimates the actual magnetic field created by the real 3D structure. The 2D model gives a very good approximation of the maximum absolute value $B_{r_{max}}$ and of the shape of the magnetic field radial component close to the rest position of the voice-coil (i.e. $z = -3mm$ and $z = 3mm$) but is less accurate near the center of the structure (i.e. between $z = -2mm$ and $z = 2mm$) and at the extremities (i.e. below $z = -5mm$ and above $z = 5mm$).
So far, 2D calculations have been widely used, especially for the development of new structures, because of their practical use compared to finite element modeling. Nevertheless, it should be kept in mind that the accuracy of 2D results is not perfect but still acceptable when looking at the magnetic field really close to the magnet, and presents a real advantage for optimization phases.

3.3 Conclusion

This chapter presents two leakage free structures of ironless motors, one made of traditional sintered magnets and the other one using bonded magnets. Even though it is not easy yet to obtain Nd-Fe-B bonded magnets with a magnetization higher than 0.9 T, the possibility to realize almost any shape allows ingenious magnetic structures to be made in order to compensate. In particular, the ellipsoidal structure shown in this chapter permits us to create a rather intense magnetic field concentrated on the voice-coil trajectory, which is the aim of a leakage free loudspeaker motor. Furthermore, one significant advantage of bonded magnets is that the making of such structures is facilitated, since neither assembling nor fabrication are needed.

Chapter 4

Experimental results

4.1 Introduction

Following this theoretical study about the ironless and leakage free loudspeaker motor made of a bonded magnet that is supposed to optimize as much as possible the magnetic mass by directly concentrating the magnetic field on the voice-coil, and to improve the sound quality by, on the one hand, suppressing all the nonlinearities due to iron and, on the other hand, creating a radial magnetic field as constant as possible on the whole voice-coil path [48], several motor prototypes were manufactured by Hutchinson-Paulstra in order to validate the magnetic calculations. Then, a couple of loudspeaker prototypes were realized by Faital, based on a mass-produced loudspeaker designed for Renault-Nissan cars, replacing the standard motor by an ironless bonded magnet motor and adapting the voice-coil to this kind of motor in order to confirm the sound quality enhancement expectations. This permits us to compare only the effect of the motor on the quality of the reproduced sound. A blind listening session was organized with a dozen people to evaluate the subjective improvement of sound quality induced by the use of an ironless motor. The judgment of all the listeners was in favor of the loudspeaker equipped with the ironless motor. The sound seemed to be clearer, more accurate and less distorted.
In order to try to understand and quantify this sound quality enhancement, a set of measurements were performed in the University of Maine Acoustics Laboratory (LAUM, France). First, the electrical impedance and the radiated pressure as a function of frequency were measured for both speakers. Then, we measured the evolution of the harmonics created on the current flowing through the coil and thus on the sound pressure, when the loudspeaker is driven with a single tone whose amplitude increases in time. Finally, we measured the inter-modulation distortion created on the current and the sound pressure when the loudspeaker is excited with two or three simultaneous uncorrelated tones.

4.2 Loudspeakers presentation

The study has been performed on a mass-produced Faital 6.5 inch bi-cone automotive loudspeaker. Two samples were used for the measurements, which are shown in Fig. 4.1. The first one is the reference speaker, using a standard ferrite sintered magnet ($B_r = 0.4T$) and iron motor. This motor weigh around $200g$. The second one is the same speaker model

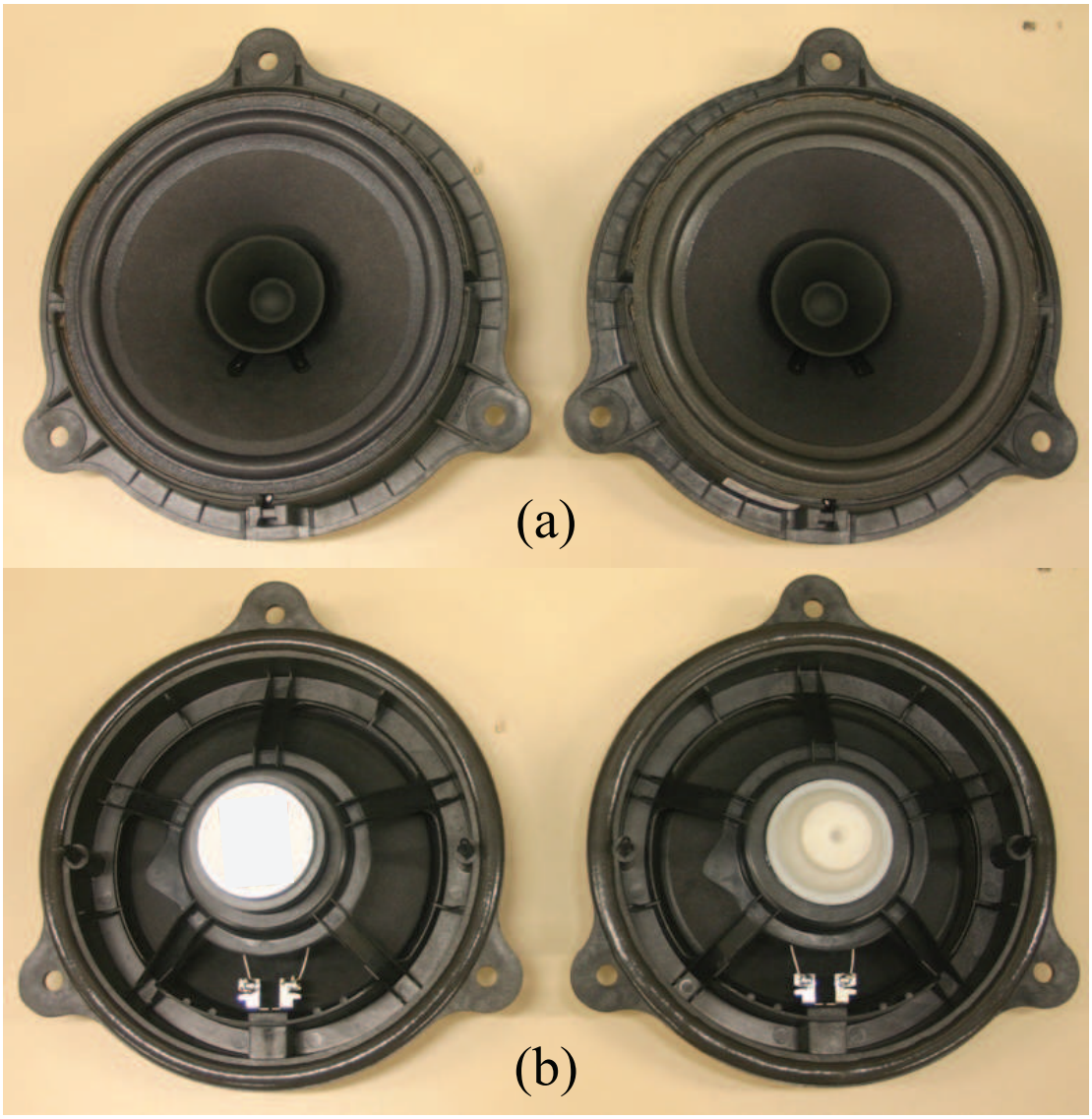

Figure 4.1: (a) Front view and (b) back view of the loudspeakers. Left: Standard speaker. Right: Ironless speaker.

but with an ironless ferrite bonded magnet ($B_r = 0.24T$) motor, whose weight is only $20g$. The voice coil was modified in order to fit with the bonded magnet structure, but keeping the same voice coil former diameter. The voice coil former is made of aluminium because of thermal dissipation reasons that will be developed further. Cross sections of both loudspeakers are presented in Fig. 4.2 and a more detailed view of both motors is shown in Fig. 4.3.

Figure 4.4 shows the way the bonded magnet motor is magnetized and the double coil winding rest position. The magnetization of the structure is done so that it is always tangent to the outer edge except on the side facing the voice-coil, where it is perpendicular to the edge. The magnetic field created by the motor is then concentrated on the voice-coil path in order to avoid magnetic flux leakage and reduce the magnetic mass as much as

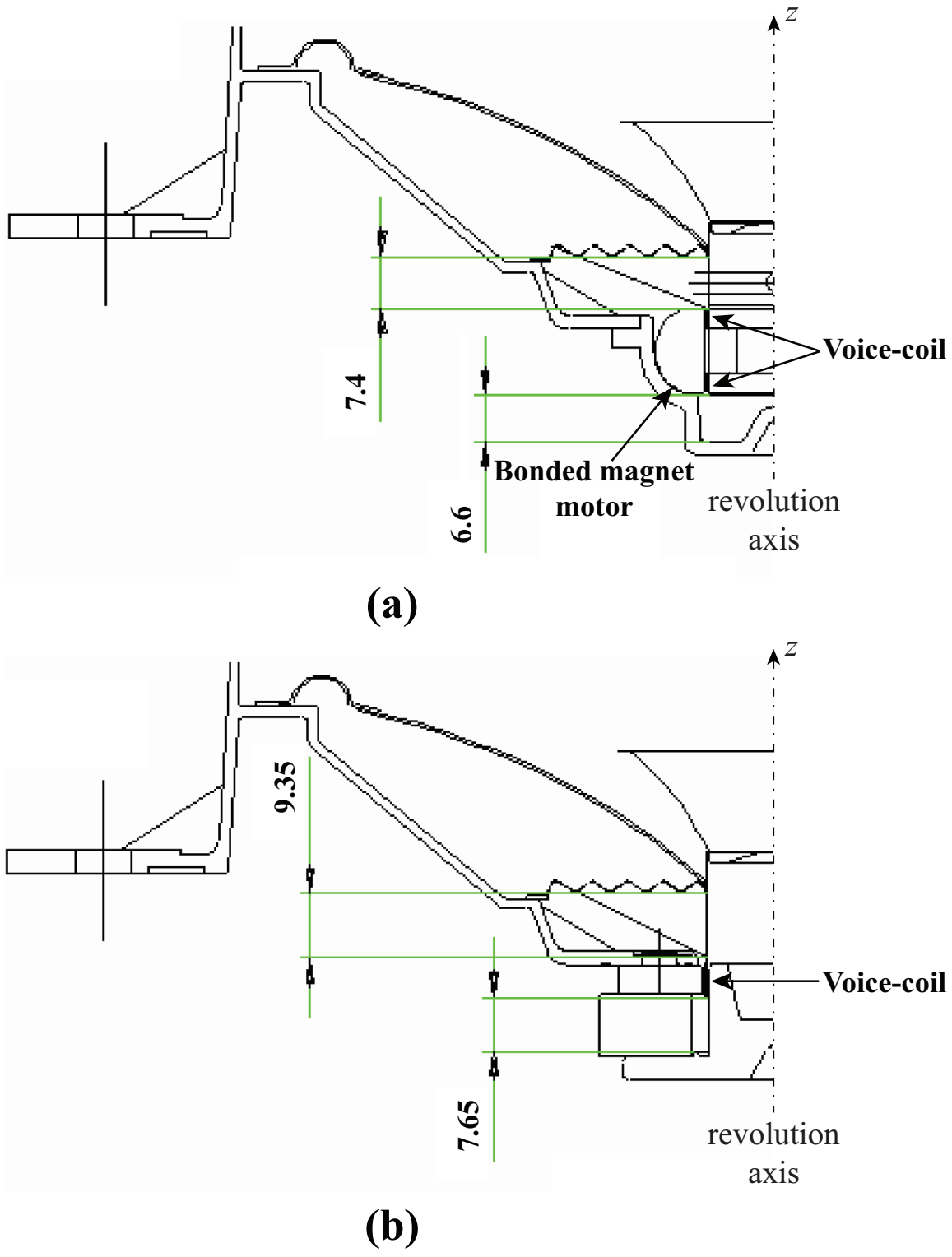

Figure 4.2: Cross sections of (a) the bonded magnet motor loudspeaker prototype and of (b) the standard reference loudspeaker (all dimensions are in mm).

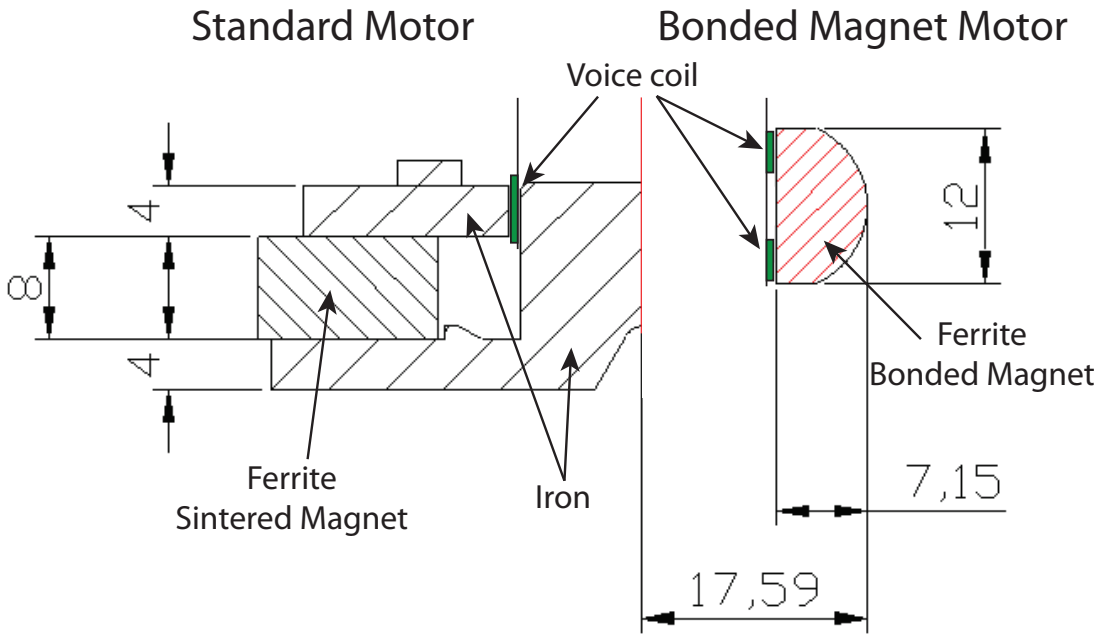

Figure 4.3: Close view of both motor structure cross sections (all dimensions are in mm).

possible.

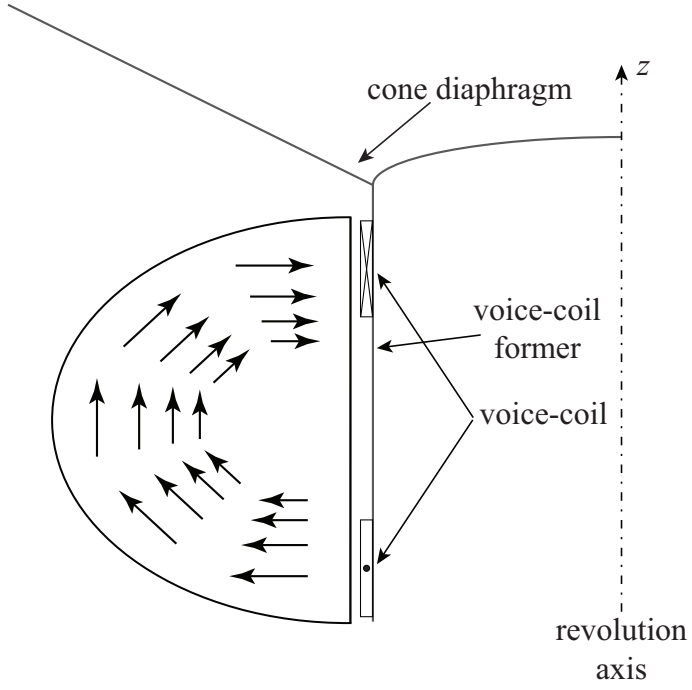

Figure 4.4: Cross section of the bonded magnet structure showing the shape of its magnetization.

4.3 Thermal considerations

Even though iron presents a certain number of defects, it has at least one quality, which is the thermal dissipation. On the contrary, bonded magnets are made of plastic and thus, are very poor heat conductors. As a consequence, the heat created by the voice coil is very badly dissipated, leading to a limitation of the maximum electrical power handling of the loudspeaker. In order to compensate this lack of dissipation, the standard Kapton voice coil former has been replaced by a aluminium one, on which the copper voice-coil is wound. In addition, several holes have been pierced to increase the forced convection.
In order to compare the thermal resistance R_{th} of each speaker, we performed a set of measurements. The measurement setup is presented in Fig. 4.5. The basket temperature T_{bask} was measured with a thermocouple and a Onsoku OMT-205A voice coil temperature meter was used to measure T_{vc}. All the results are given in Table 4.1.

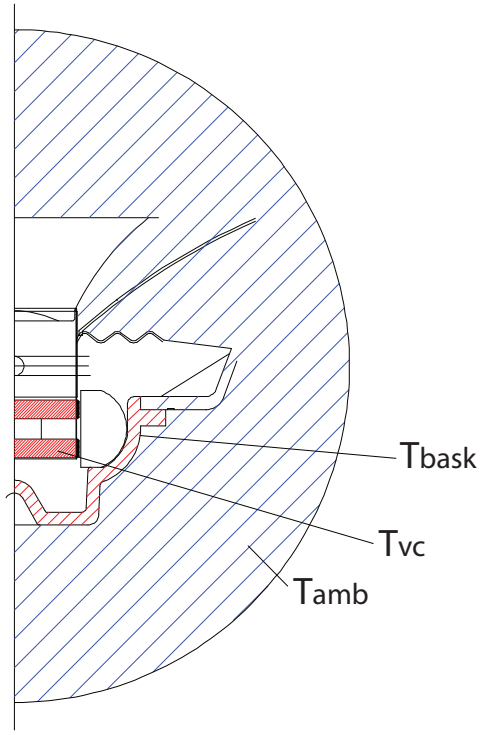

Figure 4.5: Setup used to measure the thermal resistance of both speakers. The ambient temperature, T_{amb}, the basket temperature, T_{bask} and the voice coil temperature T_{vc} were measured.

These results clearly show the advantage of the standard ferrite motor with iron for thermal dissipation. Considering standard automotive loudspeaker applications, the electrical driving power is rather low (less than 15W RMS) and should then not be a problem. But this thermal constraint could be a limitation for the use of bonded magnets in Hi-Fi or public address systems.

Bonded Magnet Motor		
Elec Power	1 W	2 W
T_{amb}	23 °C	23 °C
T_{bask}	29 °C	42 °C
T_{vc}	40 °C	53 °C
R_{th}	17 °C/W	15 °C/W
Standard Ferrite Motor		
Elec Power	1 W	2 W
T_{amb}	23 °C	23 °C
T_{bask}	25 °C	30 °C
T_{vc}	35 °C	47 °C
R_{th}	12 °C/W	12 °C/W

Table 4.1: Results of the thermal testing of both speakers.

4.4 Magnetic field measurement

This kind of bonded magnet loudspeaker motor is a new technology and manufacturing techniques are not well developed yet. In order to validate the correct orientation of the magnetic particles inside this one, a radial magnetic induction measurement was conducted along its height, 0.6 mm away from its inner surface. The instrumentation used does not permit us to go any closer to this surface because of its size and the small radius of curvature of the motor. These measurement results are compared to the FEM simulation in Fig. 4.6.

The measurement shows a good correlation with the FEM simulation even though the simulation slightly underestimates the radial magnetic induction. However, we can be quite confident in the calculation results relevance at other distances from the motor and their concordance with the actual magnetic field created by the motor at the voice coil position for instance.

4.5 Distortion: Theoretical Study

The reference loudspeaker model employed to describe the functioning of loudspeakers uses the Thiele and Small parameters (lumped parameters) and leads to a linear and stationary system of two differential equations:

$$\begin{cases} R_e \cdot i(t) + L_e \frac{di(t)}{dt} + Bl \frac{dz(t)}{dt} = u(t) \\ \\ M_{ms} \frac{d^2 z(t)}{dt^2} + R_{ms} \frac{dz(t)}{dt} + K_{ms} \cdot z(t) = Bl \cdot i(t) \end{cases} \tag{4.1}$$

where R_e is the DC resistance of the voice coil, L_e the inductance of the voice coil, Bl the force factor, M_{ms} the mechanical mass of the speaker diaphragm assembly including voice coil and air load, R_{ms} the mechanical resistance of the speaker suspension losses, K_{ms} the mechanical stiffness of the speaker suspension, u the voltage driving the speaker, i the

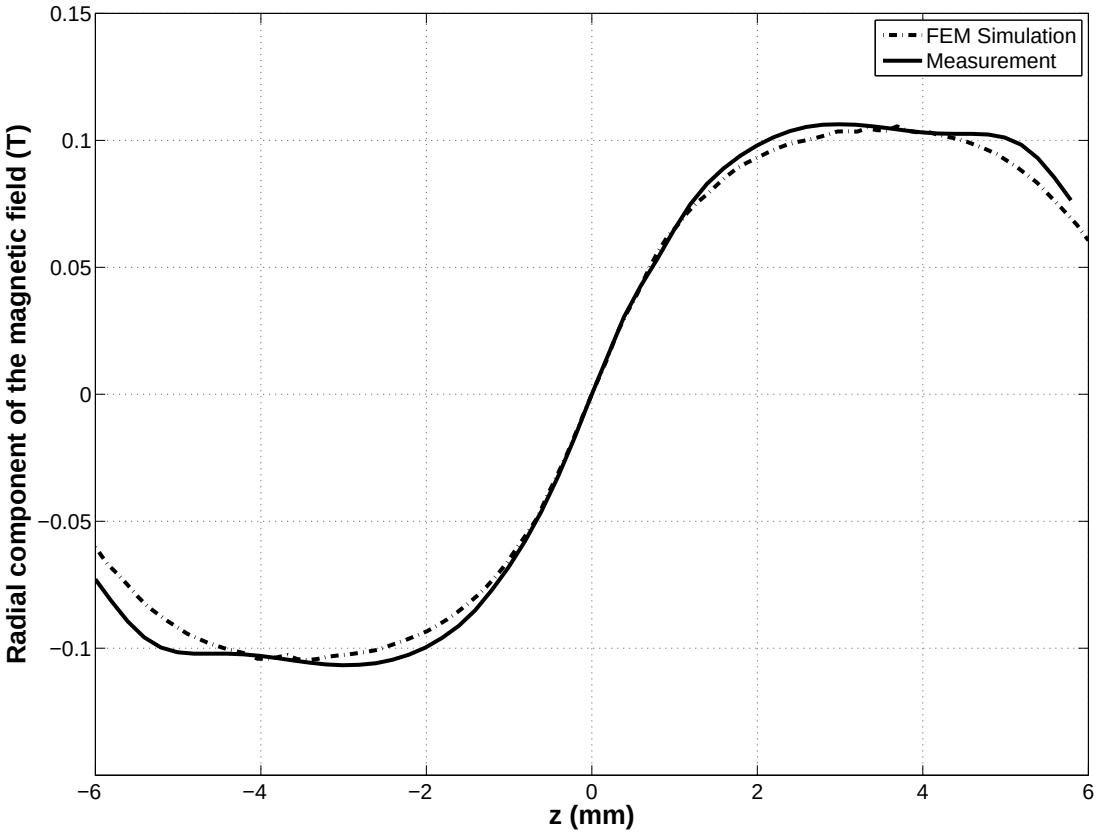

Figure 4.6: FEM Simulation (dashed line) and measurement (solid line) of the radial component of the magnetic field created by the bonded magnet motor along its height, 0.6 mm away from its inner surface.

driving current flowing through the coil and z the axial displacement of the voice coil. However, it is known that loudspeakers are highly nonlinear devices and the dependence of the force factor Bl on the displacement $z(t)$ of the coil is among the major sources of nonlinearities [49, 50]. Thus, variation of Bl versus displacement will produce two nonlinear terms in the differential equations. In both terms, time signals are multiplied. This multiplication produces new spectral components in the output signal measured and heard as harmonic and inter-modulation distortion. A symmetrical variation of Bl around the rest position of the coil leads to odd-order distortions; an asymmetry leads to even-order distortions [51].

Another great source of nonlinearities is the variation of the voice coil inductance. The moving coil creates an alternating magnetic flux in the yoke pieces. The electrical conductivity of the iron is high enough to let eddy currents appear in the iron of the motor. Eddy currents have two causes: the current variations with time and the coil movements. As a consequence, the inductance tend to diminish and the resistance to rise at high frequencies.

Another consequence is the creation of a reluctant force that can be expressed as [52]:

$$F_r = \frac{1}{2}\frac{dL_e}{dz}i^2(t). \tag{4.2}$$

This reluctant force creates a force distortion resulting directly in an audible acoustical distortion. By removing the iron from the motor, these nonlinearities should be greatly reduced.

4.6 Distortion: Numerical Study

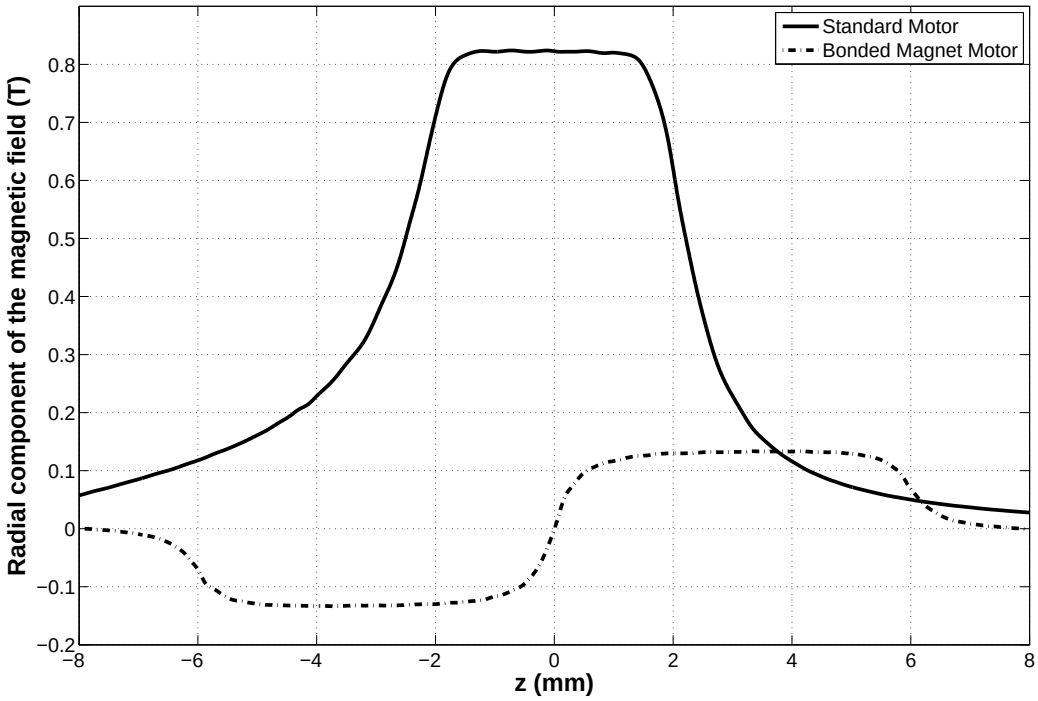

Figure 4.7: FEM Simulation of the radial component of the magnetic field created by the standard motor (solid line) and the one created by the bonded magnet motor (dashed line) along the height of both air gaps.

The radial component of the magnetic fields created in the air gap by both motors was calculated using a finite element model. The results are plotted in Fig. 4.7.
The radial magnetic field maximum of the standard motor is about seven times higher than the one of the bonded magnet motor, but the linear range is roughly about 3 mm wide whereas the bonded magnet motor offers a uniform induction over a $4mm$ range. But the real interest of the bonded magnet structure is the way it is used with the double coil winding. The standard loudspeaker has a coil that is $4.8mm$ high while the prototype's voice coil is $2x2.8mm$ high. The coil wire diameter was adjusted in order to keep the same

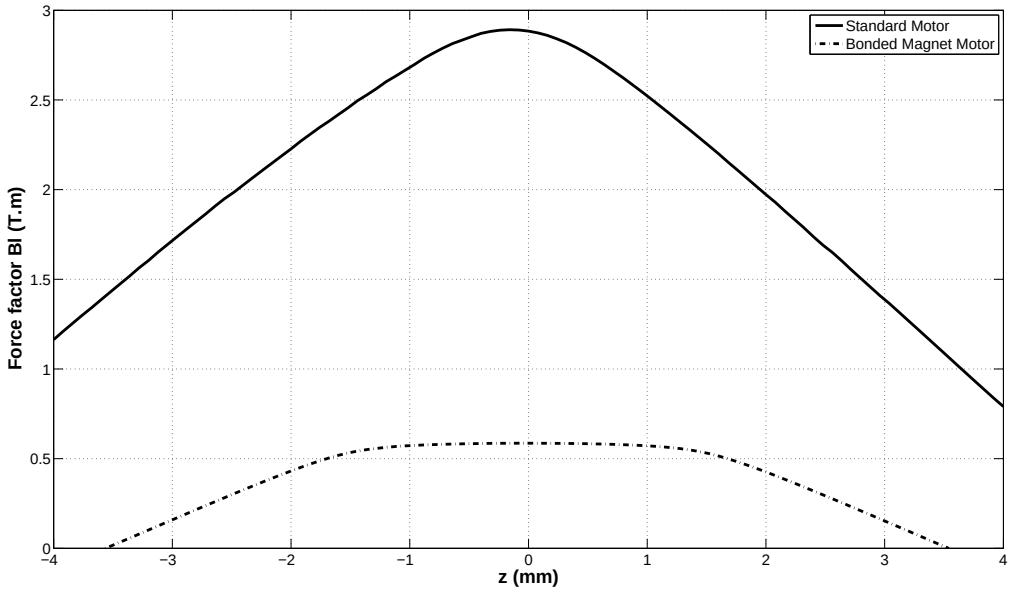

Figure 4.8: Force factors Bl calculated for the standard loudspeaker (solid line) and the prototype loudspeaker (dashed line) over a ±4 mm voice coil displacement around its rest position.

DC resistance.
Knowing the height and rest position of each voice coil, and the radial magnetic field created by each motor, the force factor of each loudspeaker has been calculated on a $\pm 4mm$ range around the rest position. The results of these calculations are presented in Fig. 4.8. Once again, the maximum amplitude of the standard motor force factor is much higher than with the bonded magnet motor, but it is as well highly nonlinear and asymmetrical around the rest position ($z = 0$ mm). On the contrary, the force factor of the speaker equipped with the bonded magnet loudspeaker is almost flat over a $3mm$ range (from $z = -1.5mm$ to $z = 1.5mm$) and then starts to decrease, but not as quickly as the standard loudspeaker. This major difference could be an explanation of the sound quality enhancement, especially at low frequencies, where coil displacements are large, and an important difference should be noticeable on the distortion measurements at low frequencies.

4.7 Distortion: Experimental Study

For all the measurements, a Devialet D-Premier amplifier was used to supply the driving voltage. This amplifier has a linear dynamic range higher than $100dB$, which permits us to drive the speaker with a perfectly linear voltage. The current was measured with a 470 mΩ N4L HF003 shunt resistance. The sound pressure level as a function of frequency was measured in an anechoic chamber, the speaker being baffled.

4.7.1 Electrical Impedance

The electrical impedance module and phase as a function of frequency of both speakers are presented in Fig. 4.9. It was measured with a constant voltage of 0.4V over the whole frequency range.

As expected, the DC resistance is the same for both speakers. However, two major

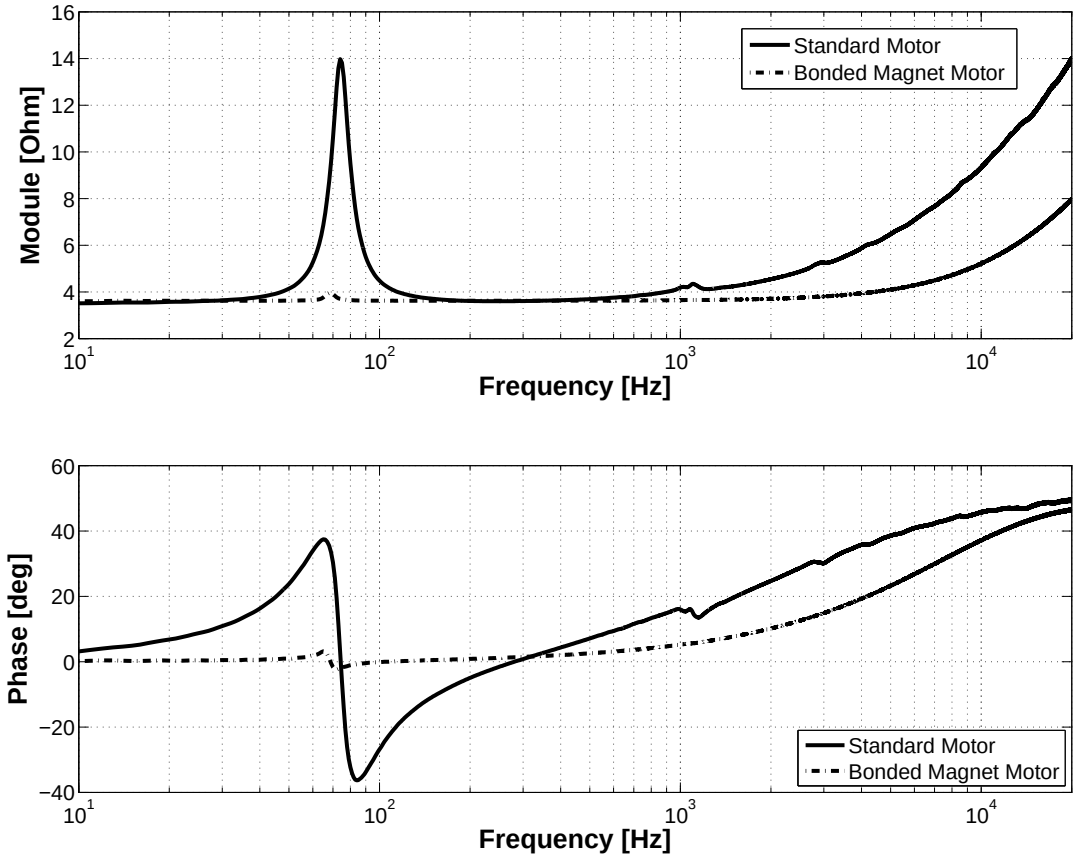

Figure 4.9: Electrical impedance module (top) and phase (bottom) as a function of frequency of the standard reference loudspeaker (solid line) and of the bonded magnet motor loudspeaker prototype (dashed line).

differences can be noticed. First, the resonance peak hardly appears for the bonded magnet loudspeaker because of the low force factor. Second, the impedance rise at high frequencies is much smaller for the ironless motor loudspeaker. This can be explained by the fact that we have an air core inductor on the bonded magnet motor, compared to the iron core inductor of the standard motor.

At high frequencies, where the displacement of the coil is negligible, the impedance of the loudspeaker can be expressed as:

$$Z_e = R_e + j\omega L_e. \tag{4.3}$$

In order to validate the assumption of the eddy currents suppression in the ironless motor, we plot the apparent resistance R_e and inductance L_e of the coil, corresponding directly to the electrical impedance real part and imaginary part divided by ω [14]. A zoom between 1kHz and 20kHz is shown in Fig. 4.10.

The difference between both speakers is obvious on the apparent inductance L_e. The

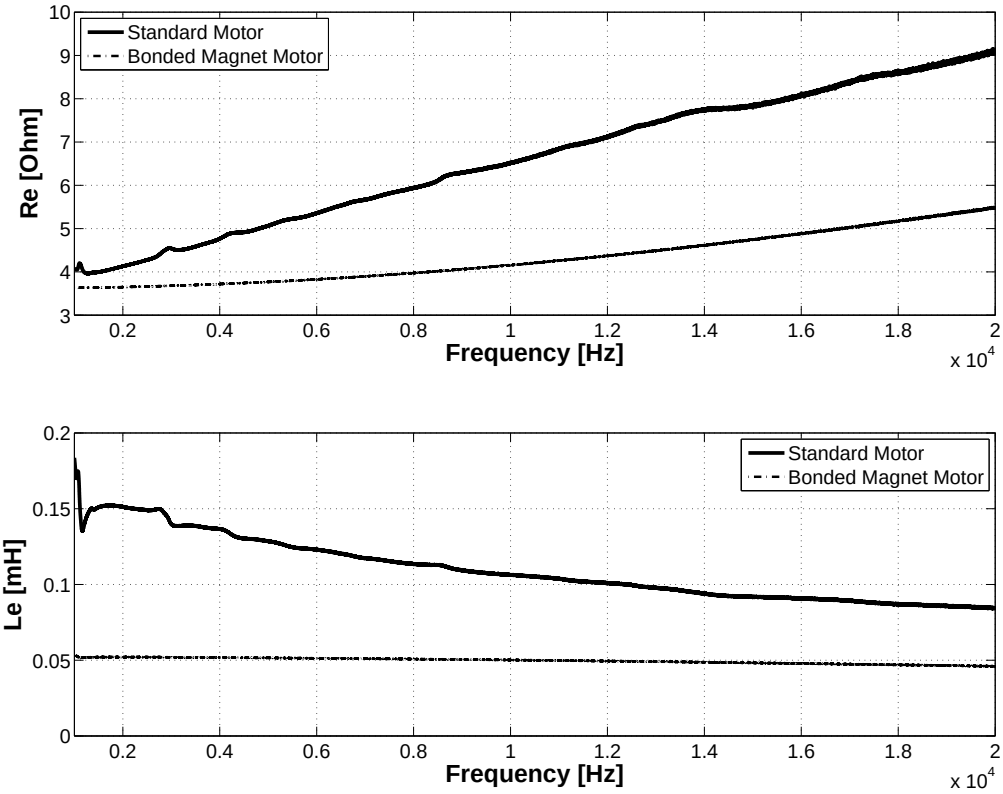

Figure 4.10: Apparent resistance (top) and inductance (bottom) as a function of frequency of the standard reference loudspeaker (solid line) and of the bonded magnet motor loudspeaker prototype using a aluminium voice-coil former (dashed line).

standard speaker inductance is divided by two between 1kHz and 20kHz whereas for the bonded magnet driver, it stays almost constant. As for the apparent resistance R_e, the rise is significantly smaller with the ironless motor. We assume that the small variation of R_e and L_e on the bonded magnet motor loudspeaker is due to small eddy currents that are created in the aluminium voice-coil former.

In order to validate this assumption, we take a loudspeaker with a kapton voice-coil former and no motor, and measure its electrical impedance. With no surprise, since it comes down to a simple air core inductor, R_e and L_e stay perfectly constant with frequency. Then, we put a bonded magnet ring around the voice-coil, block its movements, and measure again its electrical impedance. As we can see in Fig. 4.11, this does not change a thing either on R_e or on L_e. Therefore, we can conclude that the variations of R_e and L_e measured on the other loudspeaker were most probably due to the aluminium former.

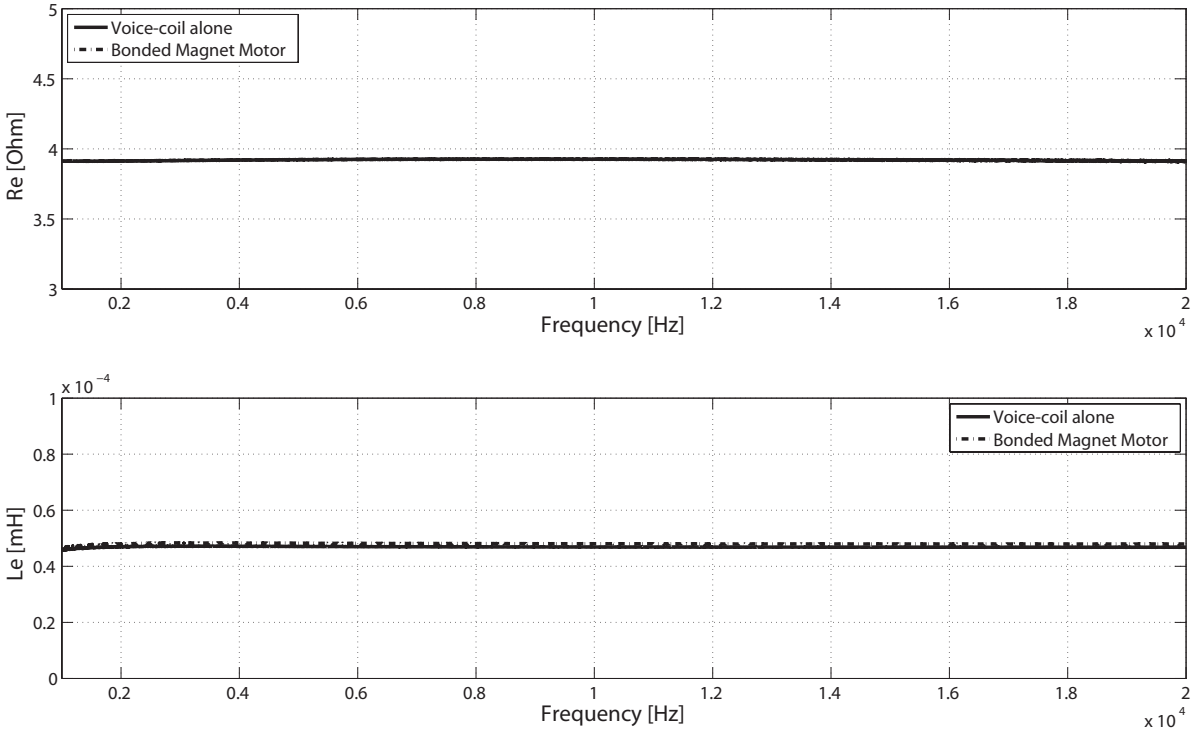

Figure 4.11: Apparent resistance (top) and inductance (bottom) as a function of frequency of the voice-coil alone (solid line) and with the bonded magnet motor around it (dashed line), using a voice-coil former made of kapton.

4.7.2 On-Axis Sound Pressure

The on-axis sound pressure level was measured for both baffled speakers in an anechoic chamber, 1m away, driven by a 2V constant voltage (nominal impedance of both speakers being 4Ω). The results of these measurements are shown in Fig. 4.12.

Two obvious differences can be discussed. First, the sensitivity of the bonded magnet motor loudspeaker is significantly smaller. It does agree with the difference between the calculated force factors (about 14dB) and with the fact that the moving part of the bonded magnet motor loudspeaker is slightly heavier (about 3dB), due to its aluminium voice-coil former. Second, the resonance peak is much more visible on the ironless loudspeaker curve. Once again, this due to the lower force factor Bl of the ferrite bonded magnet motor. Indeed, this Bl product, with B the radial induction flowing through the coil of length l, determines not only the driving force $Bl \cdot i(t)$ for a given current $i(t)$, but also an electrical damping $Bl \cdot \frac{dz(t)}{dt} = Bl \cdot v(t)$ of the loudspeaker connected to an amplifier with low impedance output.

In order to compare the spectral balance of both speakers, we add 17dB to the ironless driver SPL and plot it in Fig. 4.13.

The ironless motor driver is a little bit more generous below 100Hz due to the low resonance damping and to a 10Hz lower resonance frequency. The resonance shift is probably due to the change of voice-coil former that is heavier than the original one, and also because of the dispersion in suspension parts manufacture. Between, 100 and 700Hz, both speakers

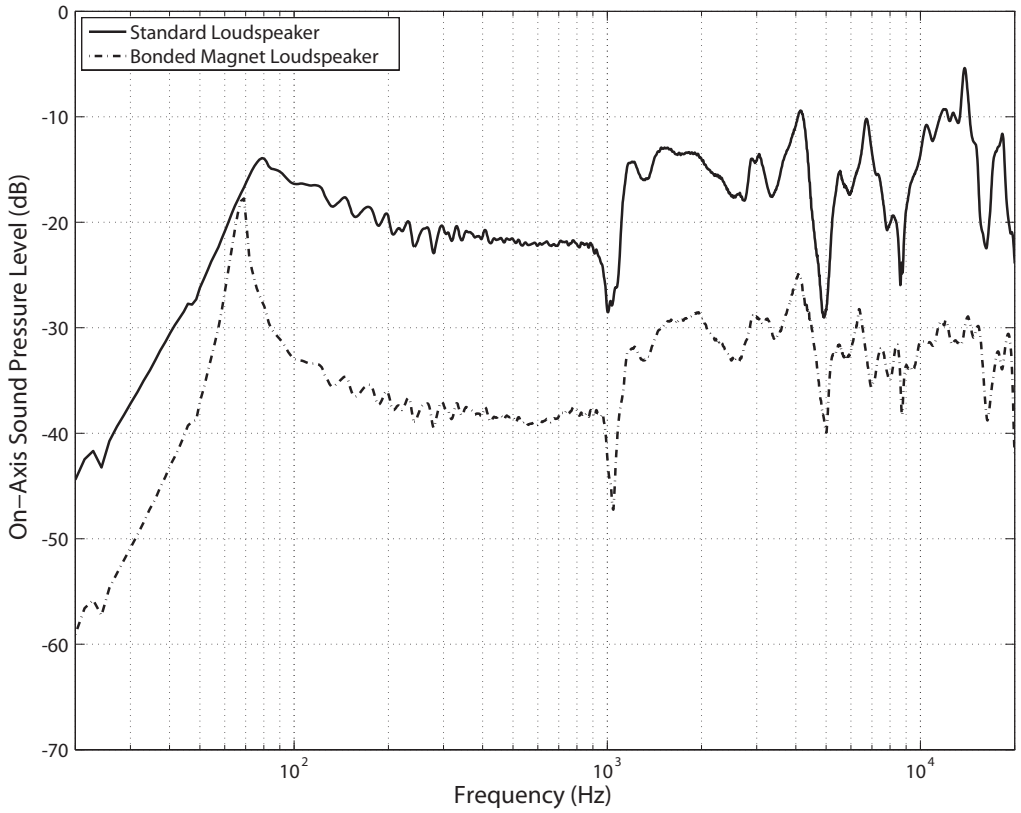

Figure 4.12: On-axis free field sound pressure level measured at 1m at 2V for the standard reference loudspeaker (solid line) and the bonded magnet motor loudspeaker prototype (dashed line). Both speakers were baffled.

responses are strictly identical. Then, approaching the first cone breakup mode (above 700Hz), the two pressure responses start to slightly differ, probably because of the different voice-coil formers.

These measurements of the electrical impedance and sound pressure level as a function of frequency give an indication about the "linear" response of both loudspeakers and confirm the suppression of eddy currents in the ironless motor but, as we expected, do not give much informations about the perceived sound quality. In order to try to quantify the latter, harmonic and inter-modulation distortion have to be measured.

4.7.3 Harmonic Distortion

This section shows the results of harmonic distortion measurements realized on both speakers. The experimental setup is the same as the one used for previous measurements. The speaker is excited by a series of tone burst whose amplitude increases step by step from 0V to the maximum voltage. The harmonic distortion created on the voice-coil current and on the sound pressure is then measured. For these experiment, the speakers

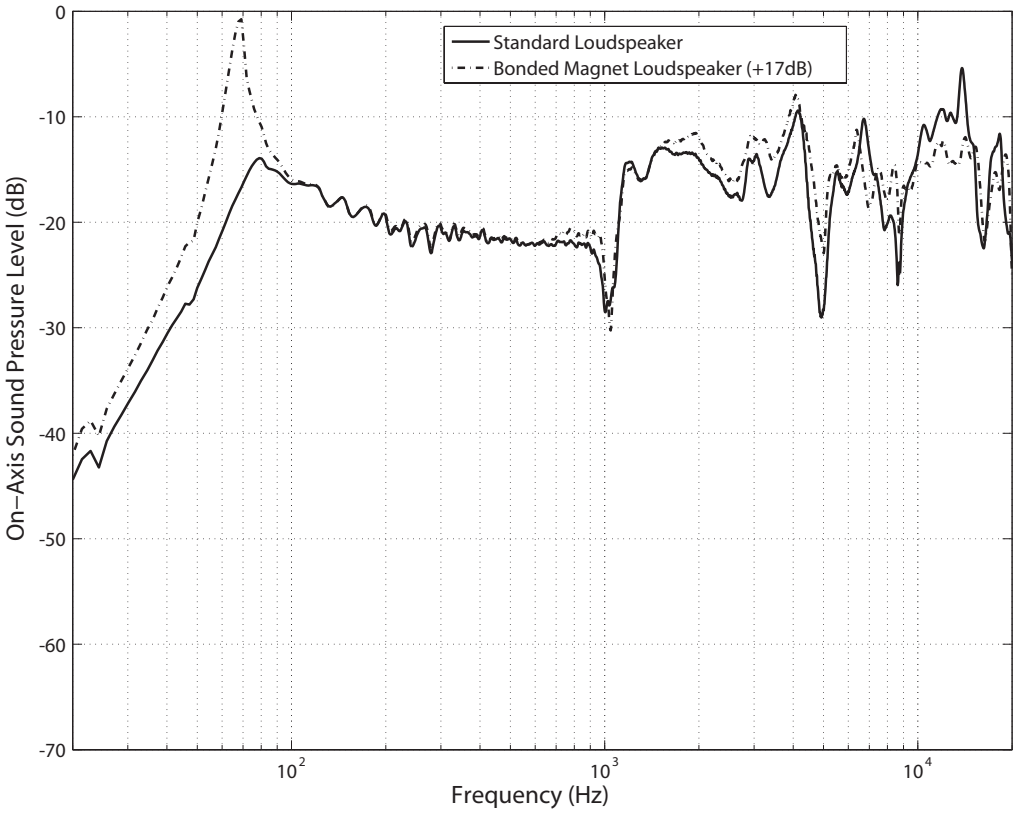

Figure 4.13: On-axis free field sound pressure level measured at 1m at 2V for the standard reference loudspeaker (solid line) and the bonded magnet motor loudspeaker prototype (dashed line) to which 17dB have been added. Both speakers were baffled.

were installed on a block of foam on the floor (grid) of the anechoic chamber, pointing upwards, without any baffle.
All the results are normalized to the maximum driving voltage and plotted in dB.

4.7.3.1 Low Frequency Harmonic Distortion

In order to try to highlight the harmonic distortion due to the force factor nonlinearity, the first measurement is conducted at low frequencies, around the resonance frequency (80Hz), in order to get large displacements of the coil. At this frequency, the efficiency of the ferrite bonded magnet loudspeaker is about 10dB lower than the standard driver. Therefore, it has been excited with a driving voltage 10dB higher in order to get the same voice-coil displacement. The harmonic distortion created on the coil current is shown in Fig. 4.14 and on the sound pressure in Fig. 4.15.

The harmonic distortion created on each voice-coil current is radically different. All the harmonics generated on the ironless motor coil current are about 50dB lower than

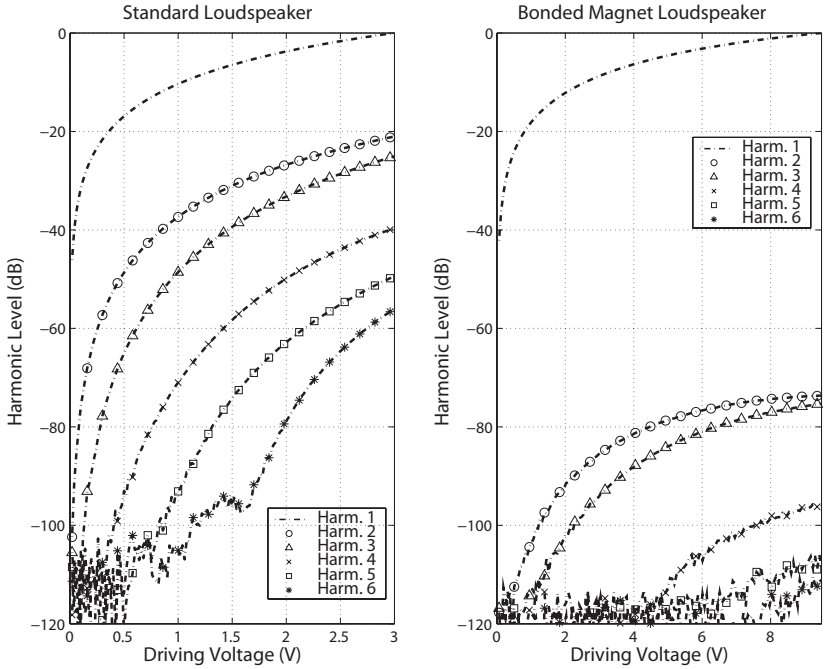

Figure 4.14: Harmonic distortion created on the voice-coil current for both speakers at 80 Hz. Fundamental (-.-), 2nd harmonic (circle), 3rd harmonic (triangle), 4th harmonic (cross), 5th harmonic (square), 6th harmonic (star)

on the standard one. The harmonic distortion measured on the sound pressure is also much lower with the ironless loudspeaker (about 20dB for harmonics 2 and 3) but this advantage is limited by the rather high noise floor of the measurement due to the lack of baffle, inducing a quite low sound pressure level at this frequency.
These results are a good example of the gain brought by a more linear force factor and an ironless motor, allowing us to get rid of the eddy currents produced by large coil displacements.

4.7.3.2 High Frequency Harmonic Distortion

At high frequencies (above 1kHz), coil displacements are really small (less than 0.1mm) which permits us to avoid nonlinearities due to the force factor. Thus, the distortion is only, or at least mainly, created by the eddy currents and the reluctant force [14]. The measurement of R_e and L_e at high frequencies showed that there were no eddy currents remaining in the bonded magnet motor.
In this case, the distortion is related to the voice-coil current and not to its displacement. At 8kHz, the impedance modulus of the standard speaker is 1.6 times higher than for the ironless speaker. Thus, the voltage driving the bonded magnet speaker is 1.6 times lower, in order to get the same current flowing through both voice-coils. The measurement results are given in Fig. 4.16 for the coil current distortion and in Fig. 4.17 for the sound pressure distortion.

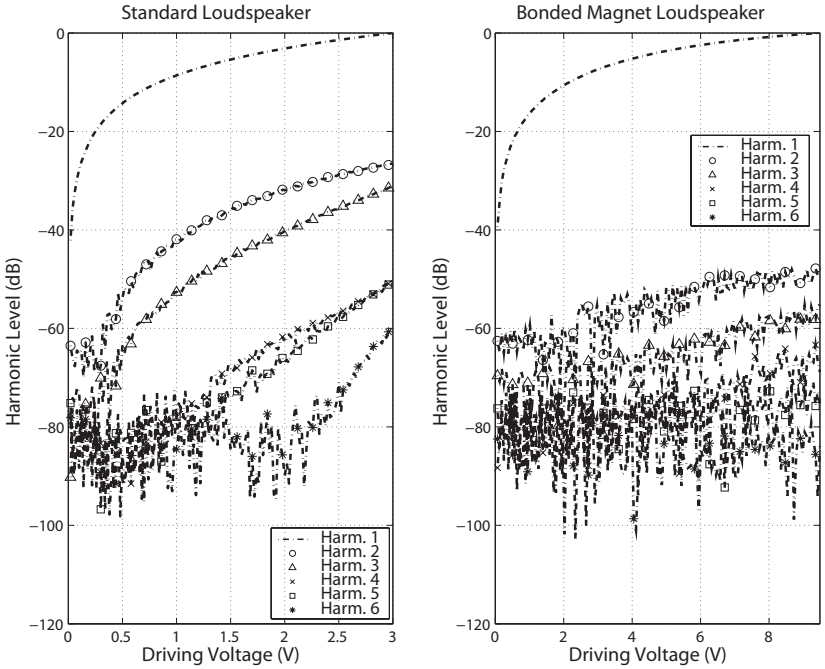

Figure 4.15: Harmonic distortion created on the sound pressure for both speakers at 80 Hz. Fundamental (-.-), 2nd harmonic (circle), 3rd harmonic (triangle), 4th harmonic (cross), 5th harmonic (square), 6th harmonic (star)

At this frequency, the ironless speaker is almost linear. The only harmonic remaining (the second one) on the voice-coil current is 90dB below the fundamental. On the contrary, the standard speaker voice-coil shows a significant level of the harmonics 2 to 5, with a predominance of the odd-order harmonics. Indeed, the third harmonic is bigger than the second one, and the fifth is bigger than the fourth. This behavior is typical of eddy currents.

The behavior is quite different on the sound pressure harmonic distortion. For the ironless speaker, the second harmonic rises up to -65dB. And for the standard driver, both fourth and fifth harmonics have disappeared and the second has become bigger than the third. This second harmonic could be due to a mechanical mode of the membrane.

The results of both high and low frequency harmonic distortion show a certain advantage in favor of the bonded magnet motor loudspeaker. This first step corroborates the listeners opinions. In order to confirm this tendency and go further, inter-modulation distortion measurements have been performed.

4.7.4 Inter-Modulation Distortion

It is known that the inter-modulation distortion components are more disturbing than the harmonic components, as much in the signal generated by the loudspeaker [53, 54, 55] as

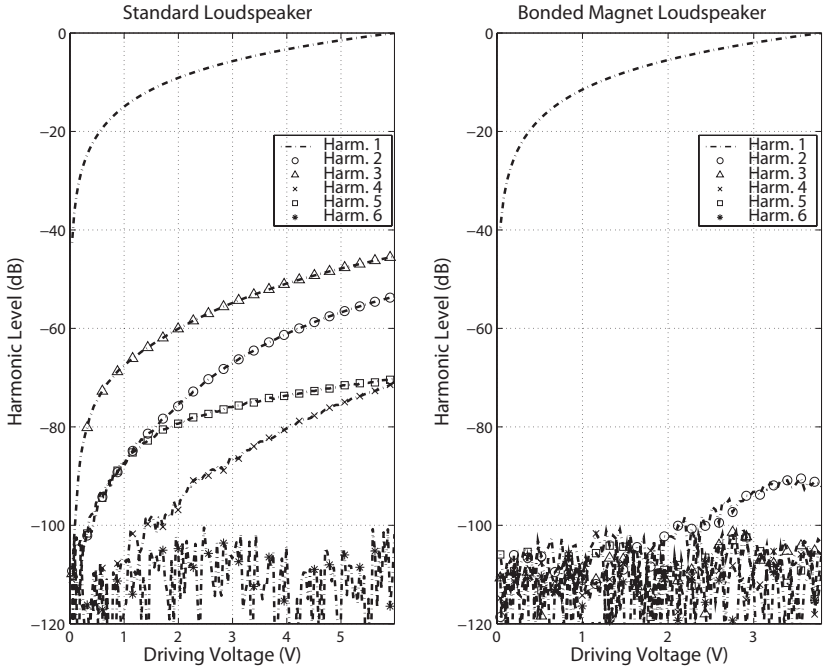

Figure 4.16: Harmonic distortion created on the voice-coil current for both speakers at 8 kHz. Fundamental (-.-), 2nd harmonic (circle), 3rd harmonic (triangle), 4th harmonic (cross), 5th harmonic (square), 6th harmonic (star)

in the auditory electric signal created by the ear itself [56]. That is why it is important to decrease these components as much as possible.
We first study the intermodulation due to iron losses but not force factor nonlinearity. Thus, we choose frequencies that are high enough to avoid large coil displacements. All the results are normalized to $0dB$.

The first example, whose results are presented in Fig. 4.18 and in Fig. 4.19, uses two uncorrelated tones, i.e. 863Hz and 3728Hz. The first measurement is realized with a driving voltage of 1V per tone (Fig. 4.18) whereas the second one is done 15dB higher, which gives 5.6V per tone (Fig. 4.19).
In the first case (1V), there is no distortion at all on the ironless motor voice-coil current whereas the current of the standard speaker shows some peaks rising up to -50dB. When the driving voltage goes up to 5.6V, the distortion peaks (harmonic and inter-modulation) already present on the previous measurement for the standard speaker tend to get bigger and new ones appear. Concerning the ironless loudspeaker, a little bit of harmonic and inter-modulation distortion starts to emerge but the higher peak is -70dB below the two driving tones.
The same experiment is done with three high frequency uncorrelated tones of equal amplitude, 943Hz, 1519Hz and 2985Hz. Figure 4.20 shows the results of this experiment with a driving voltage of 1V per tone and Figure 4.21 presents the results for 5.6V per tone, for both speakers.

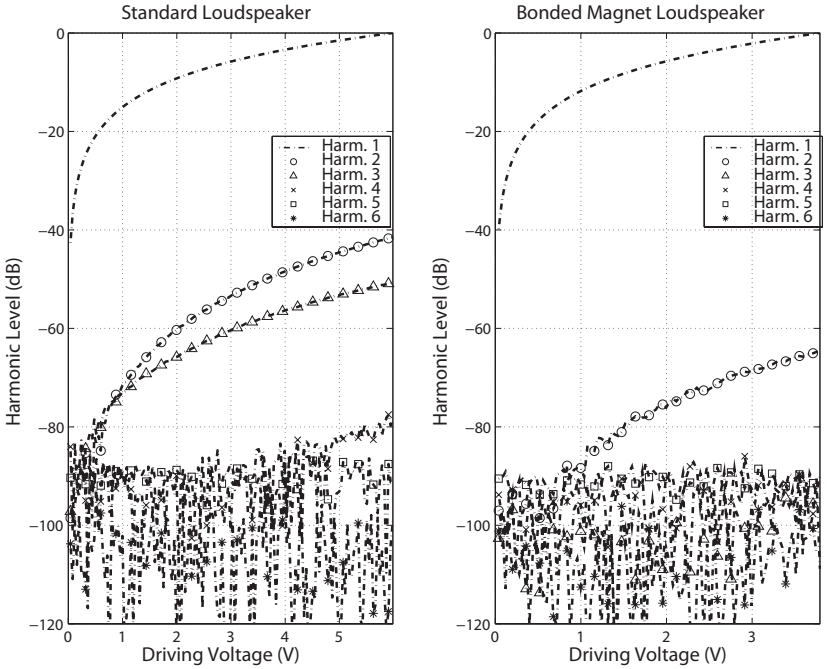

Figure 4.17: Harmonic distortion created on the sound pressure for both speakers at 8 kHz. Fundamental (-.-), 2nd harmonic (circle), 3rd harmonic (triangle), 4th harmonic (cross), 5th harmonic (square), 6th harmonic (star)

The results are similar to the experiment with two tones. The standard loudspeaker shows much more harmonic and inter-modulation distortions than the ironless speaker, for both driving voltage amplitudes.
In order to evaluate the overall distortion, including force factor nonlinearity and iron losses, a last measurement is conducted with a bass tone and two high frequency tones, the three having the same amplitude. Because of the voice-coil displacement dependence of the distortion, the standard speaker is driven at 1V per tone whereas the bonded magnet driver is fed with 5.6V per tone, representing a 15dB difference. The results are given in Fig. 4.22.

Once again, both types of distortion are much smaller on the bonded magnet motor voice-coil current. The higher distortion for this one is the second harmonic of the bass tone and is 60dB below the fundamental. On the contrary, the standard motor voice-coil current shows a high level of harmonic and inter-modulation distortion with several peaks reaching -30dB.
With a musical signal containing a multitude of simultaneous frequencies, this difference between the two speakers should be more pronounced, always in favor of the bonded magnet motor loudspeaker. This could, at least partly, explain the preference of the listeners for the ironless loudspeaker.

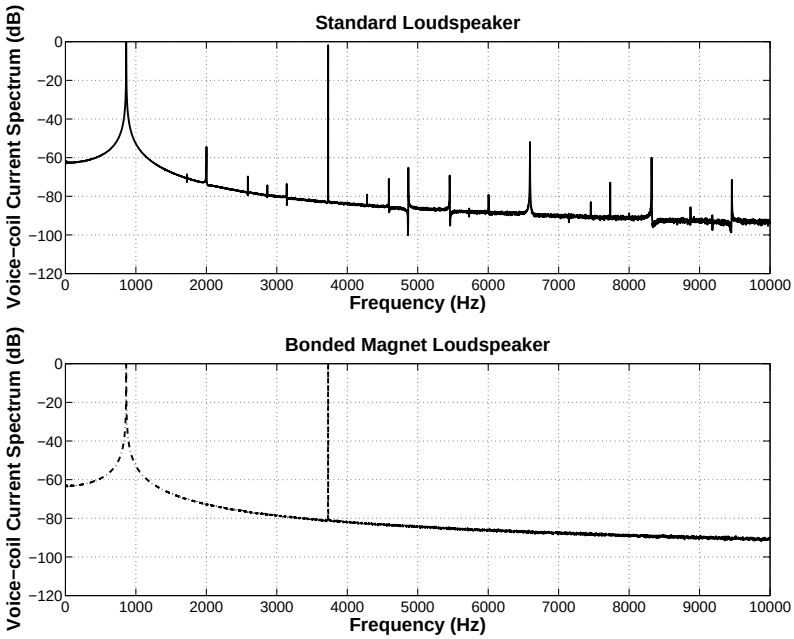

Figure 4.18: Inter-modulation distortion created on the voice-coil current for a two tone driving signal of 863Hz and 3728Hz at 1V per tone for both speakers.

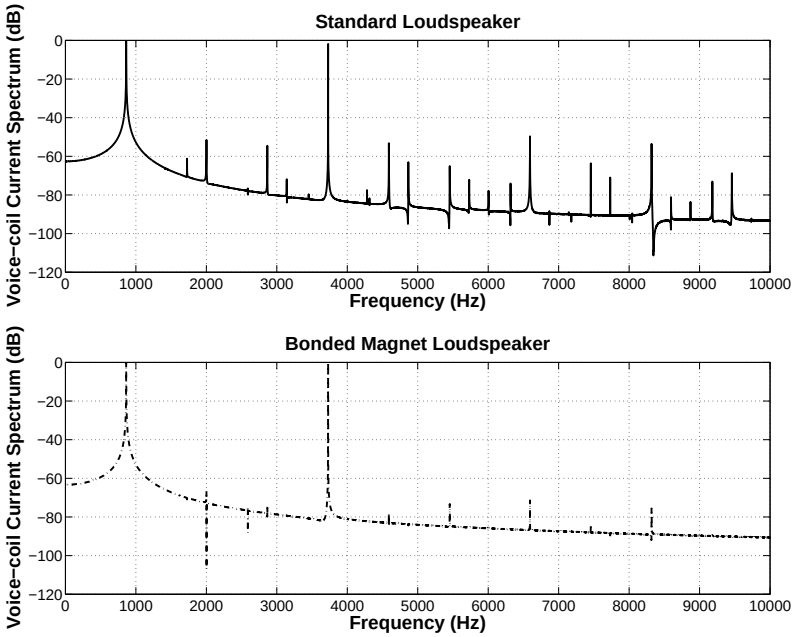

Figure 4.19: Inter-modulation distortion created on the voice-coil current for a two tone driving signal of 863Hz and 3728Hz at 5.6V per tone for both speakers.

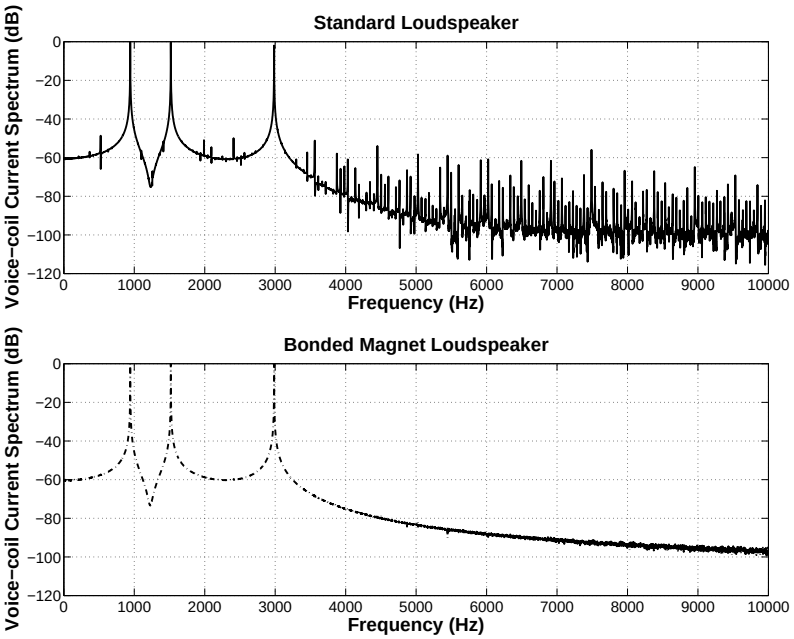

Figure 4.20: Inter-modulation distortion created on the voice-coil current for a three tone driving signal of 943Hz, 1519Hz and 2985Hz at 1V per tone for both speakers.

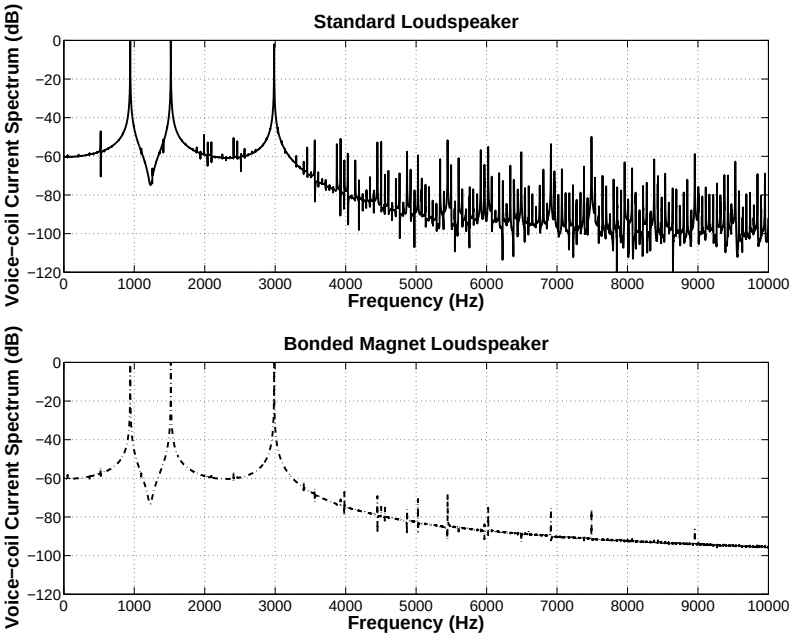

Figure 4.21: Inter-modulation distortion created on the voice-coil current for a three tone driving signal of 943Hz, 1519Hz and 2985Hz at 5.6V per tone for both speakers.

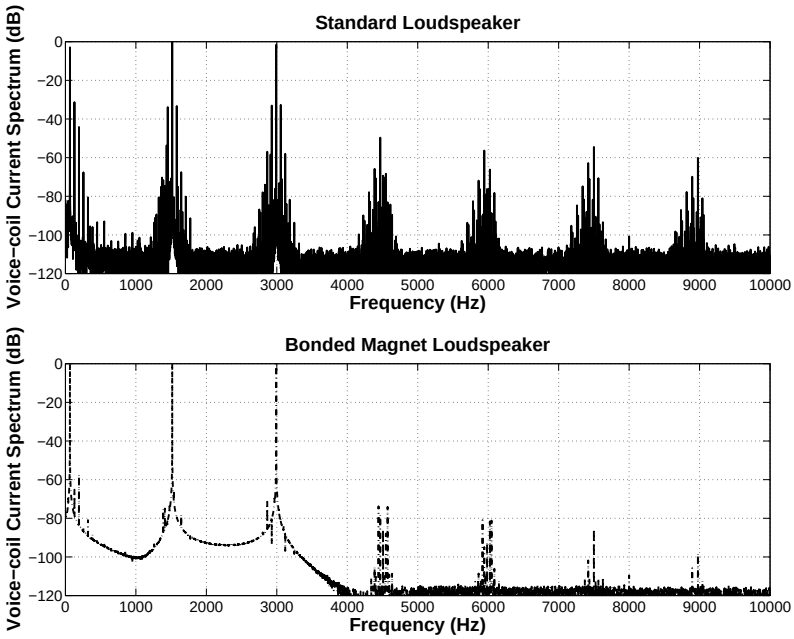

Figure 4.22: Inter-modulation distortion created on the voice-coil current for a three tone driving signal of 64Hz, 1516Hz and 2992Hz at 1V per tone for the standard speaker and 5.6V for the bonded magnet speaker (+15dB).

4.8 Conclusion

This chapter presents two automotive loudspeakers, one equipped with a traditional ferrite and iron motor and another one, on which an ironless bonded magnet motor was mounted. Following a listening session that had shown a substantial advantage for the ironless driver in terms of sound quality, a set of measurements were run in order to try to quantify this sound quality enhancement. It appears that the two main reasons of this distortion reduction are the linearization of the force factor, Bl, and the disappearance of the reluctant force and of the eddy currents.
On the one hand, low frequency harmonic distortion measurements revealed the effect of the force factor nonlinearities brought by the standard motor, compared to the more linear bonded magnet motor force factor. On the other hand, harmonic distortion measurements at high frequencies showed the interest of removing the iron from the motor. Furthermore, inter-modulation distortion was measured with several driving signals for both speakers, and the results speak for themselves. Once again, a significant advantage can easily be seen for the ironless motor loudspeaker. All these measurement results are good indicators of the sound quality enhancement, even though they are probably not the only ones.

However, at least one point was in favor of the standard loudspeaker: the efficiency. This can be explained by the fact that we tried to reduce the mass of the motor as much as possible. Indeed, it was almost divided by ten, from $200g$ to $20g$. The goal of

this study was to prove that we were able to manufacture this kind of bonded magnet motor and that the expected theoretical sound quality enhancement would actually be experimentally verified. Now that we have some concrete answers to these questions, new prototypes allowing us to approach the standard speaker efficiency, but being lighter and offering a much better linearity, will be made and tested.

Conclusion

The aim of this PhD work was to explore one or several innovative loudspeaker technologies that could have an interest in automotive audio. The main lines of inquiry that have been scouted were the weight reduction and the sound quality enhancement. These optimizations have been explored keeping in mind cost efficiency and the potential to, one day, be industrialized and put in a mass production car.

The study started from the sketch of a loudspeaker motor having a turning magnetization, on a piece of paper on the first day. The whole idea behind this concept was to design a loudspeaker motor without iron to focus the radial magnetic field on the voice-coil. Such structures had already been invented for quite a few years but either had a strong magnetic leakage flux [29, 30, 32, 37] or were almost impossible to fabricate [33], considering automotive constraints. The only way to realize a leakage free ironless loudspeaker motor, that could be produced at several million units per year and for a price that is compatible with automotive standards, was by using bonded magnets. This idea gave rise to a first patent [1] at the very beginning of the study, then followed by four others during the three years [2, 3, 4, 5].

As we discussed in this thesis, the removal of iron in the motor and the use of bonded magnets present two main advantages:

- Linearity: as previously studied and verified, the iron contained in a traditional loudspeaker motor is a great source of non-linearities. Among them, the two most important are the eddy currents and the variation of the voice-coil inductance with regard to its position, frequency and current intensity. These two non-linearities generate strong harmonic and intermodulation distortion (THD and IMD) that are heard in the sound pressure radiated by the speaker. The different measurements that we realized on our bonded magnet motor loudspeaker prototype confirmed these facts. As shown within this study, the voice-coil resistance R_e and inductance L_e both remain constant with an ironless bonded magnet motor, which indicates the disappearance of eddy currents . The several distortion (THD and IMD) measurements also gave a clear advantage to our prototype compared to a standard loudspeaker motor containing iron. However, the iron suppression is most probably not the only reason why our prototype shows less distortion. Indeed, as we also saw, the force factor Bl provided by our motor is more linear than the one offered by the other motor that we used for comparison. The scientific community agrees that the non-uniformity of the force factor represents one of the greatest distortion sources in a loudspeaker motor.

- Weight: a traditional loudspeaker motor exhibits a strong magnetic flux leakage, a remark also true for most of the ironless structures that we studied in this dissertation. This means a diminution of the global intensity of the magnetic fields created by these structures, which can become problematic when put too close to other loudspeakers or any electronic device, as was the case with old cathode ray tube (CRT) televisions or computer monitors. In other words, a part of the magnetic mass does not create a magnetic field that contributes towards making the voice-coil move. Following the work patented by Lemarquand et al. in 2006 [33], presenting an ironless structure that concentrates the magnetic field on the voice-coil path, and thus optimizes the necessary magnetic mass as much as possible, we developed our bonded magnet motor that offers both advantages to be ironless and leakage free, and solution to the manufacturing difficulties presented by the structure first proposed by Lemarquand. Indeed, since bonded magnets are realized by injection molding, it is much easier to realize complex shapes and especially complex orientations of the magnetic particles inside the magnet. With a view to mass production, the efficiency of the manufacturing process is an essential point. This flexibility is a big advantage towards weight optimization.

However, the structure we propose present as well two major drawbacks:

- Sensitivity: as seen in Chapter 4, the sensitivity achieved by the loudspeaker equipped with the bonded magnet motor is much lower than the traditional loudspeaker ($17dB$). Two reasons can explain this big difference: there is no iron to concentrate the magnetic field and increase its value in the air gap, and the remanent magnetizations that are reachable with bonded magnets are slightly smaller than with standard sintered magnets, since part of the material is plastic. The bonded ferrite powder used for the prototype had a remanent magnetization of $0.24T$, and the best bonded ferrite powder that can be found on the market hardly reach 0.28 or $0.3T$, whereas sintered ferrite powder can reach $0.4T$ or more. One way of optimizing the sensitivity of the motor is to add an inner magnet. The first prototype only had an annular magnet outside the voice-coil. However, by putting the symmetrical structure inside the voice-coil, it is possible to multiply by almost 2 the magnetic induction seen by the voice-coil, which corresponds to a $6dB$ gain. Another optimization, that is both compatible and augmentative with the first one, is to use neodymium (NdFeB) bonded magnets instead of ferrite. The remanent magnetization offered by neodymium bonded magnets can reach between $0.7T$ and $0.95T$. For instance, $0.85T$ compared to $0.24T$ represents a $11dB$ gain. Combining both optimizations, it is thus possible to increase the sensitivity of the prototype by $17dB$, which equals the standard loudspeaker, with a motor that creates much less distortion and that is still at least half the weight. Obviously, these optimizations have a certain cost that car manufacturers are not necessarily ready to pay.

- Heat dissipation: the iron contained in classical loudspeaker motors facilitates dissipation of the heat created by the electrical current flowing through the voice-coil. In the case of the prototype, the plastic present in the bonded magnet motor creates a thermal barrier between the magnetic particles, preventing the heat from being dissipated in the mass of the motor, as the thermal conductivity of plastic is close to

zero. One way to optimize the thermal dissipation, as shown in the prototype, is to use an aluminum voice-coil former, which ameliorates the thermal resistance of the speaker. However, this solution presents two disadvantages: aluminum is heavier than the kapton that is traditionally used for voice-coil formers and thus decreases the sensitivity, and as measured on the prototype, it brings back some eddy currents at high frequencies. Nevertheless, as Merit showed in his PhD [14], the eddy currents created in aluminum are not a source of distortion since this material presents a linear magnetic behavior.
This thermal restriction limits the use of this kind of motors to low power loudspeakers, which is consistent with automotive needs but prevent the extension of this technology to HiFi or even more, professional loudspeakers. Since what we are interested in is usually the maximum SPL, it is crucial to reach a high sensitivity in order to limit the intensity of the driving current.

At the end of this three years work, we developped a structure based on the ellipsoidal bonded magnet motor structure but that is not ironless anymore [5]. Indeed, we kept the magnet ring inside the voice-coil and put an iron ring outside the coil in order to shorten the magnetic path and thus increase the magnetic induction seen by the voice-coil in the air gap. Thanks to this structure, the heat dissipation is improved because of the presence of iron near the voice-coil. This structure is presented in Fig. 4.24.
This solution obviously does not offer the same benefits in terms of distortion as the

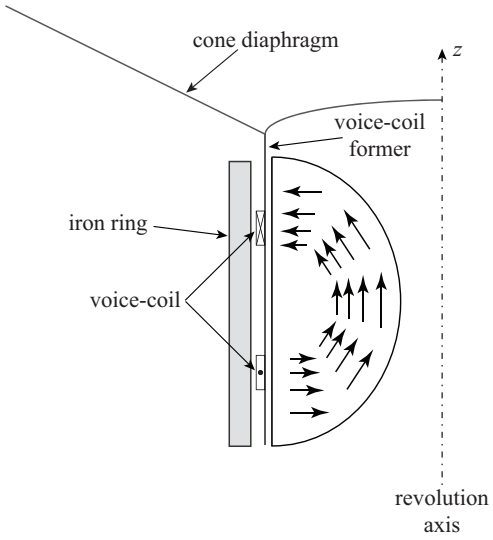

Figure 4.23: Cross section of the bonded magnet and iron ring structure.

ironless motor but could be a good compromise for automotive mass production regarding the price and the total weight of the motor. Concerning the distortions, the force factor linearity should not be affected but eddy currents and the reluctant force will appear again. New prototypes that will be soon available will permit to test this solution.

Conclusion

Le but de cette thèse était d'explorer une ou plusieurs technologies innovantes de haut-parleur pouvant avoir un intérêt pour l'audio automobile. Les axes de recherche qui ont été approfondis sont la réduction du poids et l'amélioration de la qualité sonore. Ces optimisations ont été étudiées en gardant à l'esprit les contraintes de coût et le potentiel d'être, un jour, industrialisé et intégré dans un véhicule de série.

L'étude commença, le premier jour de la thèse, par le dessin sur un bout de papier d'un moteur de haut-parleur ayant une aimantation tournante. L'idée de ce concept était de développer un moteur de haut-parleur sans fer capable de concentrer directement le champ magnétique radial sur la bobine. De telles structures avaient déjà été inventées depuis quelques années mais soit avaient un fort champ de fuite magnétique [29, 30, 32, 37] soit étaient quasiment impossible à fabriquer [33], compte tenu des contraintes du milieu automobile. La seule manière d'arriver à réaliser un moteur de haut-parleur sans fer et sans fuite, et pouvant être produit à plusieurs millions d'unités par an pour un prix compatible avec les standards de l'automobile, était d'utiliser des aimants liés. Cette idée déboucha sur un premier brevet [1] au tout début de l'étude, suivi par quatre autres pendant les trois années de mes travaux de recherche [2, 3, 4, 5].

Comme discuté dans ce mémoire de thèse, la suppression du fer dans le moteur et l'utilisation d'aimants liés présentent deux avantages principaux :

- La linéarité : comme étudié et vérifié précédemment, le fer contenu dans un moteur de haut-parleur traditionnel est une source importante de non-linéarités. Parmi elles, les deux principales sont les courantes de Foucault et la variation de l'inductance de la bobine avec sa position, la fréquence et l'intensité du courant. Ces deux non-linéarités génèrent de fortes distorsions harmonique et d'intermodulation (THD et IMD) qui sont audibles dans le son rayonné par le haut-parleur. Les différentes mesures réalisées sur notre prototype de haut-parleur équipé du moteur en aimant lié ont permis de confirmer ces affirmations. Comme montré dans cette étude, la résistance R_e et l'inductance L_e de la bobine restent toutes les deux constantes avec un moteur sans fer en aimant lié, indiquant la disparition des courants de Foucault. Les différentes mesures de distorsion (THD et IMD) ont également donné un net avantage à notre prototype comparé au moteur de haut-parleur standard contenant du fer. Cependant, la suppression du fer n'est certainement pas la seule et unique raison pour laquelle il montre moins de distorsion. En effet, nous avons également vu que le facteur de force Bl fournit par notre moteur offre une plage de linéarité plus importante que celle proposée par l'autre moteur que nous avons

utilisé en comparaison. La communauté scientifique est d'accord sur le fait que la non-uniformité du facteur de force représente une des plus importantes sources de distorsion dans un moteur de haut-parleur.

- Le poids : un moteur de haut-parleur traditionnel présente un fort champ de fuite magnétique, remarque qui s'applique également à la plupart des structures sans fer étudiées dans ce mémoire. Ce champ de fuite implique une diminution de l'intensité globale des champs magnétiques créés par ces structures, et peut devenir un problème dans le cas où le moteur est placé trop près d'autres haut-parleurs ou de toute autre équipement électronique, comme cela pouvait être le cas avec les télévisions ou écrans d'ordinateurs à tube cathodique. En d'autres termes, une partie de la masse magnétique ne crée pas de champ magnétique contribuant à faire bouger la bobine mobile. A la suite du travail breveté par Lemarquand et al. en 2006 [33], présentant une structure sans fer qui concentre le champ magnétique sur le trajet de la bobine, et ainsi optimise la masse magnétique nécessaire autant que possible, nous avons développé un moteur en aimant lié offrant les deux avantages d'être sans fer et sans fuite, et remédiant aux difficultés de fabrication rencontrées par les premières structures proposées par Lemarquand. En effet, étant donné que les aimants liés sont réalisés par injection, il est beaucoup plus facile d'obtenir des formes complexes ainsi que des orientations complexes des particules magnétiques à l'intérieur de l'aimant. Sans perdre de vue la production de masse, l'efficacité du process de fabrication est un point essentiel. Cette flexibilité est un avantage pour l'optimisation du poids.

Cependant, la structure que nous proposons présente également deux défauts majeurs :

- La sensibilité : comme montré dans le Chapitre 4, la sensibilité obtenue par le haut-parleur équipé du moteur en aimant lié est sensiblement plus faible que celle du haut-parleur traditionnel ($17dB$). Deux raisons peuvent expliquer cette différence importante : il n'y a pas de fer pour concentrer le champ magnétique et ainsi augmenter sa valeur dans l'entrefer, et l'aimantation rémanente qu'il est possible d'obtenir avec un aimant lié est légèrement plus faible qu'avec un aimant fritté, étant donné qu'une partie de la matière est du plastique. La poudre de l'aimant lié utilisé pour le prototype avait une aimantation rémanente de $0,24T$, et les meilleures poudres de plasto-ferrite que l'on peut trouver sur le marché atteignent péniblement $0,3T$, alors que les poudres d'aimants frittés peut aller jusqu'à $0,4T$ ou parfois légèrement plus. Une manière d'optimiser la sensibilité du moteur est d'ajouter un aimant à l'intérieur du support de bobine. Le premier prototype avait uniquement un aimant annulaire à l'extérieur de la bobine. Cependant, en plaçant la structure symétrique à l'intérieur de la bobine, il est possible de multiplier par presque 2 le champ magnétique vu par la bobine, ce qui correspond à un gain de $6dB$. Une autre optimisation, qui est à la fois compatible et cumulative avec la première, est d'utiliser des aimants liés en néodyme (NdFeB) à la place de la ferrite. L'aimantation rémanente offerte par ce type d'aimants peut atteindre entre $0,7T$ et $0,95T$. Par exemple, $0,85T$ comparé à $0,24T$ représente un gain de $11dB$. En combinant ces deux optimisations, il est donc possible d'augmenter la sensibilité du prototype de $17dB$, permettant ainsi d'atteindre les mêmes performances que le haut-parleur standard, avec un moteur créant nettement moins de distorsion et qui pèse au moins

deux fois moins lourd. Bien évidemment, ces optimisations ont un certain coût que les constructeurs automobiles ne sont pas forcément prêts à payer.

- La dissipation thermique : Le fer contenu dans les moteurs de haut-parleurs classiques facilite la dissipation de la chaleur créée par le courant électrique circulant dans la bobine. Dans le cas du prototype, le plastique présent dans l'aimant lié crée un isolant thermique entre les particules magnétiques, empêchant la chaleur de se dissiper dans la masse du moteur, étant donné que la conductivité thermique du plastique est quasiment nulle. Une manière d'optimiser la dissipation thermique, comme réalisé sur le prototype, est d'utiliser un support de bobine en aluminium, qui permet d'améliorer la résistance thermique du haut-parleur. Cependant, cette solution présente deux inconvénients : l'aluminium, plus lourd que le kapton traditionnellement utilisé pour les supports de bobine, diminue ainsi la sensibilité, et comme mesuré sur le prototype, cela génère des courants de Foucault à hautes fréquences. Néanmoins, comme montré par Merit dans sa thèse de doctorat [14], les courants de Foucault créés dans l'aluminium ne sont pas source de distorsion étant donné que ce matériau présent un comportement magnétique linéaire.
  Cette restriction thermique limite l'utilisation de ce type de moteurs à des haut-parleurs de faible puissance, ce qui est cohérent avec les besoins de l'automobile mais empêche une extension de cette technologie à la HiFi ou d'autant plus, aux haut-parleurs professionnels.

A la fin de ce travail de trois ans, nous avons développé une structure basée sur la structure du moteur ellipsoïdal en aimant lié mais qui n'est plus sans fer [5]. En effet, nous avons gardé l'aimant annulaire à l'intérieur de la bobine et placé un anneau de fer à l'extérieur afin de raccourcir le chemin magnétique et ainsi d'augmenter le champ magnétique vu par la bobine dans l'entrefer. Grâce à cette structure, la dissipation thermique est améliorée du fait de la présence de fer à côté de la bobine. Cette structure est représentée sur la Figure 4.24.

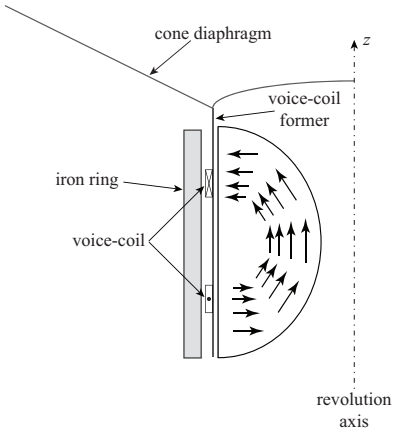

Figure 4.24: Cross section of the bonded magnet and iron ring structure.

Cette solution n'offre évidemment pas les mêmes bénéfices que le moteur sans fer en

terme de distorsion, mais pourrait être un bon compromis pour la production de masse automobile, en ce qui concerne le prix et la masse totale du moteur. Concernant la distorsion, la linéarité du facteur de force ne devrait pas être affectée mais des courants de Foucault et une force de réluctance vont apparaître à nouveau. De nouveaux prototypes bientôt disponibles devraient permettrent de tester cette solution.

Bibliography

[1] M. Remy, G. Lemarquand, and G. Guyader, "Ironless and leakage free coil transducer motor assembly." EP Patent 08103799.6, 2008.

[2] M. Remy, G. Lemarquand, and G. Guyader, "Mandrel for a coil transducer motor structure." EP Patent 08290652.0, 2008.

[3] M. Remy, G. Lemarquand, G. Guyader, and C. Peteul-Brouillet, "Optimisation de moteur de haut-parleur sans fer en aimants liés (plasto-aimants ou élasto-aimants)." FR Patent FR1050925, 2010.

[4] M. Remy, G. Lemarquand, and G. Guyader, "Moulage par injection unique de toute la partie fixe d'un haut-parleur." FR Patent FR1050926, 2010.

[5] M. Remy, G. Lemarquand, G. Guyader, and C. Peteul-Brouillet, "Suppression des plaques de champ supérieures et inférieures des moteurs de haut-parleur." FR Patent FR1150993, 2011.

[6] E. W. Siemens, "Magneto-electric apparatus for obtaining the mechanical movement of an electrical coil from electrical currents transmitted through it." US Patent 149,797, 1874.

[7] A. G. Bell, "Improvement in telegraphy." US Patent 174,465, 1876.

[8] O. J. Lodge, "Improvements in magnetic telegraphy and telephony." UK Patent GB189729505, 1898.

[9] C. Rice and E. Kellogg, "Notes on the development of a new type of hornless loudspeaker," *Transactions of the American Institute of Electrical Engineers*, vol. 44, pp. 461–475, 1925.

[10] M. Rossi, *Traité d'électricité, Vol. XXI: Electroacoustique*. Presses Polytechniques Romandes, 1986.

[11] R. P. Olenik, T. M. Apostol, and D. L. Goodstein, *Beyond the Mechanical Universe: from Electricity to Modern Physics*. Cambridge University Press, 1986.

[12] J. C. Maxwell, *On physical lines of force*. Philosophical Magazine, 1861.

[13] J. C. Maxwell, "A dynamical theory of the electromagnetic field," *Phylosophical Transactions of the Royal Society of London*, vol. 155, pp. 459–512, 1865.

[14] B. Merit, *Contribution à l'identification des non-linéarités des moteurs de haut-parleurs électrodynamiques - Sur la réalisation de moteurs tout aimant*. PhD thesis, Université du Maine, Le Mans, France, September 21st 2010.

[15] H. F. Olson, *Dynamical Analogies*. Van Nostrand Company, 1943.

[16] H. F. Olson, *Elements of Acoustical Engineering*. Van Nostrand Company, 1947.

[17] L. L. Beranek, *Acoustics*, ch. Chap. 7. Hardcover, 1986 re-edited from 1953.

[18] A. N. Thiele, "Loudspeakers in vented boxes," Presented at the 1961 I.R.E. Radio and Electronic Engineering Convention, Proceedings of the IRE Australia, March 1961.

[19] A. N. Thiele, "Loudspeakers in vented boxes: Part i," *Journal of the Audio Engineering Society*, vol. 19, pp. 382–392, May 1971.

[20] R. Small, "Loudspeakers in vented boxes: Part ii," *Journal of the Audio Engineering Society*, vol. 21, pp. 438–444, July/August 1973.

[21] M. Bruneau, *Manuel d'Acoustique Fondamentale*. Hermes, 1998.

[22] W. M. J. Leach, *Introduction do Electroacoustics and Audio Amplfier Design*. Kendall/Hunt Publishing Company, third ed., 2003.

[23] K. Honda and S. Saito, "MS magnetic steels," *Phys. Rev.*, vol. 16, 1920.

[24] J. Coey, *Rare-earth iron permanent magnets*. Oxford : Clarendon Press; New York : Oxford University Press, 1996.

[25] M. Gander, "Moving-coil loudspeaker topology as an indicator of linear excursion capability," *J. Audio Eng. Soc.*, vol. 29, pp. 10–26, Jan 1981.

[26] J. Vanderkooy, "A model of loudspeaker driver impedance incorporating Eddy currents in the pole structure," *J. Audio Eng. Soc.*, vol. 37, pp. 119–128, March 1989.

[27] C. Koh, "Magnetic pole shape optimization of permanent magnet motor for reduction of cogging torque," *IEEE Trans. Magn.*, vol. 33, pp. 1822–1827, Feb 1997.

[28] K. Atallah and D. Howe, "The application of halbach cylinders to brushless ac servo motors," *IEEE Transactions on Magnetics*, vol. 34, pp. 2060–2062, April 1998.

[29] W. House, "Transducer motor assembly." US Patent 5,142,260, 1992.

[30] S. Geisenberger and G. Krump, "Lautsprecher." EP Patent 0 804 048 A2, 1997.

[31] S. Geisenberger and G. Krump, "Loudspeaker." US Patent 6,359,997 B2, 2002.

[32] Y. Ohashi, "Magnetic circuit and speaker." EP Patent 1 553 802 A2, 2005.

[33] B. Richoux, G. Lemarquand, and V. Lemarquand, "Transducteur électrodynamique, applications aux haut-parleurs et géophones." PCT/FR2006/051133, 2006.

[34] M. Berkouk, *Contribution à l'étude des actionneurs électrodynamiques*. PhD thesis, Université de Bretagne Occidentale, France, 2001.

[35] M. Berkouk, V. Lemarquand, and G. Lemarquand, "Analytical calculation of ironless loudspeaker motors," *IEEE Trans. Magn.*, vol. 37, pp. 1011–1014, March 2001.

[36] S. Mowry, "Almost air core," *Voice Coil*, pp. 1–9, February 2009.

[37] G. Lemarquand and B. Merit, "Magnetic structure for the iron-free motor of electrodynamic loudspeaker, motors and loudspeakers." PCT/FR2008/051678, 2008.

[38] F. Bancel and G. Lemarquand, "Three-dimensional analytical optimization of permanent magnets alternated structure," *IEEE Trans. Magn.*, vol. 34, pp. 242–247, January 1998.

[39] P. Brissonneau, *Magnétisme et Matériaux Magnétiques pour l'Électrotechnique*. Hermes Sciences, 1997.

[40] H. L. Rakotoarison, J. P. Yonnet, and B. Delinchant, "Using coulombian approach for modelling scalar potential and magnetic field of a permanent magnet with radial polarization," *IEEE Trans. Magn.*, vol. 43, pp. 1261–1264, April 2007.

[41] E. P. Furlani, S. Reznik, and A. Kroll, "A three-dimensonal field solution for radially polarized cylinders," *IEEE Trans. Magn.*, vol. 31, pp. 844–851, Jan. 1995.

[42] J. P. Yonnet, *Rare-earth Iron Permanent Magnets*, ch. Magnetomechanical devices. Oxford science publications, 1996.

[43] E. P. Furlani, "Field analysis and optimization of ndfeb axial field permanent magnet motors," *IEEE Trans. Magn.*, vol. 33, pp. 3883–3885, Sept 1997.

[44] Y.Zhilichev, "Calculation of magnetic field of tubular permanent magnet assemblies in cylindrical bipolar coordinates," *IEEE Trans. Magn.*, vol. 43, pp. 3189–3195, July 2007.

[45] R. Ravaud, G. Lemarquand, V. Lemarquand, and C. Depollier, "Discussion about the analytical calculation of the magnetic field created by permanent magnets," *Progress In Electromagnetics Research B*, vol. 11, pp. 281–297, 2009.

[46] G. Lemarquand, "Ironless loudspeakers," *IEEE Transactions on Magnetics*, vol. 43, pp. 3371–3374, August 2007.

[47] Z. Jibin, Z. Jiming, and H. Jianhui, "Design and pressure control of high-pressure differential magnetic fluid seals," *IEEE Trans. Magn.*, vol. 39, pp. 2651 – 2653, Sept 2003.

[48] M.Remy, G. Lemarquand, B. Castagnede, and G. Guyader, "Ironless and leakage free voice-coil motor made of bonded magnets," *IEEE Trans. Magn.*, vol. 44, pp. 4289–4292, November 2008.

[49] B. Merit, V. Lemarquand, G. Lemarquand, and A. Dobrucki, "Motor nonlinearities in electrodynamic loudspeakers: Modelling and measurement," *Archives of Acoustics*, vol. 34, no. 4, pp. 579–590, 2009.

[50] B. Merit, G. Lemarquand, and V. Lemarquand, "Performances and design of ironless loudspeaker motor structures," *Applied Acoustics*, vol. 71, pp. 546–555, January 2010.

[51] W. Klippel, "Prediction of speaker performance at high amplitudes," Presented at the AES 111th Convention, New York, USA, December 2001.

[52] W. Cunningham, "Nonlinear distortion in dynamic loudspeakers due to magnetic effects," *JASA*, vol. 21, pp. 202–207, May 1949.

[53] E. Czerwinski, A. Voishvillo, S. Alexandrov, and A. Terekhov, "Multitone testing of sound system components - some results and conclusions. part 1 : history and theory," *J. Audio Eng. Soc.*, vol. 49, pp. 1011–1048, November 2001.

[54] A. Voishvillo, A. Terekhov, E. Czerwinski, and S. Alexandrov, "Graphing, interpretation and comparison of results of loudspeaker nonlinear distortion measurements," *J. Audio Eng. Soc.*, vol. 52, pp. 332–357, April 2004.

[55] W. Klippel, "Assessment of voice-coil peak displacement x-max," *J. Audio Eng. Soc.*, vol. 51, pp. 307–323, May 2003.

[56] M. Abuelma'atti, "Prediction of the two-tone suppression and intermodulation performance of auditory systems," *Applied Acoustics*, vol. 67, pp. 882–891, September 2006.

Appendix A

Bonded Magnet Motor Modeling

A.1 Coordinates of each surface

The origin of the coordinate system in which is defined the cross section of the discretized structure is placed in (x_0, z_0). The coordinates of all eight points defining the surfaces extremities between each magnet are expressed as a function of b, h and θ.

$$
\begin{aligned}
(x_1, z_1) &= (0, -h) \\
(x_2, z_2) &= \left(-\frac{1}{\sqrt{\frac{1}{b^2} + \frac{\mathrm{Cot}[\theta]^2}{h^2}}}, -\frac{1}{\sqrt{\frac{1}{h^2} + \frac{\mathrm{Tan}[\theta]^2}{b^2}}} \right) \\
(x_3, z_3) &= \left(-\frac{1}{\sqrt{\frac{1}{b^2} + \frac{\mathrm{Cot}[2\theta]^2}{h^2}}}, -\frac{1}{\sqrt{\frac{1}{h^2} + \frac{\mathrm{Tan}[2\theta]^2}{b^2}}} \right) \\
(x_4, z_4) &= \left(-\frac{1}{\sqrt{\frac{1}{b^2} + \frac{\mathrm{Cot}[3\theta]^2}{h^2}}}, -\frac{1}{\sqrt{\frac{1}{h^2} + \frac{\mathrm{Tan}[3\theta]^2}{b^2}}} \right) \\
(x_5, z_5) &= \left(-\frac{1}{\sqrt{\frac{1}{b^2} + \frac{\mathrm{Cot}[3\theta]^2}{h^2}}}, \frac{1}{\sqrt{\frac{1}{h^2} + \frac{\mathrm{Tan}[3\theta]^2}{b^2}}} \right) \\
(x_6, z_6) &= \left(-\frac{1}{\sqrt{\frac{1}{b^2} + \frac{\mathrm{Cot}[2\theta]^2}{h^2}}}, \frac{1}{\sqrt{\frac{1}{h^2} + \frac{\mathrm{Tan}[2\theta]^2}{b^2}}} \right) \\
(x_7, z_7) &= \left(-\frac{1}{\sqrt{\frac{1}{b^2} + \frac{\mathrm{Cot}[\theta]^2}{h^2}}}, \frac{1}{\sqrt{\frac{1}{h^2} + \frac{\mathrm{Tan}[\theta]^2}{b^2}}} \right) \\
(x_8, z_8) &= (0, h)
\end{aligned}
$$

A.2 Surface charge densities

$$
\begin{aligned}
\sigma^*_{1-} &= -\frac{J}{\sqrt{1+\frac{\mathrm{Cot}[\theta]^2\left(b-\sqrt{b^2+h^2\mathrm{Tan}[\theta]^2}\right)^2}{b^2}}} \\
\sigma^*_{1+} &= J\left(\frac{\mathrm{Sin}[\theta]\left(h-\frac{bh}{\sqrt{b^2+h^2\mathrm{Tan}[\theta]^2}}\right)}{\sqrt{\frac{1}{\frac{1}{b^2}+\frac{\mathrm{Cot}[\theta]^2}{h^2}}+\left(h-\frac{bh}{\sqrt{b^2+h^2\mathrm{Tan}[\theta]^2}}\right)^2}}+\frac{\mathrm{Cos}[\theta]}{\sqrt{1+\frac{\mathrm{Cot}[\theta]^2\left(b-\sqrt{b^2+h^2\mathrm{Tan}[\theta]^2}\right)^2}{b^2}}}\right) \\
\sigma^*_{2-} &= J\frac{\mathrm{Cos}[\theta]\left(\frac{1}{\sqrt{\frac{1}{b^2}+\frac{\mathrm{Cot}[\theta]^2}{h^2}}}-\frac{1}{\sqrt{\frac{1}{b^2}+\frac{\mathrm{Cot}[2\theta]^2}{h^2}}}\right)-\mathrm{Sin}[\theta]\left(\frac{1}{\sqrt{\frac{1}{h^2}+\frac{\mathrm{Tan}[\theta]^2}{b^2}}}-\frac{1}{\sqrt{\frac{1}{h^2}+\frac{\mathrm{Tan}[2\theta]^2}{b^2}}}\right)}{\sqrt{\left(\frac{1}{\sqrt{\frac{1}{b^2}+\frac{\mathrm{Cot}[\theta]^2}{h^2}}}-\frac{1}{\sqrt{\frac{1}{b^2}+\frac{\mathrm{Cot}[2\theta]^2}{h^2}}}\right)^2+\left(\frac{1}{\sqrt{\frac{1}{h^2}+\frac{\mathrm{Tan}[\theta]^2}{b^2}}}-\frac{1}{\sqrt{\frac{1}{h^2}+\frac{\mathrm{Tan}[2\theta]^2}{b^2}}}\right)^2}} \\
\sigma^*_{2+} &= J\frac{-\mathrm{Cos}[2\theta]\left(\frac{1}{\sqrt{\frac{1}{b^2}+\frac{\mathrm{Cot}[\theta]^2}{h^2}}}-\frac{1}{\sqrt{\frac{1}{b^2}+\frac{\mathrm{Cot}[2\theta]^2}{h^2}}}\right)+\mathrm{Sin}[2\theta]\left(\frac{1}{\sqrt{\frac{1}{h^2}+\frac{\mathrm{Tan}[\theta]^2}{b^2}}}-\frac{1}{\sqrt{\frac{1}{h^2}+\frac{\mathrm{Tan}[2\theta]^2}{b^2}}}\right)}{\sqrt{\left(\frac{1}{\sqrt{\frac{1}{b^2}+\frac{\mathrm{Cot}[\theta]^2}{h^2}}}-\frac{1}{\sqrt{\frac{1}{b^2}+\frac{\mathrm{Cot}[2\theta]^2}{h^2}}}\right)^2+\left(\frac{1}{\sqrt{\frac{1}{h^2}+\frac{\mathrm{Tan}[\theta]^2}{b^2}}}-\frac{1}{\sqrt{\frac{1}{h^2}+\frac{\mathrm{Tan}[2\theta]^2}{b^2}}}\right)^2}} \\
\sigma^*_{3-} &= J\frac{\mathrm{Cos}[2\theta]\left(\frac{1}{\sqrt{\frac{1}{b^2}+\frac{\mathrm{Cot}[2\theta]^2}{h^2}}}-\frac{1}{\sqrt{\frac{1}{b^2}+\frac{\mathrm{Cot}[3\theta]^2}{h^2}}}\right)-\mathrm{Sin}[2\theta]\left(\frac{1}{\sqrt{\frac{1}{h^2}+\frac{\mathrm{Tan}[2\theta]^2}{b^2}}}-\frac{1}{\sqrt{\frac{1}{h^2}+\frac{\mathrm{Tan}[3\theta]^2}{b^2}}}\right)}{\sqrt{\left(\frac{1}{\sqrt{\frac{1}{b^2}+\frac{\mathrm{Cot}[2\theta]^2}{h^2}}}-\frac{1}{\sqrt{\frac{1}{b^2}+\frac{\mathrm{Cot}[3\theta]^2}{h^2}}}\right)^2+\left(\frac{1}{\sqrt{\frac{1}{h^2}+\frac{\mathrm{Tan}[2\theta]^2}{b^2}}}-\frac{1}{\sqrt{\frac{1}{h^2}+\frac{\mathrm{Tan}[3\theta]^2}{b^2}}}\right)^2}} \\
\sigma^*_{3+} &= J\frac{-\mathrm{Cos}[3\theta]\left(\frac{1}{\sqrt{\frac{1}{b^2}+\frac{\mathrm{Cot}[2\theta]^2}{h^2}}}-\frac{1}{\sqrt{\frac{1}{b^2}+\frac{\mathrm{Cot}[3\theta]^2}{h^2}}}\right)+\mathrm{Sin}[3\theta]\left(\frac{1}{\sqrt{\frac{1}{h^2}+\frac{\mathrm{Tan}[2\theta]^2}{b^2}}}-\frac{1}{\sqrt{\frac{1}{h^2}+\frac{\mathrm{Tan}[3\theta]^2}{b^2}}}\right)}{\sqrt{\left(\frac{1}{\sqrt{\frac{1}{b^2}+\frac{\mathrm{Cot}[2\theta]^2}{h^2}}}-\frac{1}{\sqrt{\frac{1}{b^2}+\frac{\mathrm{Cot}[3\theta]^2}{h^2}}}\right)^2+\left(\frac{1}{\sqrt{\frac{1}{h^2}+\frac{\mathrm{Tan}[2\theta]^2}{b^2}}}-\frac{1}{\sqrt{\frac{1}{h^2}+\frac{\mathrm{Tan}[3\theta]^2}{b^2}}}\right)^2}} \\
\sigma^*_{4-} &= -J\times\mathrm{Sin}[3\theta] \\
\sigma^*_{4+} &= -\sigma^*_{4-} \\
\sigma^*_{5-} &= -\sigma^*_{3+} \\
\sigma^*_{5+} &= -\sigma^*_{3-} \\
\sigma^*_{6-} &= -\sigma^*_{2+} \\
\sigma^*_{6+} &= -\sigma^*_{2-} \\
\sigma^*_{7-} &= -\sigma^*_{1+} \\
\sigma^*_{7+} &= -\sigma^*_{1-}
\end{aligned}
$$

Moteur de Haut-parleur Sans Fer Innovant Adapté à l'Audio Automobile

Thèse de Doctorat en Acoustique, Université du Maine, Le Mans, France, 2011

Ce travail de thèse (CIFRE, Renault) porte sur la conception, le développement et la pré-industrialisation d'un nouveau type de moteur de haut-parleur sans fer utilisant des plasto-aimants, permettant à la fois de réduire très nettement la distorsion due au moteur, ainsi que d'alléger le haut-parleur grâce à une optimisation de la masse magnétique utile. Cette structure a donné lieu à cinq brevets déposés par Renault et le LAUM.

La première partie est consacrée à un rappel sur le fonctionnement du haut-parleur, sa modélisation, les différentes non-linéarités qui lui sont propres et leur impact sur la pression acoustique rayonnée par celui-ci, afin de mieux comprendre les enjeux de la réduction de ces imperfections, et plus particulièrement celles liées au moteur du haut-parleur. L'accent est mis sur la suppression du fer dans le moteur qui représente une des principales sources de distorsion de la transduction électro-mécanique. Un historique des différentes structures de moteurs de haut-parleur sans fer réalisées en aimants frittés existant à ce jour est alors présenté.

La seconde partie présente ensuite une nouvelle structure de moteur de haut-parleur tout aimant réalisée en plasto-aimant. Cette matière permet de réaliser par injection, des aimants de formes très variées et surtout, possédant des profils d'aimantation nettement plus complexes que ceux qu'il est possible d'obtenir avec des aimants traditionnels frittés. Une étude théorique complète de cette nouvelle structure est alors proposée, puis agrémentée d'un certain nombre de mesures réalisées sur un prototype et sur le haut-parleur équipé du moteur standard afin de vérifier les attentes théoriques et de pouvoir quantifier les avantages et les inconvénients de ce nouveau type de moteur. Ce prototype a été réalisé sur la base d'un haut-parleur automobile standard sur lequel le moteur a été changé. Les prototypes ont été réalisés par des sous-traitants automobiles (Paulstra/Hutchinson et Faital S.p.A.) dans des conditions telles que ces haut-parleurs soient industrialisables. Ce travail de thèse sert d'outil aux personnes en charge du développement de cette technologie en vue d'une éventuelle industrialisation et d'une mise en série sur véhicule.

Innovative Ironless Loudspeaker Motor Adapted to Automotive Audio

PhD Thesis in Acoustics, Université du Maine, Le Mans, France, 2011

This PhD work (CIFRE, Renault) deals with the conception, development and pre-industrialization of a new kind of ironless loudspeaker motor using bonded magnets, allowing to highly reduct the distortion due to the motor, as well as making the loudspeaker lighter thanks to an optimization of the useful magnetic mass. This structure led to the filing of five patents by Renault and the LAUM.

The first part is dedicated to remind the reader the general laws that describe the functioning of a loudspeaker: how it is modelized, the different intrinsic non-linearities and their impact on the radiated acoustic pressure. This is done in order to understand the stakes of reducing these imperfections, and more particularly those directly linked to the loudspeaker motor. In addition, a history of the different ironless motor structures realized in sintered magnets known today is presented.

The second part presents a new ironless structure made of a bonded magnet that we developed during these three years. The use of this material, that is fabricated by injection molding, allows to realize a great variety of magnet physical shapes and complex magnetization shapes. A complete theoretical study of this new structure, presenting the magnetic model and the design of the motor, is proposed and completed with several measurements realized on a prototype and on the standard loudspeaker in order to verify the theoretical expectations, with regard to harmonic and intermodulation distortion reduction, and quantify the advantages and disadvantages of this new kind of motor. This prototype was based on the design of a standard automotive loudspeaker on which the motor was replaced by a bonded magnet motor. The motor was fabricated by Paulstra/Hutchinson and then assembled on the loudspeaker by Faital S.p.A., both of whom are certified automotive suppliers. The methods used to realize this prototype could be directly derivated for mass production. This PhD work is used by the people in charge of the development of this technology with a view to a potential industrialization for mass market.